Quantifying feedbacks

in the plant–atmosphere–cloud continuum

MARTIN SIKMA

Quantifying feedbacks in the plant-atmosphere-cloud continuum

Martin Sikma

Thesis committee

Promotors
Prof. Dr Niels P.R. Anten
Professor of Crop and Weed Ecology
Wageningen University & Research

Prof. Dr Jordi Vilà-Guerau de Arellano
Professor of Atmosphere and Land Interactions
Wageningen University & Research

Co-promotors
Dr Jochem B. Evers
Associate Professor, Centre for Crop System Analysis
Wageningen University & Research

Dr Bert G. Heusinkveld
Senior Researcher, Meteorology and Air Quality group
Wageningen University & Research

Other members
Prof. Dr Marten Scheffer, Wageningen University & Research
Prof. Dr Diego G. Miralles, Ghent University
Prof. Dr Gerard van der Steenhoven, Royal Netherlands Meteorological Institute
Dr Hugo J. de Boer, Utrecht University

This research was conducted under the auspices of the C.T. de Wit Graduate School for Production Ecology and Resource Conservation.

Quantifying feedbacks in the plant-atmosphere-cloud continuum

Martin Sikma

Thesis
submitted in fulfilment of the requirements for the degree of doctor
at Wageningen University
by the authority of the Rector Magnificus,
Prof. Dr A.P.J. Mol,
in the presence of the
Thesis Committee appointed by the Academic Board
to be defended in public
on Wednesday, 16, October, 2019
at 4.00 p.m. in the Aula.

Martin Sikma

Quantifying feedbacks in
the plant-atmosphere-cloud continuum

128 pages

PhD thesis, Wageningen University, Wageningen, The Netherlands (2019)
With references, with summary in English

ISBN: 978-94-6343-554-3
DOI: 10.18174/478363

Contents

Chapter 1	Introduction	1
Chapter 2	Interactions between vegetation, atmospheric turbulence and clouds under a wide range of background wind conditions	13
Chapter 3	Substantial reductions in cloud cover and moisture transport by dynamic plant responses	41
Chapter 4	Quantifying the feedback between rice architecture, physiology and microclimate under current and future CO_2 conditions	57
Chapter 5	Impact of future warming and enhanced [CO_2] on the vegetation-cloud interaction	77
Chapter 6	General discussion	93
	References	103
	Summary	117
	Acknowledgements	121
	List of journal publications	125
	PE&RC Training and Education Statement	127

1

Introduction

1.1 Motivation

Weather plays an essential role in our lives. It can have a profound impact on our daily life, by means of precipitation or temperature anomalies, though its societal impact is often correlated with the population's wealth. The scientific community is aligned as regards that our daily weather is changing, with increasing global temperatures and anomalous precipitation patterns. However, how fast and how much this change will be, is unclear. Over the last decades, enormous progress has been made to predict the progression of the atmosphere more accurately, with significant help from satellite observations (Bauer et al., 2015). As these satellites gathered observational data from today's atmosphere and phenology, they did not directly improve our understanding of how this atmosphere will progress. In other words, satellite data greatly improved the accuracy of the model initialization, but only slightly improved model physics.

Around the world, many scientific groups are actively working to improve the models used for weather and climate prediction. Some groups focus on the understanding of fundamental processes, while others translate that understanding into equations to be used in the weather and global climate models. Although great progress is occurring on that end, with for instance the recent ocean-atmosphere coupling in the European weather prediction model ECMWF, numerical weather prediction (NWP) and global climate models (GCM) are still constrained by the computer resources at hand. With current supercomputers, NWP models and GCMs reach horizontal model resolutions of around 12 km and 50 km, respectively. This means that processes occurring on spatial scales smaller than the model resolution cannot be resolved and need to be

approximated through equations (i.e. they need to be parameterized), with uncertainties as a consequence (see e.g., Cox et al., 2013). This uncertainty affects the forecast on multiple scales, for instance, on short scales we cannot accurately model the location of an afternoon thunderstorm, while problems arise on the interaction between the vegetation and atmosphere. This has a profound impact on the sub-weekly land-atmosphere interactions that affects the forecast's progression. Even in GCMs, uncertainties of small scale processes affect long-term climate projections. Recent research shows that surface controlled boundary layer clouds explain more than half of the temperature variance for the year ~2100 (Boucher et al., 2013; Stevens & Bony, 2013). The likely mechanism behind this process is occurring on small spatiotemporal scales, involving local plant transpiration, turbulent moisture and heat transport and cloud development. Since this latter determines the Earth's albedo by shortwave radiative cloud reflection and scattering, small errors in these processes affect the accuracy of these models such that large uncertainties arise.

In this thesis, we deal with the fundamental understanding of the daily feedback mechanisms that occur on small spatiotemporal scales and which influence the atmospheric state and subsequent boundary-layer cloud development. Our focus will be on the negative (balancing) feedbacks between plant physiological processes and cloud shading over land, which process determines atmospheric turbulence and was found to cause dynamic and heterogenetic surface patterns to arise. Our methodology focuses on low vegetation and is based on first principles by utilizing a state-of-the-art high-resolution model, which is able to simulate the full spectrum of moist convection; from plant physiology, atmospheric turbulence to cloud development.

1.2 Atmospheric feedbacks and their impact on the modelled future atmosphere

Understanding feedback mechanisms is essential to be able to accurately predict the future atmosphere. Feedbacks are present at all spatiotemporal scales and can both amplify or diminish the effects of an external forcing (e.g. solar irradiance) (Soden et al., 2008). An illustration of the relevance of a feedback is shown in the distribution of solar energy: from a global mean perspective, the Earth is close to radiative equilibrium, meaning that the shortwave radiation received from the sun is nearly balanced by the longwave radiation emitted from the Earth. However, the incoming radiation is unevenly distributed, causing large-scale atmospheric circulations to arise between the tropical and polar regions. By redistributing heat, those circulations tend to diminish the effects of the unevenly distributed solar energy by reducing spatial gradients in temperature.

Feedbacks and interactions occur on a wide range in spatiotemporal scales, but it is their overall interconnectivity that determines their efficiency to equilibrate, or destabilize, an external forcing. For instance, in-canopy plant-atmosphere interactions

occur on spatiotemporal scales of meters and seconds, while on the longer term (days to weeks) they can destabilize the atmospheric system. For instance, during the European summer of 2003, a destabilization of the atmospheric system caused severe droughts and extreme temperatures (Seneviratne et al., 2006). Related to atmospheric continental blocking events, soil moisture levels reduced caused by plant transpiration. As a consequence, more solar energy was converted into sensible heat, meaning rising canopy and air temperatures. Note that this process was a positive feedback, that forced the atmosphere into a new base state.

Although a negative feedback is not a physical phenomenon, but rather a consequence from interconnected physical processes, it determines the overall efficiency with which the Earth's system moves towards equilibrium. As such, feedbacks comprise integrated quantities of, for instance, key state variables as moisture, temperature or momentum, that entail small scale non-linear responses to external perturbations. To predict the evolution and impact of atmospheric feedbacks in NWPs and GCMs, small-scale interconnected processes need to be simplified and parameterized. Especially processes that are physically smaller than twice the finer NWP model resolution (~12 km; i.e., "grey zone") –such as cloud development and vegetation-atmosphere interactions– cannot be resolved explicitly and need to be represented by parameterizations. This entails all processes smaller than approximately 12 x 12 km for NWP and 50 x 50 km for GCM. Since those parameterizations coarsely represent the physical processes and the global models use different modelling approaches, extrapolation of these processes will cause misrepresentations to amplify (Berner et al., 2012), resulting in increased inter-model spread. Examples are present in the perturbed NWP ensemble forecast (i.e. 'plume') or in the climate projections.

Especially processes and their feedbacks related to short-lived continental cumulus cloud development (i.e. shortwave radiative effects) have shown to cause a wide inter-model spread regarding climate sensitivities. This process is thought to explain up to half of the variance in equilibrium climate sensitivity (Sherwood et al., 2014), which is the expected increase in temperature when CO_2 concentration doubles. Main uncertainties arise due to disturbances in shortwave radiation by these clouds. Since this directly impacts the surface energy fluxes, this process controls the development and stability of the atmosphere, the transport of moisture and heat and thus influences the large-scale circulations patterns. Understanding the non-linear processes that drive cumulus convection is thus one of the current major challenges in NWP and GCM modelling (Bony et al., 2015). Since large-scale atmospheric models do not represent the actual physics involving cumulus cloud development, fundamental research is needed to understand the interactions and feedbacks across spatial and temporal scales.

1.3 Radiative forcing on diurnal land-atmosphere feedbacks

At the surface, absorbed solar irradiance is converted into soil heat fluxes and turbulent energy fluxes. This partitioning of the radiative flux into an energy flux depends on the soil and vegetation conditions. Over land, a minor part of the incoming energy is transferred into the soil, while the major part of the incoming energy is redistributed into temperature (sensible heat) and moisture (latent heat) fluxes, whose distribution is constrained by the soil moisture state and plant transpiration. Over vegetated surfaces, plants respond to their environment and *vice versa*. Plant leaf area and physiology play a crucial role in this response, as it determines the surface roughness, interception rate of radiation and the in-canopy vertical exchange of momentum, heat, moisture and CO_2. Plants extract carbon dioxide (CO_2) from the atmosphere and convert this into chemical energy for internal use (i.e. photosynthesis). The uptake of CO_2 takes place through small openings –stomata– in the leaf and stems. Stomatal aperture is partly determined by the demand for CO_2 from the photosynthetic process which in turn also requires light as a source of energy. Thus, stomata will open more when there is much light and close more when there is less. Depending on the stomatal aperture, temperature and atmospheric humidity levels, a certain amount of water is released through these plant pores (i.e. transpiration) (Lambers et al., 2008). As plant transpiration is driven by both stomatal aperture responses to solar radiation as well as the soil and atmospheric state variables (e.g. temperature, moisture availability and deficit), the plant-atmosphere interaction is highly non-linear. Furthermore, since plant stomata mechanistically adapt to internal, atmospheric and radiative perturbations, a lagged response is observed, which mechanist response is asymmetric and species dependent (Vico et al., 2011). Furthermore, plants generally close their stomata faster than they open. This is believed to be a water saving strategy ensuring that stomata do not remain too open for too long when light availability and demand for CO_2 is low (e.g., Vico et al., 2011).

Under daytime conditions, the solar energy re-enters the atmosphere through the latent and sensible heat fluxes, which drives turbulent convection that cause the lower atmosphere to mix. This well-mixed layer overlaying the surface is called the atmospheric boundary layer (ABL), which is topped by a temperature inversion (Stull, 1988; Garratt, 1992). Under clear sky conditions (i.e. no clouds), high photosynthetic levels –thus transpiration– are maintained, leading to high sensible and latent heat fluxes that cause a strong land-atmosphere coupling (provided of course that there is enough water in the soil to support this transpiration). When surface temperatures and moisture levels are higher compared to the overlying atmosphere, the near surface density is lower compared to their surroundings. As a consequence of the decreased density, vertically rising motions (i.e., thermals) arise that contain high levels of humidity

and heat. These rising motions are more intense and reach deeper levels when the temperature strongly differs with the surroundings, meaning buoyancy levels are high. Depending on its strength (i.e., momentum), the thermals might be able to overcome the ABL inversion and reach the cloud layer. In the cloud layer, the absolute temperate quickly lowers, causing water to condensate. Atmospheric boundary layer cumulus clouds thus embody the top of moist thermals and represent the highways of atmospheric moisture transport from the surface into the cloud layer (Figure 1.1). In this capacity, they make a substantial contribution to the hydrological balance and Earth's energy balance through albedo effects, of which the latter cause the wide range in inter-model spread of current climate models (Sherwood et al., 2014).

With cumulus clouds developing, it can be stated that the plant-atmosphere-cloud system is coupled, since changes on plant transpiration will directly impact cumulus development through atmospheric thermals (Fig. 1.1). When cumulus clouds grow, they interfere with the solar radiation directed towards the surface. Part of the radiation is reflected back into space (i.e., albedo effect), while the major part enters the cloud and is scattered by cloud droplets. As a consequence, the diffuse component of radiation (i.e., the part that is scattered) strongly increases, while the direct component (i.e., uninhibited solar beams) of radiation decreases. This process is dependent on cloud thickness; with thin clouds overhead, the reduction in global radiation is relatively minor –with a high diffuse-direct ratio–, while thick clouds cause a vast reduction in both components of radiation. Since the diffuse component of radiation penetrates more efficiently into the canopy compared to the direct component of radiation, distinct plant responses occur (Freedman et al., 2001; Pedruzo-Bagazgoitia et al., 2017). As explained in detail in Chapter 2, this has consequences for the surface energy balance where thin clouds could enhance the latent heat flux –thereby likely having a positive feedback on cloud development–, while thick clouds always initiate a negative feedback on cumulus growth (Fig. 1.1). In this thesis, this is called dynamic heterogeneity, which contrasts with static heterogeneity. In short, dynamic surface heterogeneity is local and short-lived caused by atmospheric driven perturbations, while static heterogeneity covers a spatially larger area and is controlled by the vegetation type and state. Since dynamic heterogeneity, other than static heterogeneity, is spatially smaller than the large-scale model resolution, it has not been taken into account in the current numerical weather prediction and climate models.

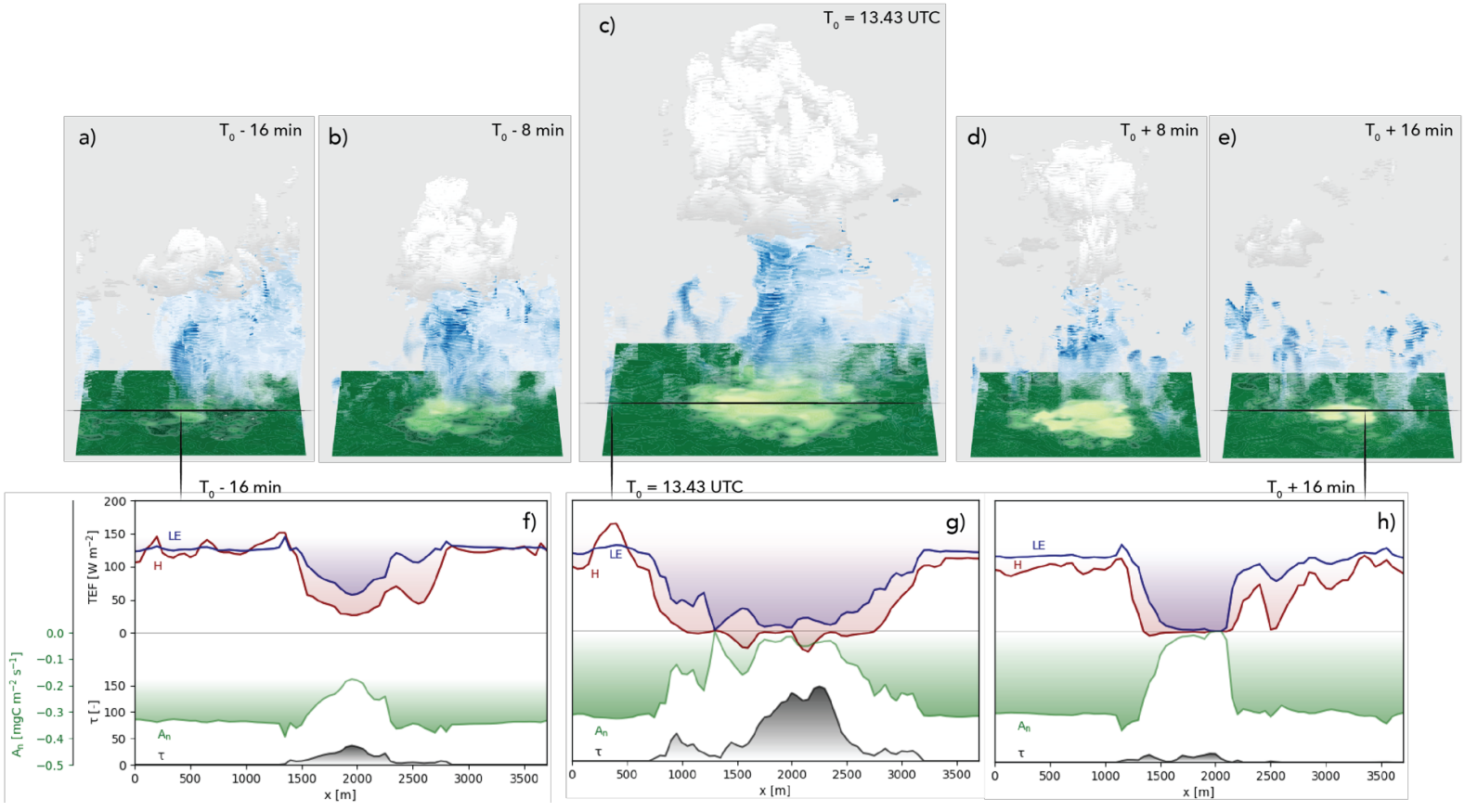

Figure 1.1 Life cycle of a cumulus cloud developing over a vegetated surface (a-e). The middle panel c) shows a mature cumulus cloud with its moisture updraft rooted into the vegetation (blue). The green surface shading denotes photosynthesis levels, with green maximum levels and yellow a strongly reduced CO_2 uptake. The bottom subplots f-h) denote slices through the middle of the cloud, as shown with the black stripes, for T_0 and 16 minutes prior and after T_0. The axis for subplots f-h) is similar and shown in f). Blue and red colors denote latent (LE) and sensible (H) heat fluxes, respectively, while assimilation of CO_2 (A_n) and the cloud optical depth (τ) are shown in respectively green and black. The color gradient of subplots f-h) is for visualization only.

1.4 Anthropogenic forcing on the diurnal land-atmosphere feedbacks: towards a bottom up approach

The human induced exponential increase in atmospheric CO_2 concentration ($[CO_2]$) has strong consequences for the land-atmosphere interactions, as the elevation in $[CO_2]$ acts as an additional forcing (Ciais et al., 2013). The increased amount of CO_2 molecules affects the atmospheric radiation profile in multiple ways, while it also influences the plant physiological state and subsequent feedback to the atmosphere. Focusing at the leaf level, the elevation in atmospheric $[CO_2]$ increases the difference in partial pressure between the plant intercellular and atmospheric levels. Resulting from this, the plant stomatal aperture narrows causing leaf temperatures to rise due to reduced transpirational cooling. This has direct consequences on the surface energy fluxes, as sensible heat fluxes increase at the costs of the latent heat fluxes. Consequently, ABL feedbacks are altered that have a profound impact on the hydrological cycle and radiation balance at the daily scales (Vilà-Guerau de Arellano et al., 2012).

These interactions do not behave similarly over the globe, as was found during a Free-Air CO_2 Enrichment (FACE) experiment. In a FACE experiment, CO_2 is fumigated over a crop or canopy and the response of this canopy to elevated $[CO_2]$ is monitored (e.g., Nakamura et al., 2012). Data from this experiment is shown in Figure 1.2. Here, the turbulent energy fluxes over an irrigated rice paddy are shown. A clear distinction in the latent heat fluxes is visible between clear and cloudy skies, though minimal effects

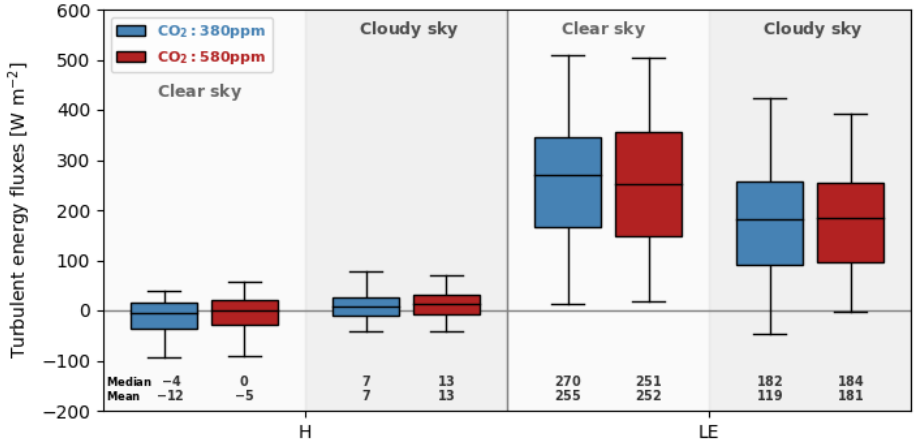

Figure 1.2 Aggregated observations of the sensible (H) and latent heat (LE) turbulent energy fluxes over an irrigated rice paddy are shown for clear and cloudy skies in ambient and elevated CO_2 situations during daylight conditions (i.e., ~6 am till ~6 pm local time). The data is taken from a Free-Air CO_2 Enrichment (FACE) campaign during the Japanese summer of 2015. The campaign, measurement specifics and methodology are described in Chapter 4. In blue, natural CO_2 conditions are shown, while red visualizes an elevated CO_2 environment. At the bottom, both median and mean values are presented.

are found in the case of enriched CO_2 conditions. The reason was an enhanced evaporative flux of surface water from the flooded rice paddies, which compensated for the decrease in plant transpiration. Furthermore, the direction (amplitude) in sensible heat fluxes becomes negative (small) due to a sea-breeze initiated warm air advection. Although the rice plants responded as expected as regards to stomatal closing and increased canopy temperatures, the response in surface fluxes was distinct. This shows the importance of a fundamental understanding of the non-linear vegetation-atmosphere interactions, in order to be able to extrapolate these mechanisms to future land-atmospheres interactions. For further details, the reader is referred to Chapter 4.

The uncertainty related to future feedback mechanisms is an additional cause of inter-model spread. Our current knowledge and understanding of current feedbacks is insufficient to be used to extrapolate for future scenarios. The main issue is the upscaling of results as well as the non-linearity of processes, which causes small errors to grow rapidly when extrapolated due to the chaotic behavior of the atmosphere. However, these extrapolated results, or climate projections, provides the benchmark with which climate scenarios are developed. This approach is questionable, since these scenarios only include the currently known feedback mechanisms, and do not capture the change in non-linear interactions that control these feedbacks. For example, using this benchmark to predict future crop yields will cause misrepresentations, or large uncertainties, and results have to be adjusted regularly when knowledge advances (see e.g., Wang et al., 2017). This top-down approach, with which future expectations are determined by focusing on the atmospheric forcings, yields large-uncertainties and does not provide the full spectrum of possibilities. In this thesis, a bottom-up approach is used, in which focus is laid on the small spatiotemporal scales that determine and control the strength of interactions that eventually affect larger-scale feedback mechanisms. Although this approach also entails uncertainties, it is more systematic and enhances our fundamental understanding more than a top-down approach would.

1.5 Brief overview of past research

1.5.1 Current understanding of cumulus development over vegetated surface

Although ideas on the influence of vegetation on cumulus development were already discussed in the early 20th century (Mon., 1907), it took until the mid-80's before it was observationally shown that cumulus development is related to processes occurring in the atmospheric boundary layer (ABL) (LeMone & Pennell, 1976). Shortly after, investigations were focusing on the role of static heterogeneity (i.e., spatially fixed heterogeneity) in vegetation type on triggering large-scale convective patterns related

to precipitation (Anthes, 1984; Garratt, 1992) and parameterizations were developed (Avissar & Pielke, 1989). In the early 90's, Avissar & Pielke (1991) linked plant stomatal processes to variations in sensible and latent heat fluxes and demonstrated that the incorporation of stomatal mechanisms –as well as sub-grid processes– are required to improve the simulated land-atmosphere interactions (Fig. 1.1). Utilizing satellite data, the strong interaction between vegetation cover and local cloud development became apparent in the years that followed (Rabin et al., 1990; Carleton et al., 1994). Following from their findings, progress was made on the modelling aspect, although focus on the larger scales was maintained (e.g., Chen & Avissar, 1994; Hong et al., 1995; Jacobs & de Bruin, 1997; Freedman et al., 2001).

Nearly one century later than the question raised by the anonymous writer (Mon., 1907), the computational power and scientific understanding allowed for three-dimensional studies on the vegetation-cloud interaction utilizing the large-eddy simulation (LES) technique. As the LES technique is based on first principles, more accurate simulations were possible that enhanced the understanding. The early LES investigations focused on the effects of surface boundary conditions, as for instance the leaf-area index (i.e., the amount of leaf area per unit soil area; e.g., Albertson et al., (2001)) or soil moisture content (e.g., Golaz et al., 2001). It was Schumann et al. (2002) who first simulated the effects of local cumulus cloud shading on the surface, with subsequent effects on the latent and sensible heat fluxes. However, their focus was only on the radiative aspect of cumulus shading, while the vegetative aspects were not taken into account. As a next step, Jiang & Feingold (2006) coupled the LES to an interactive land-surface submodel (LSM) and found that changes in cloud optical properties caused spatial effects on the surface energy fluxes. It was only recently that the computational capabilities allow for dynamic simulations between interactive vegetation and cumulus cloud development. Nearly simultaneously, both Lohou & Patton (2014) and Vilà-Guerau de Arellano et al. (2014) shared their findings on the effects of local cumulus shading on an interactive surface that caused subsequent local effects on the ABL, which hampered cumulus development. With the addition of instantaneous stomatal mechanistic responses (see Jacobs & de Bruin, 1997), Vilà-Guerau de Arellano et al. (2014) opened the path to investigate vegetation behavior and the occurrence of dynamic surface heterogeneity in the energy fluxes that were found to have an effect on cumulus behavior.

To deepen our understanding on the processes occurring in the layer between the surface and cumulus, Horn et al. (2015) investigated the length scales related to updrafts and cumulus population. With these advancements on quantifying the plant-cumulus interaction as well as increased computational capabilities, more complex radiative aspects were investigated. More specifically, the effects of solar zenith angles

on the onset of secondary circulations (spatial scale ~10 kilometers; Gronemeier et al., 2017), the role of three-dimensional radiative transfer on the organization of cumulus convection and cloud street formation (Jakub & Mayer, 2017), as well as in-cloud radiative scattering effects on the partitioning in direct and diffuse radiation (Pedruzo-Bagazgoitia et al., 2017). The latest publication to date regarding land-cloud interactions over realistic land surfaces showed that cloud shading-induced dynamic surface heterogeneities can have a larger impact on cumulus development than static heterogeneity (Xiao et al., 2018).

In this thesis, we extend on the research by investigating detailed plant-atmosphere-cloud responses for a wide range of wind conditions (i.e. cloud population clustering), as well as the influence of increased carbon dioxide (CO_2) levels and air temperatures, on the plant-atmosphere-cloud interaction. By doing so, this thesis adds to the fundamental understanding of vegetation-atmosphere-cloud interactions at the sub-kilometer and sub-daily scales and contributes to the fundamental knowledge needed to increase model accuracy and reduce the inter-model spread.

1.5.2 Anthropogenic effects on land-atmosphere interactions

The rising levels in carbon dioxide (CO_2) profoundly impact the land-atmosphere interactions. As a primary atmospheric greenhouse gas, it affects the radiative forcing and subsequently the Earth's temperature (Ciais et al., 2013). In the 2000 years prior to the industrial revolution, the concentrations of greenhouse gases were relatively stable and mainly controlled by natural processes. Since the 18th century, this balance has been drastically affected by human activity, such as fossil fuel emissions, land-use change and consumption (e.g., Le Quéré et al., 2009; Pielke et al., 2016). As a consequence, an exponential increase in [CO_2] is observed (Ciais et al., 2013), which is likely to be maintained in the coming years. As it is unequivocal that human behavior strongly affects the increase in atmospheric CO_2, scientists try to understand and predict the consequences and impact of future CO_2 concentrations on our environment.

The first investigation of elevated CO_2 levels on plant growth was performed by de Saussure (1804). In the two centuries that followed, much research has focused on the physiological effects of increasing levels of CO_2 for numerous species using controlled environments (i.e. greenhouses and climate chambers), which are summarized by Kimball (1983). With the establishment of the Intergovernmental Panel on Climate Change (IPCC) in 1988, awareness was raised on the global effects of increased levels of CO_2 on the surface and radiative forcing. During the same period, FACE facilities were developed to assess the effects of increased [CO_2] on plant communities (Nagy et al., 1994), which technique had the advantage that plants could grow in natural (i.e.,

outside) conditions. A few years later, a modelling study of de Bruin & Jacobs (1993) showed the effects of CO_2 enrichment on regional evapotranspiration. They recommended to accurately model land-atmosphere feedbacks in order to properly capture their forcing on the climate, although simulation experiments from Field et al. (1995) showed small effects globally. In the years that followed till the time of writing, articles published as regards to climate change research in relation to the surface energy balance increased tenfold.

Since the start of this century, science has advanced considerably as did the increased focus on land-atmosphere research. With the increasing global temperatures and extreme weather events (e.g., Seneviratne et al., 2010), focus on extreme heat waves in relation to land-atmosphere couplings has increased (Fischer et al., 2007; Miralles et al., 2014; Seneviratne et al., 2006). However, until this date, only one study focused on the effects of elevated CO_2 in relation to boundary layer cloud development (Vilà-Guerau de Arellano et al., 2012). In this thesis, we extend on current research by means of combining results from detailed microclimate measurements in elevated CO_2 environments with atmospheric high-resolution modelling, which allows us to fundamentally understand how the plant-atmosphere-cloud interaction might be affected in a changing climate.

1.6 Aims and content

In this thesis, detailed micro-climate and boundary-layer observations are combined with high-resolution land-atmosphere simulations. With the current technical incapability to measure the whole spectrum of interactions related to the plant-atmosphere-cloud system, we make use of the Large-Eddy Simulation (LES) technique to predict the impact of vegetation-atmosphere interactions on regional scales. Our Dutch Atmospheric LES model, which in this thesis has been initialized with observations from Western Europe, gives us a unique tool to systematically study the interactions and feedbacks occurring between the vegetated surface and the atmospheric boundary layer. By utilizing results from a FACE experiment, we took our analysis one step further and investigated a virtual future (year 2050) atmosphere in order to understand the non-linearities in the plant-atmosphere-cloud system.

To fundamentally understand the non-linear responses and interactions occurring over a wide range in spatiotemporal scales and to be able to perform a bottom-up approach, rather than a top-down approach, widely-used plant-atmosphere models, as for instance Soil-Vegetation-Atmosphere Transfer (SVAT) models, do not provide sufficient detail and resolution needed for the objectives of this thesis. The LES technique has the advantage to explicitly represent atmospheric dynamics and land-atmosphere interactions in three dimensions at very high resolution over time (Fig. 1.1).

By doing so, it is possible to perform sensitivity analysis on **plant responses and determine their influence on the atmosphere and subsequent cloud development**, which is our **first objective** and presented in Chapter 2. Furthermore, by analyzing cumulus development in different wind regimes, we were able to investigate the strength of the plant-atmosphere-cloud coupling and determine their significance by means of plant-cloud coupling. Results of this study are presented from a plant perspective in Chapter 2 and from a cloud perspective in Chapter 3. In Chapter 2, we identified streak-wise patterns in the (initially homogeneous) vegetated surface that caused dynamic and regional heterogeneity, thereby influencing the cloud distribution. Our work in Chapter 3 brought attention to two short-lived (15-30 minutes) plant-cloud coupling regimes, which were related to the distribution in cloud population (e.g. cloud streets). This showed that plant responses caused spatial dynamic surface heterogeneities in the energy fluxes that couple with the atmospheric flow and subsequent development of cumulus clouds. As a result, the moisture transport from the ABL to mid-troposphere was strongly affected, which yields an important message to the global modelling community on the need to treat the vegetation-atmosphere in a coupled way.

The **second objective** of this thesis is **to understand how the plant-atmosphere-cloud coupling is affected by increasing concentrations of CO_2 and temperature**. This objective is aimed to get insight in future albedo and radiative effects that cause the wide inter-model spread. Before simulating future climates, we first quantified the effect of increasing CO_2 concentrations on the plant-atmosphere response, using the FACE facilities. In the FACE setup, two distinct rice varieties were grown that strongly differed in physiology as well as architecture, and found that strong effects on the plant-atmosphere interaction occurred caused by plant architecture. Furthermore, the effect of plant responses to atmospheric perturbations is investigated as well, with special focus on intermittent radiative conditions caused by perturbations from cumulus clouds. This work is presented in Chapter 4. With the findings from Chapters 2-4, we simulated future atmospheres by designing numerical experiments that integrate our previous findings in Chapter 5. Here, we investigated how feedback mechanisms might be altered in the year 2050, and what consequences this might have for the plant-atmosphere-cloud interactions with subsequent consequences on the Earth's radiation balance.

Chapter 6 summarizes our main conclusions and puts our findings in perspective in a general discussion. It gives as well an outline on the implications of this thesis for future research on the topic and ends with an outlook for future research.

2

Interactions between vegetation, atmospheric turbulence and clouds under a wide range of background wind conditions

The effects of plant responses to Cumulus (Cu) cloud shading are studied from free convective to shear-driven boundary-layer conditions. By using a Large-Eddy Simulation (LES) coupled to a plant physiology embedded land-surface submodel, we study the vegetation-cloud feedbacks for a wide range (44) of atmospheric and plant stomatal conditions. The stomatal relaxation time is prescribed as an instantaneous, symmetrical (10, 15 and 20 minutes) and asymmetrical (5 min closing, 10 min opening) response, and the background wind ranges from 0 to 20 m s^{-1}. We show that in free convective, non-shading (i.e., transparent) cloud conditions the near-surface updraft region is marked by an enhanced CO_2 assimilation rate (An; 7%) and increased latent (LE; 9%) and sensible heat (H; 19%) fluxes. When we introduce Cu shading, we find an enhancement in plant transpiration and CO_2 assimilation rates under optically thin clouds due to an increase in diffuse radiation. However, these effects vanish when a background wind is present and the Cu are advected. Optically thick clouds reduce the assimilation rate and surface fluxes under all simulated wind conditions.

With increasing background wind, the shaded surface area is enlarged due to Cu tilting. The consequent decrease in surface fluxes by a reduction in incoming radiation, is partly offset due to an enhancement in the surface exchange and turbulent mixing as a result of stronger wind speeds. Different and non-linear processes control the H and LE response to

This chapter has been published as Sikma et al. (2017) in Agricultural and Forest Meteorology

shading. H is mainly radiation driven, whereas plant responses dampen the shading effects on LE. As a result, the regional averaged (48 km x 48 km) reduction in H and LE are found to be 18% and 5%, respectively, compared to non-shading cloud conditions. Surprisingly, a nearly uniform regional net radiation reduction of 11% is found, with only a deviation between all 35 Cu shading cases of 0.5% (i.e. 1.2 W m^{-2}) at the moment of maximum cloud cover. By comparing four representative simulations that are equal in net available energy, but differ in interactive and prescribed surface energy fluxes, we find a relative reduction in cloud cover between 5-10% during the maximum cloud cover period when the dynamic surface heterogeneity is neglected. We conclude that the local and spatial surface heterogeneity influences Cu development, while the Cu-vegetation coupling becomes progressively weaker with increasing stomatal relaxation time and background wind.

2.1 Introduction

As long as more than a century ago, an anonymous writer raised a question in the literature regarding whether the vegetation could influence cloud development, and consequently the occurrence of rainfall (Mon., 1907). While the answer provided to that question is debatable, our understanding on the vegetation-cloud interaction is still very limited. During the 90s, progress was made on a more profound understanding of the interactive vegetation-cloud system using large scale observations (Carleton et al. 1994) and modeling (Chen and Avissar 1994; Hong et al., 1995; Wetzel et al., 1996). In those studies, the land surface was prescribed, thereby not permitting interactive surface responses to atmospheric perturbations. To understand the effect of smaller-scale processes, Montieth et al. (1995) suggested linking plant stomatal responses to a clear sky convective boundary layer (CBL) development, and vice versa. However, he concluded that *"a combined complex plant and atmosphere model would be an unmanageable monster from which useful output would be extremely hard to obtain"*, which illustrates our current limited understanding of the vegetation-cloud system.

Advances in computational power and improved understanding of fundamental modelling concepts (e.g. sub-grid representation) gave rise to systematic studies on forcings in the vegetation-cloud system, although no interactive approach was yet feasible. Investigators utilized the Large-Eddy Simulation (LES) technique to study interactions between vegetation and turbulent transport by varying the leaf-area index (e.g., Albertson et al., 2001), the sensitivity of Cumulus (Cu) development to soil moisture content (e.g., Golaz et al., 2001), or the effect of a local decrease in surface fluxes due to Cu shading on the CBL structure (Schumann et al., 2002). In the latter study, they focused on an initially homogeneous surface and modelled the surface effects to local shading as instantaneous. For hovering Cu, they found that the convective turbulent motions were significantly influenced when Cu shading was taken into account, while the solar inclination angle had no significant effects on atmospheric

structure. A subsequent step, was to couple an LES to an interactive land-surface submodel (LSM) and investigate the influence of aerosol properties on Cu clouds (Jiang and Feingold 2006). They showed that the LSM responded to changes in cloud optical properties and spatially affected the surface energy balance (SEB), leading to a reduction in the strength of convection, cloud fraction and depth. In 2014, both Lohou & Patton (2014) and Vilà-Guerau de Arellano et al. (2014) published their findings of localized Cu shading on an interactive vegetated surface and found large effects on cloud and surface properties. More specifically, Lohou & Patton (2014) showed that Cu shading leads to a non-linear SEB response, enhancing the evaporative fraction (EF) by 2-3%, with the reduction in shaded areas having a greater effect on the sensible heat flux (H; 7-15%), and less on the latent heat flux (LE; 5%). While the surface response was immediate in the case of Lohou & Patton (2014) and earlier studies, Vilà-Guerau de Arellano et al. (2014) introduced a symmetrical plant stomatal relaxation time (of ~15 minutes), based on observations from Vico et al. (2011). In their free convection case (i.e., no background wind), they showed that Cu are significantly affected by vegetation. Cu shading induced both spatial and temporal heterogeneity in the SEB, which affected the cloud liquid water path. Furthermore, they concluded that the plant response has consequences for local turbulence, and thus could affect cloud properties on short time-scales. To further quantify these results, Horn et al. (2015) investigated the effects of spatial variability in surface fluxes due to Cu shading on characteristic boundary-layer length scales for a tropical free-convection case (Ouwersloot et al., 2013). They reported that cloud shading reduces turbulent kinetic energy (TKE) production in the subcloud layer, resulting in a decrease in thermal lifetime and inter-thermal distance. They also concluded from their LES experiments that the cloud population was affected by Cu shading, which produced smaller and more clouds, while the cloud cover remained similar compared to radiatively transparent clouds.

In order to investigate the effects of cloud shading location on secondary circulations, Gronemeier et al. (2017) modelled in a free convective situation four solar inclination angles, which affected their prescribed sensible heat flux. They show that a small solar angle negatively influences Cu development, while a larger angle increases the occurrence and depth of Cu, which suggests a decoupling between the vegetation and clouds. However, no adaptations of plant response or distinctions between direct or diffuse radiation were taken into account, which makes it difficult to extrapolate their results for an interactive vegetated surface. Related to this, observations by Freedman et al. (2001) and Min (2005) showed that the partitioning into diffuse and direct radiation by Cu is essential to capture vegetation responses to Cu shading, which enhances both the light-use and water-use efficiency (WUE) of the vegetation (Freedman et al. 2001).

Near-surface environmental conditions are essential in the vegetation-Cu system, as local fluctuations in the atmospheric state (e.g., temperature, moisture, wind) introduce spatial and temporal heterogeneity in the vegetation state (e.g., see Fig. 1 in Betts et al. (1996)). As a result, vegetation patterns interact with atmospheric structures, and vice versa (e.g., visible in Fig. 1b-d in Vilà-Guerau de Arellano et al. (2014)). Focusing on the near-surface horizontal wind speed (U), which plays a major role in vegetation-atmosphere exchange, Moeng & Sullivan (1994) found streaky patterns in U that suggest line-wise patterns in the state of the vegetation (e.g., enhanced transpiration rates) as well. As these atmospheric structures can range from cellular convection under free convective conditions to roll vortices in wind-shear conditions, it is to be expected that U affects the vegetation-Cu interaction in several ways. Since the atmospheric structure not only affects the vegetation, but also Cu development and tilting, it affects the partitioning between direct and diffuse radiation reaching the surface, thereby complicating the interactions even further.

In order to understand the relationships between horizontal wind perturbations, plant adaptation time, atmospheric structure and Cu shading and development, we designed numerical experiments to systematically break down the complexity of the interactive vegetation-Cu system by performing a sensitivity analysis for five plant stomatal response times in combination with seven wind-speed cases, ranging from cellular to roll-vortex convection. To better understand the effects of Cu shading, we also included a radiatively transparent Cu case. To the best of our knowledge, no research on the combination of plant relaxation time, cloud shading and wind conditions has been carried out on this detail. We therefore systematically increased the complexity throughout the paper. After describing the numerical modelling and cases, which are introduced in section 2.2, we started by investigating the effects of horizontal wind perturbations on the vegetation (section 2.3). Next, we added the presence of Cu shading in section 2.4 and explored the effect of cloud movement on the vegetation. In section 2.5, we combined the knowledge gained thereby explaining the effects of Cu shading on the vegetation, and its feedback to Cu development for all wind and plant adaptation cases. Finally, our results are put into perspective in a discussion (Section 2.6), which is followed by the conclusions in Section 2.7.

2.2 Numerical simulations

The numerical experiments describe a typical early autumn day in the Netherlands and are validated against a complete set of observations (Vilà-Guerau de Arellano et al., 2012), where dynamically forced Cu arise over an interactive grassland (Casso-Torralba et al., 2008). To represent the formation of roll vortices properly, the simulated area covers 48 x 48 km and is for 90% covered by C3 grass. The three-dimensional atmospheric fields were solved up to a height of 5.5 km, with horizontal and vertical resolutions of 50 m and 12 m, respectively. Time integration was performed by a third-order Runge-Kutta scheme. An adaptive time-step approach was taken, limited to a maximum of 20 s, after which a 1-minute average was calculated. To numerically integrate the flow equations, we utilized the Dutch Atmospheric Large-Eddy Simulation (DALES; version 4.1) the core details of which are described in Heus et al. (2010) and recent extensions in Ouwersloot et al. (2017). At the top one-third of the domain, a sponge layer is applied that prevents the reflection of gravity waves (Heus et al., 2010). Surface characteristics were calculated by an interactive plant physiological sub-model, A-gs (Jacobs & de Bruin, 1997; Ronda et al., 2001), which enabled us to investigate localized cloud-shading effects on surface characteristics. The coupling of the surface boundary to the atmosphere is performed by applying the transfer laws of Louis (1979). For details, see Heus et al. (2010). All the experiments considered a situation in which the sun is directly above the cloud, although the amount of radiation depends on the solar angle (Pedruzo-Bagazgoitia et al., 2017). This idealizes the interactions, as the maximum decrease in radiation occurs directly below the cloud, thereby reducing the turbulent intensity in its updraft (Gronemeier et al., 2017; Schumann et al., 2002). Using the Delta-Eddington approach (Joseph et al., 1976), the time dependent incoming shortwave radiation is partitioned into a diffuse and a direct component depending on the cloud's optical depth, as described in Barbaro (2015). To distinguish between direct and diffuse radiation, Pedruzo-Bagazgoitia et al. (2017) introduced a two big-leaf approach in the A-gs submodel that takes different extinction coefficients for direct and diffuse radiation into account, as well as in-canopy light scattering by the soil, sunlit and shaded leaves (Jacobs and de Bruin, 1997). For a detailed explanation of the two big-leaf approach and implementation, see Pedruzo-Bagazgoitia et al. (2017). The simulations start at 7 UTC (9 LT) and simulate 11.5 hours of daylight.

The 7 numerical base experiments differ in stomatal response (interactive versus homogenized) and cloud transparency (transparent versus shading), and are summarized in Table 2.1. The stomatal response experiments are repeated for 7 geostrophic wind speeds, ranging from 0 till 20 m s^{-1} (Table 2.2). In total, 44 situations were simulated. Except for the aforementioned differences, these were identical in

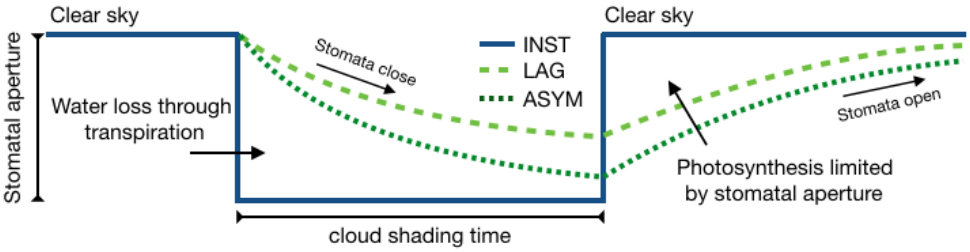

Figure 2.1 Conceptual representation of the stomatal relaxation time for the INST, LAG15 and ASYM case when perturbed by a Cu cloud at leaf scale.

initial atmospheric profiles and soil and plant characteristics, and are based on the LES case described in Vilà-Guerau de Arellano et al. (2014). Note that the FIX case was only evaluated for the 0 and 10 m s^{-1} wind situations, while the other cases cover the full range (0-20 m s^{-1}) of wind conditions.

In our first base experiment (TRA), we disabled cloud shading by making the clouds radiatively transparent. This experiment was set as the control case to determine the effects of cloud shading on the surface and its influence on the atmospheric structure. Note that the dynamic characteristics of cloudy boundary layers such as cloud venting between the sub-cloud and cloud layer (van Stratum et al., 2014) are maintained. To explore the maximum impact of atmospheric circulations on the surface, the plants' stomata adapt instantaneously to atmospheric perturbations.

In the second base experiment (INST), cloud shading, which depends on the cloud optical depth (τ; Stephens, 1978), was enabled similar to Horn et al. (2015), where τ is a function of the liquid water path. By enabling cloud shading, we can determine the interactions between the plants and Cu through atmospheric turbulence, as shading decreases the total amount of radiation reaching the surface and affects its partitioning into direct and diffuse radiation, thus locally affecting the SEB. In this second experiment, the stomatal response to Cu shading is set to instantaneous.

Base experiments LAG10, LAG15 and LAG20 differed in terms of the plants' stomatal relaxation time compared to experiment two. The relaxation time is applied following Sellers et al. (1996) as

$$\frac{\partial g_c}{\partial t} = -k_g \left(g_c - g_{c_{inf}} \right), \tag{2.1}$$

where k_g denotes the time-constant for the stomatal relaxation time (s^{-1}), g_c the actual canopy conductance (m s^{-1}) and $g_{c,inf}$ the g_c at t = ∞, which is illustrated conceptually in Figure 2.1. Note that g_c is the inverse of r_c. To encompass the most relevant stomatal response times observed in nature (Vico et al. 2011), the stomatal relaxation times are

set for experiments three to five as 10, 15 and 20 minutes e-folding, respectively. The range in relaxation time gives us an idea on the sensitivity of the stomatal response to atmospheric and cloud dynamics. In these experiments, the relaxation is set as a symmetrical function; the stomatal opening time thus equals the closing time.

Table 2.1 List of base experiments addressed to study the role of the stomatal response. The 6 stomatal response cases are repeated for the 7 wind conditions shown in Table 2.2. FIX is only repeated for the 0 and 10 m s^{-1} wind case.

Case	Stomatal response	Remarks
TRA	Instantaneous	Radiatively transparent clouds
INST	Instantaneous	Closing = opening (0 min)
LAG10	Symmetrical	Closing = opening (10 min)
LAG15	Symmetrical	Closing = opening (15 min)
LAG20	Symmetrical	Closing = opening (20 min)
ASYM	Asymmetrical	Closing = opening (5 vs 10 min)
FIX	None	Homogenized surface fluxes

Table 2.2 Range of wind speeds and non-dimensional indicators to determine the dominant atmospheric structure. Values are based on the ASYM case and averaged over 15 min (14–14.15 UTC). No significant differences in the non-dimensional indicators between the other stomatal relaxation cases were found. The classification (I–V) is based on Grossman (1982).

Initial U_g	$-z_i/L$	u_*/w_*	Cat.	Structure	Fig. 2
0.0 m s^{-1}	59.860	0.089	V	Cellular	a
2.5 m s^{-1}	322	0.122	V	Cellular	
5.0 m s^{-1}	69	0,190	V	Transition	b
7.5 m s^{-1}	27	0.255	IV	Transition	
10 m s^{-1}	14	0.317	III	Transition	c
15 m s^{-1}	6	0.425	II	Roll	
20 m s^{-1}	3	0.521	I	Roll	d

In the sixth base experiment (ASYM) the stomatal response is asymmetrical. In this case, the stomata close with an e-folding time of 5 minutes, but opening occurs at a slower rate of 10 minutes, following Eq. 2.1. It has been shown that an asymmetric response is closer to nature (e.g., McAusland et al., 2015; Ooba & Takahashi, 2003; Vico et al., 2011), as several factors (e.g. air temperature, ion (K^+) transport in the guard cells) affect the opening and closing speed differently.

In the final base experiment (FIX), we prescribed the surface fluxes according to the domain-averaged values of the INST case. At every time-step, the domain-averaged value was prescribed for all grid points in order to homogenize the surface and to neglect the effects of atmospheric perturbations and Cu shading. Note that this experiment was only evaluated for a 0 and 10 m s^{-1} wind.

As shown by Vilà-Guerau de Arellano et al. (2014), the vegetation-cloud system can be identified as a coupled interactive system, which continuously adapts to new atmospheric and vegetation conditions. On the basis of their research, we hypothesize that persistent structures arise due to atmospheric and vegetation forcings. For example in a roll-vortex situation (Table 2.2), cloud streets shade the vegetation in lines, thus influencing the SEB by lowering stomatal conductance. As a consequence of the cloud streets, clear streaks of sky appear, favoring photosynthesis and thus transpiration rates. As this spatial and dynamic heterogeneity is affected by the stomatal relaxation time and horizontal wind speed, we explored the sensitivity of stomatal responses (Table 2.1) to a wide range of wind conditions. We repeated the first six base simulations (Table 2.1) for seven wind speeds (Table 2.2), whose four selected situations are shown in Figure 2.2. In this figure, the up- and downdraft areas clearly show cell structures for low wind speeds (Fig. 2.2a) and roll vortices for high wind speeds (Fig. 2.2d). Figs. 2.2b-c show a transition from cellular-dominated convection towards roll vortex-dominated convection. Based on the classification scheme of Grossman (1982), the stability parameter $-z_i/L$ is used as a proxy to determine the dominant turbulent state of the atmosphere (e.g., cellular or roll vortices), where z_i denotes the CBL height and L the Obukhov length. The classification scheme is based on the BOMEX case (Holland and Rasmusson 1973). A classification of I corresponds to roll-vortex motions only, while V indicates only random cellular structures. The categories II-IV correspond to a gradual

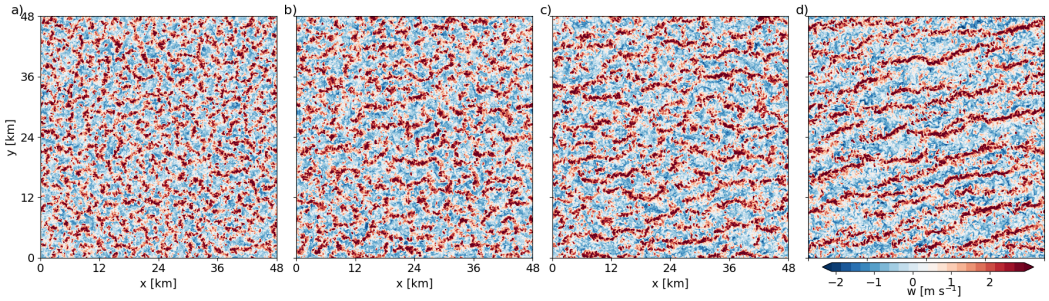

Figure 2.2 Instantaneous horizontal cross-sections of the vertical wind-speed of LAG15 at 900 m showing a transition from (a) dominant cell structure (0 m s^{-1}) to (d) dominant roll-vortex situation (20 m s^{-1}) at 14 UTC. (b) and (c) show the transition cases of 5 and 10 m s^{-1}, respectively (Table 2.2). Red color denotes updrafts, while blue indicates downdrafts. The wind direction is from left to right.

increase from a dominant shear (i.e., roll vortex) to buoyancy-driven (i.e., cell) boundary layer. Based on the value of $-z_i/L$, we categorize the 5 to 10 m s^{-1} as transition cases, where neither cellular nor roll vortices are dominant. However, note that contradictory results have been reported that describe a CBL dominated by roll vortices under very unstable conditions ($-z_i$ /L of 250 & 136 in Ferrare et al., 1991; Kristovich, 1993, respectively).

For completeness, we also show the u_*/w_* as a proxy to determine the atmospheric structure (Table 2.2). Sykes & Henn (1989) reported that when this ratio between the surface friction velocity and the convective velocity scale is larger than 0.35–0.40, rolls dominate the turbulent flow, although Kristovich (1993) showed the dominance of roll vortices in a lower (0.13–0.15) u_*/w_* regime. It is still unclear why these differences in $-z_i$ /L and u_*/w_* are found between the observational studies. One reason could be the difficulty to measure the z_i, L, u_* and w_* correctly, while on the other hand external factors could influence roll formation (e.g., convection waves, for a review, see Young et al., 2002). In this study, we follow the classification scheme of Grossman (1982) to determine the dominant atmospheric structure, as shown in Table 2.2.

2.3 Impact of atmospheric turbulence on the surface

Before we start to investigate localized cloud shading effects on vegetation-atmosphere-cloud interactions, we need to understand how the vegetation responds to atmospheric fluctuations in e.g., radiation, temperature and water vapor deficit. Therefore, we focus in this section on a free convective non-shading clouds situation (i.e., no background wind; TRA case) where the canopy instantaneously responds to atmospheric perturbations. Note that this idealized setup with free convective conditions is characterized by a low surface exchange rate, which is strongly affected by small perturbations in the horizontal wind due to up- and downdrafts. As such, surface fluxes of heat, moisture and CO_2 are enhanced in the regions characterized by convergent motions. Furthermore, as no cloud shading is taken into account, the feedback between the Cu and the vegetation is absent. By doing so, we isolate the interactions in the LSM for a non-shading clouds situation, which is needed to understand the complexity and feedback mechanisms in the vegetation-Cu system due to Cu shading in the cloud shading cases later on.

Focusing on the LSM description (Jacobs and de Bruin, 1997; Ronda et al., 2001), three (indirectly) interrelated equations play key roles in the vegetation-atmosphere exchange. Note that this description is widely used in atmospheric models (e.g., ECMWF; Boussetta et al., 2013). The surface net radiation is partitioned into three surface fluxes: the sensible heat (H), latent heat (LE) and ground (G) flux. As the G flux is found to be ~9% of the net radiation (Q_{net}) and fluctuations due to atmospheric

circulations are found to be negligible (more in Section 2.5), we will mainly focus on the H and LE fluxes. These compete for energy, and thus have a strong influence on each other. The sensible heat flux is regulated through

$$H = \frac{\rho c_p}{r_a}(\theta_c - \theta)\,, \tag{2.2}$$

Here, ρ denotes the surface air density, c_p the specific heat of air, θ_c the canopy temperature, θ the near-surface air temperature and r_a the aerodynamic resistance, which is the inverse of the surface drag coefficient (C) times the horizontal wind speed (U).

The LE flux is defined as

$$LE = \frac{\rho L_v}{r_a + r_{cH_2O}}(q_s(\theta_c) - q)\,, \tag{2.3}$$

where L_v denotes the heat of vaporization, r_{cH_2O} the canopy resistance regarding water vapor, T_c the canopy temperature and $q_s(T_c)$ and q the saturated specific moisture content and actual specific moisture content of air near the vegetation, respectively. Note that in general, r_c is larger than r_a, which is also the case in our experiments.

The interrelationships in the LE flux increase the complexity of the system, as they take into account the vegetation state and the vapor pressure deficit (*VPD*, defined as $q_s(T_c) - q$) on the canopy scale, which depends non-linearly on temperature. Note that the radiation effects are introduced indirectly through T_c, r_c and q, which result is similar to that found using the Penman-Monteith equation.

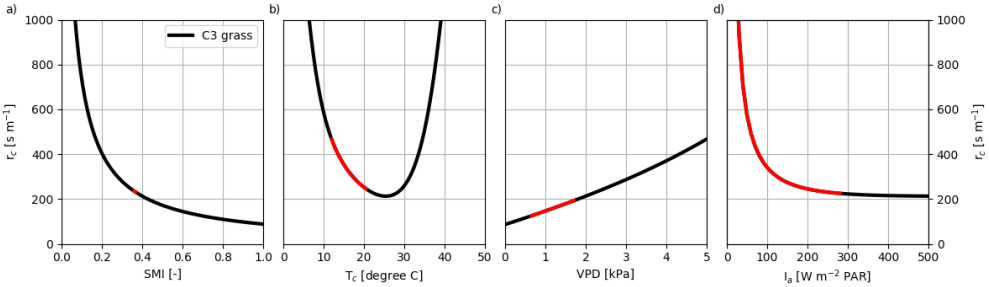

Figure 2.3 The relationship between canopy resistance (r_c) versus (a) soil moisture index (SMI), (b) canopy temperature (T_c), (c) vapor pressure deficit (VPD) and (d) absorbed photosynthetically active radiation (I_a) is shown. Unless specified, all relationships were calculated under constant conditions of Tc = 25 °C, I_a = 500 W m^{-2} PAR, VPD = 2 kPa and current CO2 conditions of 350 ppm. The red areas denote the spatial surface variability due to Cu shading for the INST free convective case at 14 UTC.

The vegetation reacts to the partitioning between direct and diffuse radiation, thereby affecting photosynthesis and transpiration rates. Since both transpiration and CO_2 uptake are regulated by the stomatal aperture, which is modelled as its resistance (r_c), plants continuously modulate their stomata to optimize their CO_2 uptake, while preventing additional water loss. In Fig. 2.3, we show the relationships of r_c to soil (Fig. 2.3a), atmospheric (Fig. 2.3b, c) and radiation conditions (Fig. 2.3d). It is clear that all relationships are non-linear, illustrating the interrelations involved. In red, the spatial surface variability is shown for a Cu shading case (INST). As expected, the spatial spread in the soil moisture index (SMI), which is defined as the relative saturation between wilting point and field capacity, is small. This indicates that no significant spatial soil moisture heterogeneity is present that spatially influences plant transpiration rates at sub-daily scales. The variability in atmospheric and radiation conditions due to Cu shading is found to be larger, which will be discussed in detail in section 2.4. The stomatal aperture can be seen as the gateway of the net flow of carbon dioxide into the interior of the plant. This indicates that r_c is influencing the assimilation of CO_2, which is described as:

$$A_n = \frac{\mathrm{c}_a - \mathrm{c}_i}{r_a + r_{cCO_2}}, \tag{2.4}$$

where c_a and c_i denote the atmospheric and internal CO_2 concentration, respectively. Note the difference in canopy resistance due to a difference in molecular diffusion between water vapor and CO_2, $\left(r_{cH_2O}\right)/\left(r_{cCO_2}\right)$= 1.6. Hereafter, we refer to r_{cH_2O} as r_c.

It is to be expected that atmospheric perturbations will have a direct impact on the LSM when the stomatal response is instantaneous. To understand the chain of processes involved in this atmosphere-surface coupling, we focus on the key variables that affect the A_n, LE and H. In the upper panels of Figure 2.4, four surface horizontal instantaneous snapshots at 14 UTC are shown, while the lower panels visualize the relationships between the variables. In our free convective TRA case, it is shown that cellular structures (see Fig. 2.2a) affect the horizontal wind patterns (Fig. 2.4a). The dynamic heterogeneity in horizontal wind, resulting from cellular shaped up- and downdrafts, has direct effects on the surface exchange, as the rate of energy and water transfer increases with stronger winds. This relation is shown in Fig. 2.4e, where the aerodynamic resistance (r_a) decreases as horizontal wind speed increases (U). As a result of the advection of moist air towards the updraft, the vapor pressure deficit (VPD,

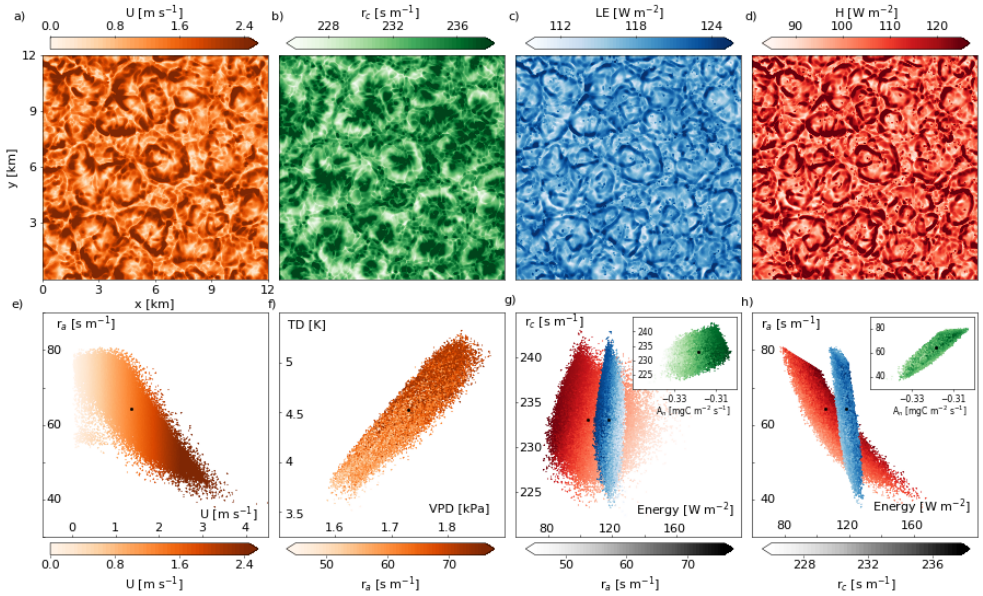

Figure 2.4 The upper panels show the zoomed (12 km x 12 km) instantaneous horizontal cross-sections at the surface for the TRA free convection case (i.e., no background wind) at 14 UTC. The upper panels show: (a) the horizontal wind speed (U), (b) canopy resistance (r_c), (c) latent heat flux (LE), (d) sensible heat flux (H). The lower panels show the relation between several variables with the color bar showing the relation of a specific variable within this relation. (e) shows the relation between the aerodynamic resistance (r_a) and U. In (f) the relation between temperature deficit (TD; $(\theta_c - \theta)$) and vapor pressure deficit (VPD; $q_s(\theta_c) - q$), with in color the relation of r_a. In (g), the relation between r_c and surface energy is shown. The inset shows the relation between r_c and CO_2 assimilation rate (A_n). While the color bar showing the gradient in r_a in grey, the colors show the relation of r_a for H (red), LE (blue) and A_n (green). In (h), the same data is shown as in (g), but now r_a is a function of energy (or A_n for the inset), with in colors the relation of r_c. The black dot in panels (e–h) represents the domain averaged value.

defined as $q_s(T_c) - q$) is reduced (Fig. 2.4f). This has direct effects on the stomatal aperture, which widens, thereby lowering the canopy resistance (Figs. 2.3c and 2.4b). Due to the increase in wind speed near updraft region and the combined effect of enhanced (5%) transpiration rates, the canopy temperature decreases (~2 K) thereby lowering the temperature deficit (*TD*, defined as $\theta_c - \theta$; Fig. 2.4f).

The wind induced spatial heterogeneity in the vegetative state is affecting the surface fluxes in a similar way. As Figs. 2.4c and d show, both H and LE are enhanced ~10 (~9%) and ~20 (~19%) W m^{-2} near updraft region, respectively. The A_n increases ~7% at the similar areas. In order to determine whether the plants' stomata or the efficiency in surface exchange (i.e. low r_a) drives the increase in surface fluxes and A_n, we show the relationship between r_a and r_c on the A_n, LE and H in Figs. 2.4g and h. Starting with 2.4g,

we find no strong relationship between r_c and the surface fluxes. However, the horizontal color gradient indicates that r_a is more dominant in driving the surface energy than r_c. Focusing on the inset, this relationship is less obvious in A_n, as the r_c has an effect as well. In a plant physiological perspective this is understandable, as the decrease in r_c limits CO_2 uptake, thereby decreasing A_n. Fig. 2.4h shows a clear relationship between r_a and both surface fluxes. This indicates that r_a rather than r_c dominates the surface-energy flux. However, a color gradient is still apparent, indicating an influence of r_c. Focusing on the inset, it is clear that r_a has a larger effect on the A_n than r_c. Note that, thanks to our plant physiology-based LSM, we capture the large heterogeneity in surface and plant processes that are mainly controlled in this case by atmospheric perturbations. Larger-scale models that only capture the average response lack the relevant vegetation-atmosphere interactions, as represented by the small black dot in the lower panels of Fig. 2.4.

These results show that CBL turbulence influences the surface responses by governing the exchange between the surface properties and the atmospheric layer nearby. This leads to an enhancement in surface fluxes at and near updraft regions. As a result, it amplifies the heating and moistening effects on the updrafts itself that enhances convergence at the surface, thereby increasing the horizontal wind perturbations generated by turbulence.

2.4 Impact of Cu shading on the surface: a 2-dimensional perspective

As reported by Vilà-Guerau de Arellano et al. (2014) and Horn et al. (2015), a local decrease in radiation by Cu shading has an immediate impact on the SEB and thus, on Cu development. However, it is still an open question whether this is mainly due to a local coupling between vegetation and clouds, or is driven by the regional averaged (i.e. domain averaged) change in surface properties due to the presence of clouds.

As our modeled area covers 48 km x 48 km, we refer from here on to domain scales as regional scales to make a clearer distinction between local (~500 m^2) and regional effects.

Before heading into the results, we start by introducing conceptually the main Cu shading effects in free convective and shear-driven boundary layers, as illustrated by Fig. 2.5. In a free convective situation (Fig. 2.5a), the Cu remain above their shadow. In this idealized situation, the Cu are so called 'rooted' into the vegetation (Vilà-Guerau de Arellano et al., 2014), as they have shown to respond to surface perturbations. The main processes are described as follows: the solar irradiance is, depending on cloud

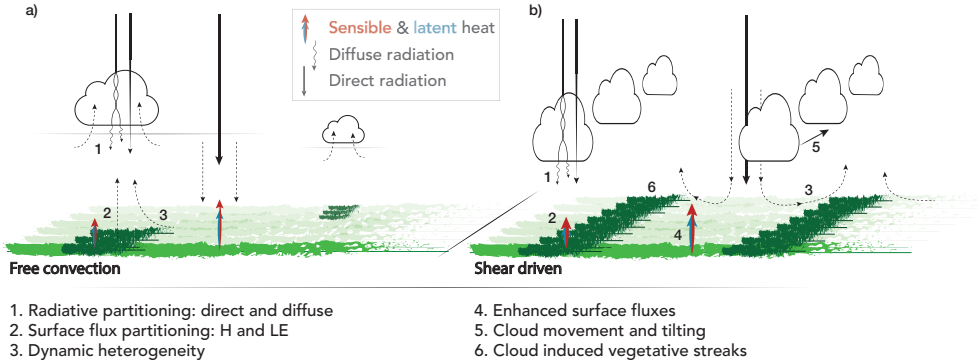

Figure 2.5 Illustrative representation of the Cu–vegetation interaction for a (a) free convective and (b) shear-driven boundary layer. The darker green areas indicate stomatal closure. The LES numerical experiments explore systematically the different Cu–vegetation interactions by increasing wind and varying stomatal relaxation time.

thickness, (1) partitioned into direct and diffuse radiation, thereby lowering the local net radiation at surface. This affects the (2) strength and partitioning of H and LE that negatively affect the updraft towards the cloud. As a result of this surface energy change, a (3) dynamic heterogeneity arises alongside the updraft core, affecting the surface exchange due to horizontal wind speed variations.

The shear-driven situation (Fig. 2.5b) is more complex as the interactions are not idealized and less profound. With increasing background wind, the surface exchange is increased as well. This leads to an (4) enhancement in surface fluxes compared to free convective conditions. This increase in energy level is compensated by an increase in Cu development, venting air from the CBL into the cloud layer. As a result, Cu grow taller. However, due to wind shear the Cu start to tilt, thereby lowering the net surface radiation less as would expected. Next to tilting, the (5) Cu move along the wind and form in streets due to the presence of roll vortices. Combining this latter with a plant stomatal relaxation time, causes the Cu surface effects to be lingered, thereby forming (6) streaks of lowered plant transpiration.

To explore the interrelated processes in the vegetation-cloud system, we first analyze a free convective situation (i.e., no background wind) to maintain the clouds directly above their shaded area (Fig. 2.5a). The plant stomatal response is prescribed as a 15 minutes symmetrical e-folding time (LAG15 case; upper panels of Fig. 2.6). Later in this section we focus on the effects of a 10 m s^{-1} initial background wind as well (lower panels of Fig. 2.6; Fig. 2.5b).

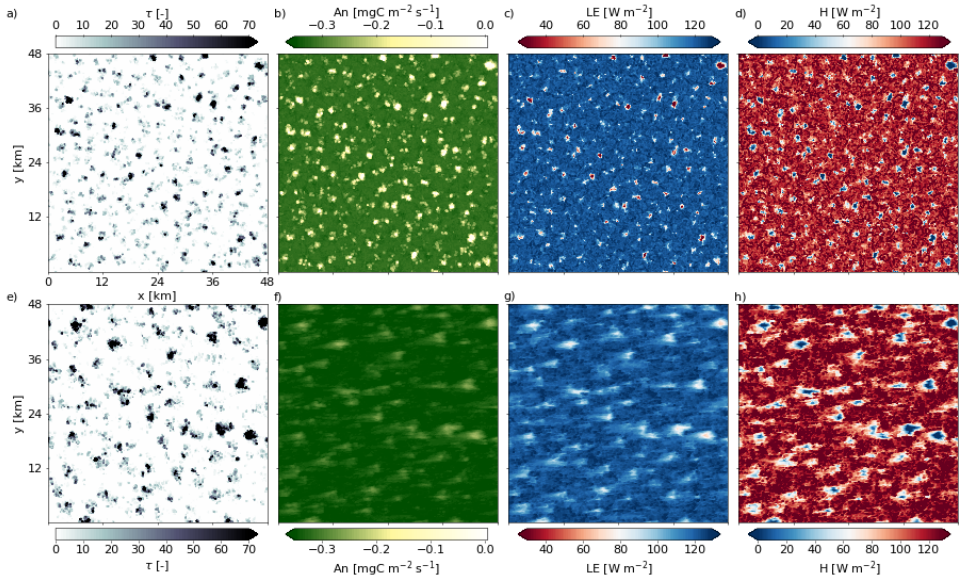

Figure 2.6 Instantaneous horizontal cross-sections at the surface for the LAG15 case at 14 UTC. The effect of the (a) cloud optical depth (τ) on the (b) assimilation of CO_2 (A_n), (c) latent heat flux (LE) and (d) sensible heat flux (H) is shown for a free convective situation (upper panels) and 10 m s^{-1} initial geostrophic wind (lower panels). Note that H and LE have inverse coloring. The wind direction is from left to right.

The free convection case is visualized in Figure 2.6a-d, where an instantaneous surface cross-section is shown for 14 UTC. At this time, the cloud cover (*N*), which is defined as the fraction of the domain where liquid water is present in the vertical air column, is maximum and stable (0.18 [-]; not shown). Furthermore, the wide range in cloud optical thicknesses (τ; ranging from 1 until 120) indicates that the clouds are actively growing (Fig. 2.6a). The impact of the presence of clouds is shown by the local decrease in CO_2 assimilation rate (max. 85%), similar to the LE (max. 81%) and H (max. 100%) fluxes. As also shown in Figs. 2.6c-d, the LE and H respond differently within the shaded areas. This is mainly due to the Clausius-Clapeyron relation that enters in $q_c(T_c)$ (i.e. LE) due to the decrease in T_c (Eqs. 2.2 & 2.3).

Focusing on the processes affecting LE and H, we identify several factors that play a role on this distinct Cu shading response. Regarding H, we describe the following steps:

1. Clouds directly reduce the net radiation (Q_{net}) at the surface, which in turn lowers canopy temperature (θ_c).
2. This locally reduces the buoyancy flux, increasing the relative importance of turbulent mixing by shear near the surface (i.e., through r_a).
3. Due to this local decrease in Q_{net}, perturbations of *U* become weaker as a result of

the reduction in local convection, thereby limiting energy exchange at the Cu shaded areas (i.e., increasing r_a).
4. Eventually, this diminishes H even further, thereby affecting the updraft.

Focusing on LE, the spatial variability is mainly affected through stomatal responses:

1. As a result of Cu shading, the canopy temperature (θ_c) falls, which decreases the VPD, thereby hampering the local LE flux near the updraft region (Eq. 2.3).
2. The plant relaxation time determines the delayed impact of canopy resistance on the LE flux. As a result, the local impact of a gradually adapting surface below a cloud will always be less compared to an instantaneous responding surface, which is reflected in the LE response (Fig. 2.6g).

It is interesting to note that Cu shading acts as a local negative feedback on the surface fluxes near the updraft region, compared to the local enhancement effects due to horizontal wind perturbations generated by turbulence, as described in section 2.3.

If sufficient background wind (U_g > 10 m s^{-1}) is introduced in the CBL, roll vortices form due to shear (Grossman 1982). Figure 2.6e-h illustrates the effects of 10 m s^{-1} background wind on the cloud optical depth, CO_2 assimilation rate and LE and H fluxes. Figure 2.6e suggests that clouds broaden when wind increases, thereby increasing the cloud cover (N = 0.22). As will be explained in detail in section 2.5, this result is mainly due to cloud tilting. As cloud tilting occurs in wind sheared areas, it enlarges the shaded area. However, due to their tilt the local cloud optical thickness decreases. As a consequence, the partitioning between direct and diffuse radiation changes, thereby affecting the surface fluxes.

Turning to Figure 2.6f, it is clear that horizontal wind increases the CO_2 exchange and photosynthetic rates through a reduction in aerodynamic resistance compared to free convective conditions (Eq. 2.4). Furthermore, due to the combination of cloud advection and delayed plant responses, the local effect on CO_2 assimilation is reduced (max. 33%) compared to free convective conditions. However, the affected area is increased due to the delay in plant recovery, thereby reducing the CO_2 uptake due to limitations in stomatal aperture (Fig. 2.1). This effect in plant recovery has comparable consequences for the LE flux (max. 41%; Fig. 2.6g), while different effects in H (max. reduction of 100%) are found that are comparable to free convective conditions. Regarding the effect on the canopy-atmosphere gradients expressed in equations 2.2 and 2.3, the decrease in θ_c also has a negative impact on transpiration rates through a decrease in VPD. However, since θ_c reacts fast to the incoming radiation, this effect is more localized. Moreover, stomatal closure tends to increase θ_c, as less transpirative

cooling occurs. In general, the impact of the local and lagged increase in canopy resistance due to Cu shading turns out to be dominant in controlling the reduction in LE when a relatively strong background wind is present. This is due to the significant decrease in r_a with increasing wind and the relative high absolute value of r_c (~230 s m^{-1}) compared to r_a (~40 s m^{-1}).

When we focused outside the shading-affected areas, we found that LE and H increase with rising background wind, which is explained through the reduction in aerodynamic resistance (from 90 to 30 s m^{-1} for a background wind of 0 to 20 m s^{-1}, respectively).

The H flux (Fig. 2.6h), however, has no direct consequences of the r_c increase by Cu shading and is mainly affected by the localized fall in surface temperature. In the sunlit areas, H is enhanced more strongly by a reduction in r_a compared to LE and free convective conditions.

To summarize the feedbacks described in this section (note that we will elaborate on this in the following section by combining all experiments):

1. Near-surface horizontal wind perturbations generated by turbulence enhance surface exchange, thus increasing H and LE near the updraft region.
2. This favors convection, which increases the likelihood of Cu occurring above the updrafts.
3. The development of Cu reduces the Q_{net} at the surface, which locally reduces canopy temperature as well as plant transpiration and assimilation rates.
4. These are much affected by Cu movement due to the background wind condition:
    a. In free convective situations, the lower H and LE for optically thick Cu negatively affect the updraft, which lowers near-surface turbulence and hampers Cu development.
    b. Under situations characterized by a background wind, LE is less affected than free convective conditions, due to the plant relaxation time combined with Cu movement. Furthermore, the Cu tilt enlarges the shaded area, thereby affecting the partitioning of radiation reaching the surface.

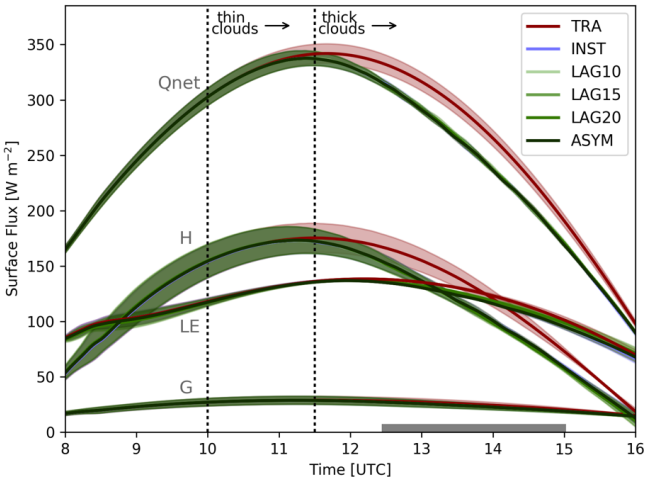

Figure 2.7 Temporal evolution of the domain- and wind-experiment (Table 2.2) averaged surface fluxes are shown per base case (Table 2.1). The thick line represents the mean of the wind experiments, while the spread denotes the standard deviation. At 10 UTC, optically thin clouds arise, while optically thick clouds are present from 11.5 UTC onwards. The grey bar denotes the maximum cloud cover period. Note that only 2 colors are visible, which is due to all the base experiments exhibiting the same dependencies with the exception of TRA.

2.5 The Cu-vegetation interaction in shear and buoyantly driven boundary layers

Moving on in complexity, we analyze the combined effects of the horizontal wind in relation to the delay in plant responses, by discussing all (44) experiments. First, we analyze the regional averaged SEB, following up with the effects of the atmosphere and vegetation on Cu.

2.5.1 Regional SEB: effects of wind and plant response

To determine the effects of local cloud shading on the regional SEB, the SEB components are spatially averaged over time. Combining all wind-speed (Table 2.2) and base (Table 2.1) experiments enables us to understand the general effects of the stomatal relaxation responses to cloud shading. The regional SEB components and corresponding standard deviations between the averaged wind cases are presented in Fig. 2.7. Here, the main feature is the spread in the SEB components, which is mainly due to near-surface horizontal wind effects (i.e., r_a). Note that only 2 colors are visible, which is due to all base experiments exhibiting the same dependencies, with the exception of TRA.

In Fig. 2.7, the time at which optically thin and thick clouds arise is indicated; the quantification is based on the partitioning between direct and diffuse radiation. As shown by Pedruzo-Bagazgoitia et al. (2017) (Fig. 1 therein), direct radiation decreases rapidly towards zero as cloud optical depth (τ) increases below 10 τ. In turn, the diffuse radiation increases. When $\tau > 10$, the diffuse radiation also falls slowly towards zero. The threshold between optically thin and thick clouds is set at $\tau = 15$ throughout the

simulation. Our criteria are based on a more favorable plant environment at canopy level, where below a τ of 15 the A_n and transpiration rates were increased as optical thickness increases at 14 UTC. The onset of cloud development is equal for all cases; however, the increase in cloud cover is faster with stronger background winds.

It is evident that H has the largest spread (~159–183 W m^{-2}) before optically thick shading clouds arise (11.30 UTC), which is due to its sensitivity to horizontal wind through r_a (Eq. 2.2, 2.4b). Furthermore, during the maximum cloud-cover period (12.30–15 UTC), the regional H is reduced (max. reduction: 18%) due to cloud shading. A relevant feature is that the standard deviation decreases when thick clouds arise, which offsets the effects of r_a on H. This indicates that the vegetation-Cu system adapts in the direction of a steady-state condition when sufficient radiation (positive feedback) is present to form Cu clouds (negative feedback). In other words, an increase in CBL energy due to enhancement of surface fluxes by wind is balanced by an increase in Cu development that decreases the θ_c at surface. The sequence of the mechanism that affects H is explained as follows:

1. Cu clouds start to tilt in sheared environments, thereby enlarging the shaded areas.
2. As a result, the local τ decreases slightly, affecting the partitioning between direct and diffuse radiation.
3. As this feedback mechanism acts during the period when optically thick clouds ($\tau >$ 15) are present (Fig. 2.7), the total radiation reaching the surface is much reduced, which results in a decrease in θ_c. Note that fluctuations in θ_c due to Cu shading are more than 20 times as large as fluctuations in the near-surface potential air temperature, θ (not shown).
4. As a result of the combination of decreased r_a due to the background wind and the increase in the cloud-shaded area due to cloud tilting, which decreases θ_c, the effects are almost equally offset.

Our results also show that this relation is independent of the stomatal relaxation time, as in all the experiments, H converges and the spread (95–100 W m^{-2} at 14 UTC) is small.

The impact of optically thick Cu on the regional LE flux (maximum reduction: 5%) is less than H (max. reduction: 18%). The reason for the difference in response is found in the dependence of LE on vegetation responses (through r_c) and VPD. Depending on cloud thickness, the amount of diffuse and direct radiation reaching the plants is affected, which has consequences for the magnitude and feedback of the plant's response. As described in detail by Pedruzo-Bagazgoitia et al. (2017), when the vegetation reacts immediately, optically thin clouds enhance A_n and transpiration rates,

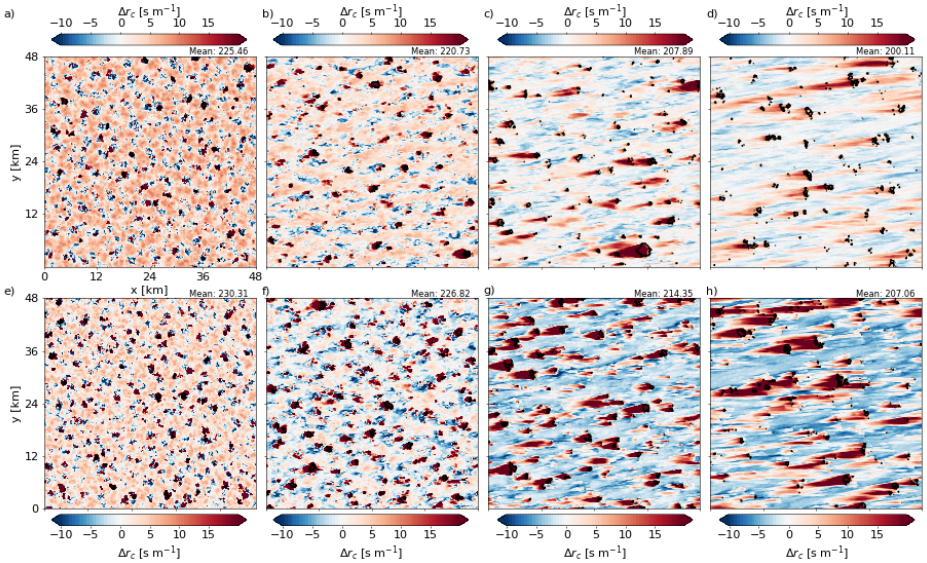

Figure 2.8 Instantaneous horizontal cross-sections of the canopy resistance deviation compared to the domain averaged value (Δrc) at the surface is shown at 14 UTC for the (a–d) LAG15 and (e–h) ASYM cases, regarding wind speeds of (a,e) 0, (b,f) 2.5, (c,g) 7.5 and (d,h) 15 m s^{-1}. The black contour lines indicate the Cu clouds that are thicker than 50 τ. The wind direction is from left to right.

due to an increase in diffuse radiation (positive effect on LE), while some direct radiation is still present. On the other hand, under optically thick clouds, A_n and plant transpiration are reduced, since only a small proportion of the radiation reaches the surface.

Under these conditions, r_c is the dominant term (r_c is ~3–4 times larger than r_a; Fig. 2.4b, e). As a result, fluctuations due to wind (thus r_a) on the LE flux are less effective, while its response is mostly due to Cu shading effects on r_c (Eq. 2.3).

Besides LE and H, the ground heat flux (G) is also affected by Cu shading. A maximum reduction due to Cu shading is found to be 8%. However, due to its relatively small contribution to Q_{net} (9%), no major effects on the vegetation-cloud coupling are evident.

To conclude, H has important effects on the net radiation. Regarding the TRA case, a relatively large spread is found, due to the sensitivity of H to r_a (Fig. 2.4b). Furthermore, when optically thick Cu shading occurs, the spread is drastically reduced and the plant adaptation cases converge. The net regional SEB reduction (i.e. Q_{net}) due to Cu shading is found to be 11%, with a deviation between cases of 0.5% (i.e. 1.2 W m^{-2}), which regional decrease in Q_{net} is comparable to the finding of Lohou & Patton (2014) (10%).

In order to understand why we found no effects of the plant relaxation time on the SEB at regional level, we focus on the effects of Cu shading on the canopy resistance, whose deviation compared to the mean is shown in Figure 2.8 for the LAG15 (upper

panels) and ASYM (lower panels) cases. As can be seen, the surface impacts on r_c due to Cu shading are distinct for different background wind conditions, as well as plant relaxation time. In general, four factors control the surface impact due to Cu shading: 1) plant relaxation time, 2) cloud thickness, 3) cloud movement and 4) cloud tilting. This means that regarding the asymmetrical stomatal response, the impact of Cu shading on the surface is expected to be the largest compared to all base cases, since due to its asymmetry a larger surface area is affected.

Under free convective conditions (Fig. 2.8a, e), canopy resistance is affected by the atmospheric cell structure and the local decrease in net radiation by hovering Cu. As a result, spatial heterogeneity is large, due to the more profound impact of Cu shading on the surface. When wind is present ($U_g \geq 2.5$ m s^{-1}), the spatial and temporal SEB is powerfully affected by the plant's relaxation time (Fig. 2.8). For instance, when the plants react rapidly, the fluctuations in LE are larger than when plant reaction time is slower. This suggests that the plants partially affect atmospheric turbulence, as they induce a dynamic heterogeneity in the SEB. Furthermore, in some situations the plants are unable to recover significantly, as a new cloud perturbs the incoming radiation. This mostly occurs when roll vortices are present and the clouds move along the vortex in streets (Fig. 2.8d, h). Due to this effect, an optimal situation between background wind and plant relaxation time would be expected, which could significantly impact spatial canopy resistance. However, in the symmetrical LAG10-20 cases, the cloud cover (N = 18–22%) is too low to maintain those situations effectively, as the plants have time to recover significantly.

In the asymmetrical response case (ASYM), this situation is more evident. Along with the vortex, Cu clouds perturb the vegetation in streaks (Fig. 2.8h). As a result of the asymmetrical response to radiation, areas of higher r_c start to develop. Next to areas of cloud streets, clear sky areas persist. Due to the combination of wind and maximum radiation (see for details section 2.3), the r_c remains at a low level in clear sky areas, which counteracts the cloud shaded areas of higher r_c, resulting in a net effect near zero.

2.5.2 Atmospheric and vegetation effects on cumulus

As background wind-speeds increase, the momentum and surface fluxes gradually increase (e.g. at 12 UTC, Q_{net} increases from 327 to 352 W m^{-2} regarding a background wind of 0 to 20 m s^{-1}, respectively). As a result, convection and cloud development are enhanced (not shown), with Cu growing larger and thicker. To understand how Cu growth relates to Cu tilting in sheared environments, we studied the effects of the background wind on cloud cover and cloud area fraction (Fig. 2.9). The cloud area fraction is defined as the fraction of clouds on each level independently. As Fig. 2.9 shows, cloud cover increases with rising background wind speed. This is explained by

the effect of cloud tilting, which is caused by wind shear. The negative effects of cloud shading on cloud cover are clearly identified with respect to the TRA case. In general, a decrease in cloud cover of 11% was found, with the exception of the 20 m s^{-1} case (14%). This exception is explained by the fact that with a strong background wind the radiatively transparent clouds reach the sponge layer (i.e., a numerical artifact; not shown) due to the missing cloud-shading feedback. When Cu shading is present, the decrease in regional SEB lowers the Cu vertical extent, thereby preventing them to spread artificially at this sponge layer. It is noteworthy that the plant relaxation time does not affect the cloud area fractions and cover, which led us to conclude that the localized vegetation response to Cu shading has little impact on the formation of Cu, that is mainly driven by the (local) decrease in r_a.

To determine the cloud tilting effects on the cloud cover, the area fraction of clouds is calculated at 2 heights. Figure 2.9 shows the area fraction at 2 and 3 km heights, both of which are above the cloud base that was found around 1900–1950 meters. We found that the area fraction at 2 km increases with increasing background wind-speed. This is explained by the growing amount of forced clouds when the background wind increases, as more air parcels are forced towards the lifting condensation level (LCL).

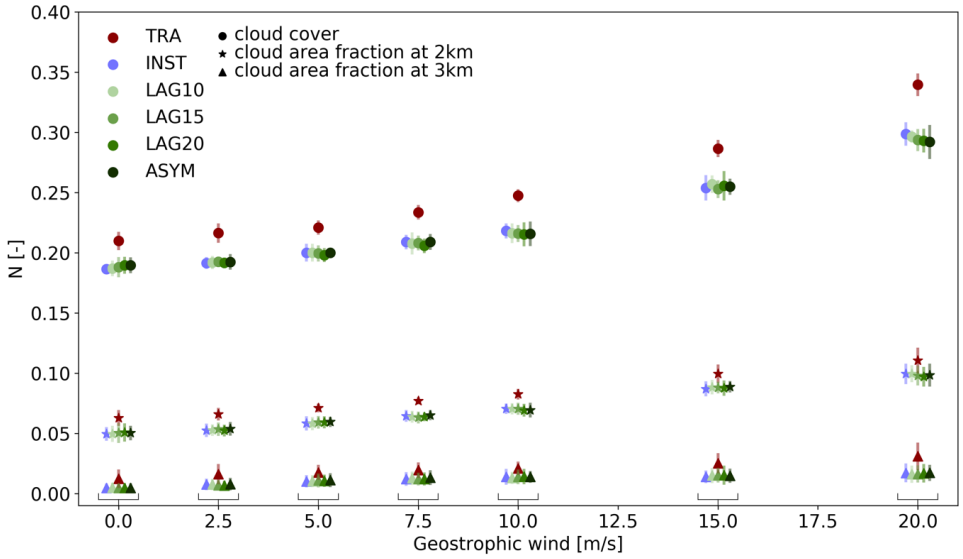

Figure 2.9 Half-hourly averages (13.45–14.15 UTC) and standard deviation (vertical lines) of cloud cover (circles) and area fraction of clouds at 2 (stars) and 3 (triangles) km in relation to the initial geostrophic wind speed. Note that the horizontal spread in the plant response cases is for visualization only.

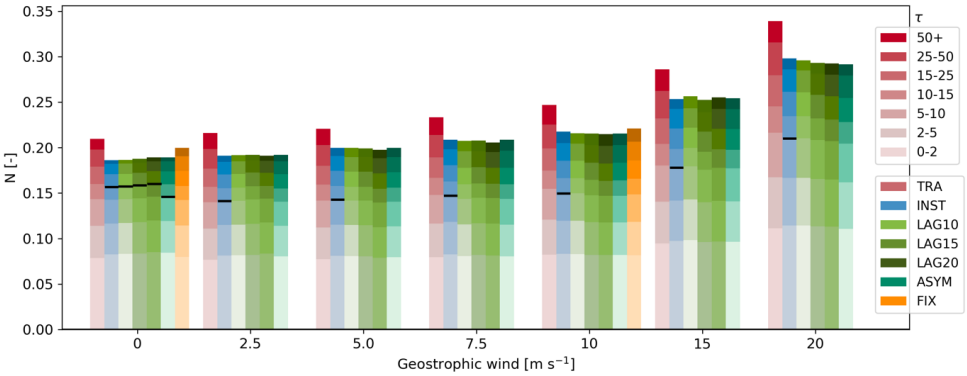

Figure 2.10 The aggregated fraction of the cloud optical depth (τ) for all wind and base experiments is shown at 14 UTC. The horizontal black line denotes the threshold value where clouds have a positive (below black line), or negative (above black line) effect on A_n and transpiration. When no black line is present, all clouds contribute negatively to An and transpiration.

Focusing on the 3 km level, which is above the level of free convection (i.e. no forced clouds present), it is clear that the rise in area fraction with wind speed is much less. The fact that the increase in cloud cover is not mirrored by a similar relative increase in cloud-area fraction at 3 km indicates that the rise in cloud cover is mainly due to the tilt as a result of wind shear.

Our finding that local plant responses do not affect the area fraction of clouds and cloud cover suggests that the regional decrease in energy level is dominant and local interactions become less important. To determine whether this is true, we homogenized the surface fluxes based on the INST case for the 0 and 10 m s^{-1} wind cases (i.e. FIX case). We thus simulate the same surface energy level as in the INST case, but without local interactions based, for instance, on Cu shading affecting the local SEB. We introduce the FIX case in Fig. 2.10, where the aggregated fraction of the regional averaged cloud optical depth is shown. The horizontal black lines denote the threshold value where above (below) these lines an increase in cloud thickness decreases (increases) the photosynthetic and transpiration rates. When no black line is visible, all clouds contribute negatively to the photosynthetic and transpiration rates. From the figure is clear that only optically thin clouds in a free convection situation have a positive effect on the photosynthetic and transpiration rates, and in cases when the plants' stomata react instantaneous. Regarding free convective conditions, the threshold is found around 15τ for the INST and LAG10-20 cases, while it is approximately 10τ for the ASYM case. When a background wind is introduced and clouds are moving, the A_n and transpiration rates are always reduced as cloud optical depth increases for the cases with an (a)symmetrical relaxation time. However, the INST case retains a threshold,

which is approximately 10τ .

In order to understand the effects of Cu shading on cloud development, we aggregated the cloud optical depth in stacked bins (Fig. 2.10). Instead of focusing on the trend in cloud cover, as shown in Fig. 2.9, we focus here on the influence of Cu shading on the occurrence of the aggregated cloud optical depth. We start our analyses with the clouds of $0–2\tau$. As Fig. 2.10 shows, those optically thin clouds are not affected by Cu shading and stomatal response time as the aggregated fraction remains stable around N = 0.08 [-] for all cases with wind speeds up to 10 m s^{-1}. When the wind speed is higher than 10 m s^{-1}, more optically thin clouds appear. This is explained by the generation of forced clouds, as can also be seen in Fig. 2.9. This pattern is nearly similar for cloud optical depths till 10τ, showing no response on Cu shading or stomatal relaxation time. When the clouds are thicker than 10τ, a clear difference between the TRA and stomatal response cases is visible. This indicates that Cu shading only has an impact when the clouds sufficiently decrease the net radiation below the cloud. Note that this process is mainly due to the canopy temperature and thus on H, as no clear response between the stomatal response cases is found. When the surface fluxes are prescribed and homogenized as in the INST case (i.e. FIX), we find comparable results for the optical thin ($0–10\tau$) clouds, while an intermediate result is found compared to the TRA and stomatal response cases.

Neglecting the local variability in surface fluxes leads to an increase in the incidence of thicker ($\geq 10\tau$) clouds. This leads us to conclude that the local variability and heterogeneity in surface fluxes due to atmospheric perturbations and Cu shading acts as a negative feedback on cloud growth. If this response is not taken into account, the growth of Cu clouds will be overestimated, increasing cloud cover with 1–2% (i.e. relatively with 5–10%).

2.6 Discussion

The results presented in previous sections showed the sensitivity of Cu and atmospheric dynamics to stomatal relaxation times for a wide range in wind conditions. We focused on the impact and feedbacks in the vegetation-cloud system when Cu perturb the partitioning between direct and diffuse radiation reaching the surface. Due to our systematic approach to identify key vegetation-clouds feedbacks, we initialized the simulations with homogeneous surface conditions. In this section, we address the effects of this initialization and put our results in perspective with the current understanding found in literature.

In all our simulations, we start with an initially homogeneous distribution in soil moisture content as in vegetation type and state. However, it is well known that a horizontal variability in those variables affect the surface fluxes, thereby influencing

convection rates and Cu occurrence. For instance, Chen & Avissar (1994) and Clark & Arrit (1995) have shown that a horizontal variability in soil moisture strongly affects Cu and precipitation fields. This was confirmed by the observational study of Taylor et al. (1997), who showed that in the semiarid Sahel region soil moisture patterns play a role in determining rainfall locations. Although we explicitly simulate the soil moisture in the top layer, its distribution was homogeneously prescribed. Next to this, the soil moisture content is lower than field capacity, thus (slightly) hampering transpiration rates in our simulations, which indicates that soil moisture is affecting the surface fluxes through plant transpiration as well. If spatial variations in soil moisture would develop, this would influence the stomatal aperture, thus surface fluxes. For instance, the modelling study of Rieck et al. (2014) shows that a variation in surface fluxes has strong impacts on the transition from shallow to deep convection and on the cloud size distribution. This would indicate that when Cu are advected over different vegetation and soil types, the variation in surface fluxes could accelerate Cu development due to enhanced surface fluxes.

Besides our initial homogeneous surface setup, we idealized the vegetation-Cu interaction by considering the sun directly overhead the clouds. This idealizes the interactions as the maximum decrease in radiation is found directly below the cloud. By fixing the solar angle, we prevent any additional interactions due to cloud tilting and movement, which enabled us to compare and identify feedbacks in the Cu-vegetation system. For instance, when the clouds tilt in a wind sheared environment towards the sun, the radiation is partitioned in a different way than when the clouds tilt in another direction. As this is highly dependent on the background wind direction and speed, we chose to fix the sun's location throughout all experiments to have a fair comparison and analysis between the simulations. Note that the amount and cloud transmissivity of radiation still depends on the solar angle (Pedruzo-Bagazgoitia et al., 2017). Furthermore, as shown by Schumann et al. (2002), the location of the cloud shading on a spatially homogeneous surface has only a very small impact on the turbulent motion field. However, Jakub & Mayer (2017) recently found in a LES sensitivity study that the organization of Cu convection and formation of clouds streets is influenced by the position of the cloud's shadow. In a similar line of research, Gronemeier et al. (2017) focused on the effects of the cloud shading's location on secondary circulations and the effects of surface heterogeneity. They concluded that the effects of cloud shading are small for situations where the shading is perpendicular on a static heterogeneous (striped) surface, while the effects are stronger if the cloud shadows are cast parallel to the striped surface. It would be very interesting to include the processes and radiation schemes described in Gronemeier et al. (2017) and Jakub & Mayer (2017) with the interactive and dynamic plant stomatal heterogeneity presented in this study.

In our LES setup, all water within an air parcel saturates when the local lifting condensation level is reached. We assume all droplets to maintain an effective radius of 10 μm, a size typically found in Cu (Baker and Latham, 1979; Siebert and Shaw, 2016). In reality, this process will be more subtle and cloud droplets will grow gradually in size. However, the effect of droplet size on the shortwave downward radiation would only be minor (Pedruzo-Bagazgoitia et al., 2017). Next to this, we simulate warm clouds, thereby neglecting the possibility of ice crystallization at the top of the clouds (Taylor et al., 2016). This process could acts as a negative feedback as it generates precipitation, which negatively influences the updraft, thus Cu development, and increases the spatial variability in surface fluxes as patches of relatively high soil moisture arise (Chen et al., 2012). In our simulations, we only investigate the development of fair-weather non-precipitating warm Cu. Due to the missing feedback of ice crystallization and precipitations, our conclusions are only valid for non-precipitating Cu clouds.

In this study, we were interested in the effects of local plant stomatal responses to a decrease in radiation on the Cu development. In all our cases, we start with an initially equal and idealized surface and radiation setup. Since we draw conclusions on the comparison with our control case (i.e., INST) our results remain valid, even though our simulations do not necessarily compare perfectly with the processes and feedbacks occurring in nature itself.

2.7 Conclusions

The interactions in the vegetation-cloud coupling were systematically studied in order to understand the regional effects of local cumulus (Cu) cloud shading. To determine the main processes in the plant-atmosphere-cloud interaction, the coupling was investigated for a wide range (44) of atmospheric and vegetation conditions. The plant relaxation time is prescribed as an instantaneous, symmetrical (10, 15 and 20 minutes) and asymmetrical (5 min closing, 10 min opening) response. The background wind speeds ranged from 0 to 20 m s^{-1} to obtain a range from free-convective to shear-driven boundary layers. By using the LES technique, the interactive vegetation reacted to the atmospheric state variables and intermittent light perturbations due to clouds. The latter introduced a partitioning between diffuse and direct radiation reaching the canopy, which was dependent on the optical cloud thickness. Also within-canopy radiative transfer was taken into account. In order to investigate the effects of cloud shading, we also simulated a case with transparent clouds.

In our vegetation-cloud system, we systematically increased the complexity of the system by successively adding processes that would affect the interaction. First, we focused on a free convective situation with radiatively transparent clouds. In this idealized setup, we found that the dynamic heterogeneity of the horizontal near-surface

turbulence influences the vegetation, leading to an enhanced CO_2 assimilation rate (A_n; 7%) and latent (LE; 9%) and sensible heat (H; 19%) fluxes near the updraft region, thereby intensifying the local turbulent convection.

When we permitted clouds to provide shade in a free convection situation, a different response between LE and H was found in the shaded areas. Under optically thin clouds, plant transpiration and A_n increased (5–7%) were comparable to the regional averaged value in the INST case, whereas this enhancement became smaller (3–5%) when the plants needed time to adapt. We explain this effect by the positive canopy response to an increase in diffuse radiation, leading to decrease the canopy resistance by 5% (INST). For H, no such effects were found as it was mainly radiation-driven, thus leading to a decrease of 31%. When optically thick clouds develop, both A_n (85%) and LE (81%) were greatly reduced, although to a lesser degree than was H (100%).

When we focused at the influence of a background wind, the enhancement effect of optically thin clouds vanished. If the clouds were sufficiently vertically developed, we found that as wind-speed increases they broaden due to tilt. As a result, the shaded surface area expanded, while the cloud optical thickness locally decreased, thereby influencing the partitioning between direct and diffuse radiation reaching the canopy. In roll-vortex situations (U_g > 10 m s^{-1}), the vegetation was affected in a streak-wise pattern where the surface fluxes were lowered below the Cu streets. The combination of cloud movement and plant relaxation time resulted in a smaller reduction in A_n (33%) and LE (41%) compared to free convective conditions, while its effect was distributed over a larger area, resulting in a negligible net effect. H was not affected differently (max. reduction 100%). As a result of the spatial Cu organization, a similar streak-wise clear sky area was evident. Here, the maximum solar radiation effectively maintained high levels of photosynthesis, and thus a low canopy resistance. Due to the strong background wind, the aerodynamic resistance was also low, thereby maintaining high surface fluxes. This effect compensated for the negative effects of Cu shading, resulting in similar surface fluxes for all atmospheric and vegetation cases. The effects of turbulence and Cu shading on H and LE were found to be distinct due to the plant relaxation time involved in the LE flux, as the canopy resistance was three times as large as the aerodynamic resistance, and therefore played a dominant role in controlling plant transpiration.

By combining and interpreting the entire set of plant responses and wind combinations (44 experiments), our findings show that during the period of maximum cloud cover, regional reductions in H and LE of 18% and 5%, respectively, were found compared to the TRA case, while the net radiation (Q_{net}) was reduced by 11%. A regional deviation in Q_{net} of 0.5% (i.e. 1.2 W m^{-2}) was found among the wide range of atmospheric and vegetation conditions. By comparing four simulations that are equal

in net available energy, but differ in interactive (i.e. INST) and prescribed (i.e. FIX) surface energy fluxes, we find a relative reduction in cloud cover between 5–10% during the maximum cloud cover period when the dynamic surface heterogeneity is neglected. Taking into account that cloud cover is independent of the plant relaxation time and the development of optically thin Cu clouds was not hindered due to shading, we conclude that the local and spatial dynamic surface heterogeneity is affecting Cu development, while the coupling between vegetation and clouds becomes progressively weaker as stomatal relaxation time and background wind speeds increase.

2.8 Acknowledgements

This study was supported by a grant from the Netherlands Organisation for Scientific Research (NWO; 823.01.012). The numerical simulations were performed with the supercomputer facilities at SURFsara and were sponsored by the National Computing Facilities (NCF) foundation and NWO under project SH-312-14. We thank four anonymous reviewers for their helpful comments on the manuscript.

3

Substantial reductions in cloud cover and moisture transport by dynamic plant responses

Cumulus clouds make a significant contribution to the Earth's energy balance and hydrological cycle, and are a major source of uncertainty in climate projections. Reducing uncertainty by expanding our understanding of the processes that drive cumulus convection is vital to the accurate identification of future global and regional climate impacts. Here, we adopt an interdisciplinary approach that integrates interrelated scales from plant physiology to atmospheric turbulence. Our explicit simulations mimic the land-atmosphere approach implemented in current numerical weather prediction and global climate models enable us to conclude that neglecting local plant dynamic responses leads to misrepresentations in the cloud cover and mid-tropospheric moisture convection of up to 21% and 56%, respectively. Our approach offers insights into the key role played by the active vegetation on atmospheric convective mixing that has recently been identified as the source of half of the variance in global warming projections (i.e. equilibrium climate sensitivity).

This chapter has been published as Sikma & Vilà-Guerau de Arellano (2019) in Geophysical Research Letters

3.1 Introduction

With an average daily occurrence of around 25% in mid-latitude and tropical continental regions (Eastman & Warren, 2014), cumulus convection has a significant influence on regional radiation balance (Lohou & Patton, 2014; Schumann et al., 2002; Vilà-Guerau de Arellano et al., 2014) and moisture recycling (Waite & Khouider, 2010; Wright et al., 2017). By perturbing the incoming radiation, cumuli modulate plant stomatal aperture (Min, 2005) and surface temperature (Pedruzo-Bagazgoitia et al., 2017) near updraft regions (Figure 3.1). In this capacity, cumuli initiate a chain of events that dynamically affect their development (e.g., Manoli et al., 2016; Sikma et al., 2017), as well as the distribution of atmospheric moisture (e.g., Spracklen et al., 2012) and terrestrial carbon uptake (Min, 2005).

Observation-based experimental and simulation studies have revealed that cumulus radiative perturbations have a bi-directional effect on local photosynthesis and transpiration rates (Min, 2005; Pedruzo-Bagazgoitia et al., 2017). Optically thin clouds enhance those rates, due to an increase in the diffuse radiative component, while optically thick clouds lead to significant decreases in evapotranspiration (Pedruzo-Bagazgoitia et al., 2017). In the perspective of moisture recycling (Wright et al., 2017), this early transpiration enhancement stimulates cumulus growth and subsequent upward moisture transport, thereby pre-conditioning the mid-tropospheric cloud layer for regional-scale deep convection on a sub-weekly scale (Keil et al., 2008; Waite & Khouider, 2010; Zhang & Klein, 2010; Spracklen et al., 2012). This underlines the predominant role of plant physiology as a key driver related to mid-tropospheric moisture convection, and demonstrates that only a profound understanding of the fundamental processes involved can lead to progress in the modelled land-atmosphere continuum (Katul et al., 2012; Stevens & Bony, 2013; Sherwood et al., 2014; Bony et al., 2015; Yano et al., 2018).

In current numerical weather-prediction and climate models, the land-atmosphere continuum is separately treated and parameterized (WMO, 2015; Hov et al., 2017). As a result, global models lack dynamic and static heterogeneity on small spatiotemporal scales (i.e., seconds/meters), thereby missing essential interactions that play a vital role in the formation of cumuli. This underlines the need for high-resolution simulations that adopt a holistic approach by dynamically coupling plant responses to atmospheric mesoscale circulations. Here, by explicitly resolving relevant and essential sub-grid scale processes and interactively coupling the atmosphere to plant physiology (Figure 3.1), we systematically study feedbacks and sensitivities in the plant-atmosphere-cloud system. Special focus is placed on the combined effects of local and dynamic cloud radiative perturbations on characteristic plant physiological responses (Ooba &

Takahashi, 2003; Vico et al., 2011; McAusland et al., 2015), and in turn on the subsequent effects of their responses to the atmosphere and clouds.

3.2 Proof of concept: numerical simulation strategy

Current technological limitations and scientific inability to integrally measure the spatiotemporal interactions covered in this study, mean that no all-encompassing observations are available. More specifically, in order to take all the relevant scales (i.e., from leaf level to cloud convection) into account, we need to study the coupled processes simultaneously. Moving forward to overcome these limitations, we performed 20 novel three-dimensional numerical experiments (DALES4.1; DALES model details in Heus et al. (2010) and Ouwersloot et al. (2017)) that offer an unprecedentedly detailed diurnal description of atmospheric dynamics as well as the physiological response to environmental perturbations. The experiments describe a typical Western European early autumn day, with cumuli developing over well-moistened grassland. Our 48 km x 48 km domain is 90% covered by C3 grass and the three-dimensional atmospheric fields were explicitly solved for an entire day up to a height of 5.5 km, with horizontal and vertical resolutions of 50 m and 12 m, respectively (i.e. 420 million grid points). The surface characteristics were mechanistically solved by an interactive plant physiological sub-model (Jacobs & de Bruin, 1997; Ronda et al., 2001; Boussetta et al., 2013), A-gs, which was coupled to DALES to provide a dynamic representation of the vegetation. Note that plant physiological responses were affected by the soil-moisture state. The A-gs sub-model utilizes a two big-leaf (sunlit and shaded)

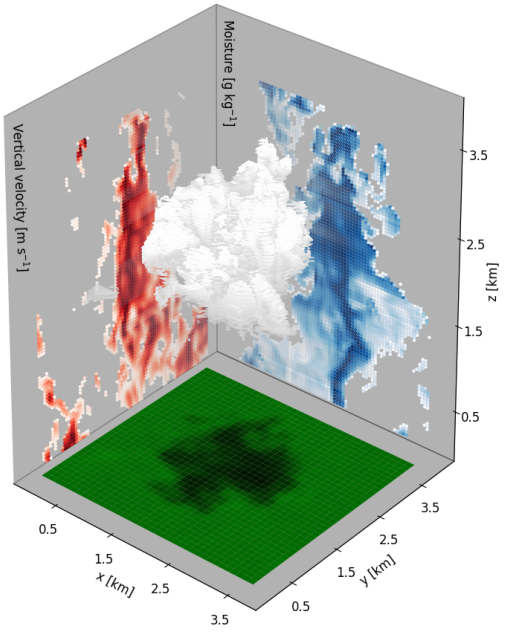

Figure 3.1 Virtual cumulus cloud and its shading on plants in the simulated land-atmosphere continuum. The cloud reduces and partitions the solar radiation into direct and diffuse components, leading to different levels of photosynthesis (green colors at surface) and transpiration (not shown) at the surface. Vertical planes show the upward vertical velocity (red) and total atmospheric moisture content (blue) as a vertical slice through the cloud (i.e., x, y = 2 km). For a regional view see Fig. S3.1 in the supporting information.

approach (Pedruzo-Bagazgoitia et al., 2017), which simultaneously treats both direct and diffuse radiative effects caused by cloud scattering, as well as in-canopy radiative scattering (Pedruzo-Bagazgoitia et al., 2017). Furthermore, the A-gs sub-model has recently been implemented in the ECMWF global model to account for the land-surface CO_2 uptake (Boussetta et al., 2013). Cloud-induced scattering was solved by the Delta-Eddington approach (Joseph et al., 1976), which partitions direct and diffuse components based on the incoming shortwave radiation and cloud optical depth. To ensure a fair comparison between experiments, the solar inclination angle was fixed at zenith, although the amount of radiation depends on the virtual diurnal evolution in solar angle (i.e. its path through the atmosphere) representative for mid-latitude conditions (Pedruzo-Bagazgoitia et al., 2017).

In order to ensure that our simulations are representative, we first evaluate our numerical experiments with a comprehensive surface and upper atmospheric data set. Our comparison entails a holistic view on the sub-daily processes that drive the plant-atmosphere system, which includes the surface and boundary-layer dynamics. As an example, the boundary-layer height evolution (Figure 3.2a) exhibit the integrative effects of the surface (Figure 3.2b) and atmospheric processes. The simulated diurnal variability of warming (Figure 3.2c) and moistening (Figure 3.2d) further confirms that our turbulent-resolved results are able to connect the surface processes with the boundary-layer dynamics, by adequately simulating the entrainment of warm and dry air into the atmospheric boundary layer.

The accurate representation of processes and their coupling is key for the development and daily cycle of boundary-layer clouds. Buoyancy rates driven by atmospheric turbulence provide the necessary energy to form and intensify cloud growth. As the measured diurnal evolution of integrated thermodynamic variables (Figure 3.2) is close to our virtual simulated atmosphere, and our simulated vegetation-cloud system covers the myriad of spatiotemporal scales related to plant physiology, atmospheric boundary layer and cloud development, it confirms the validity of our integrative approach.

In order to ensure that our results maintain representative and to encompass the relevant biophysical aspects, we systematically designed four numerical large-eddy simulation experiments that are aimed to unravel the magnitude of sensitivities in the vegetation-cloud system:

1. ASYM, our control experiment, represents a realistic asymmetric plant stomatal response to light fluctuations (Fig. 1) (Ooba & Takahashi, 2003; Vico et al., 2011; McAusland et al., 2015). The asymmetric stomatal response was modelled as

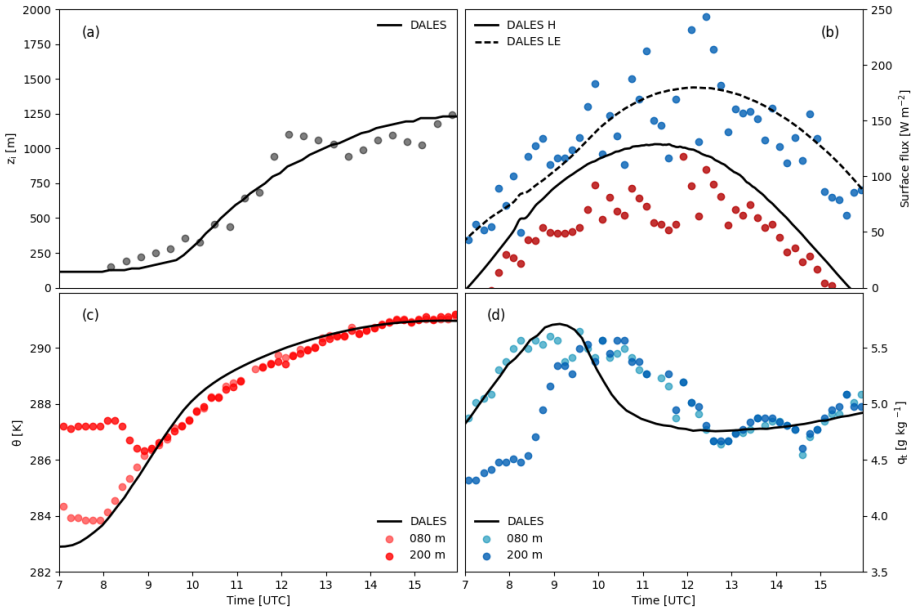

Figure 3.2 Diurnal variability of atmospheric state variables measured at Cabauw, the Netherlands (25 September 2003), and modeled with DALES. The (a) boundary layer height, (b) sensible (red) and latent (blue) fluxes, (c) potential temperature, and (d) total specific moisture content are shown as a function of time. In (c) and (d), two measurement heights are shown.

relaxation time (Sellers et al., 1996), with a closing (opening) e-folding time of 5 (10) minutes and based on observations that encompass a wide range of functional plant types (Vico et al., 2011; McAusland et al., 2015). By so doing, we explicitly account for the direct effects of light perturbations and its surface feedback to the atmosphere on very fine spatiotemporal scales. In this capacity, this experiment is the most detailed simulation of the actual feedback that occurs in nature.

2. INST experiment: an instantaneous plant stomatal response to fluctuating light, which is designed to understand the impact of the (asymmetry in) stomatal responses. In other words, a lingered plant stomatal surface response might alter atmospheric patterns by a change in the surface energy balance. This experiment represents an extreme case on which the plant stomata, thus surface energy balance, instantaneously responds to changing light, which has subsequent effects on vertical atmospheric movements.
3. DOMAIN experiment: surface fluxes are adjusted at each time step (~2 seconds) based on the domain averaged properties of the coupled INST experiment. These adjustments ensures that in DOMAIN the energy is conserved and exactly similar to INST, but is homogeneously distributed over the entire domain. The focus of this

experiment is to understand how a domain averaged response influences cloud properties. It mimics an approach used in numerical weather models that parameterize the influence of clouds on radiative transfer and its effects on the surface energy balance, though don't account for the sub-grid effects (i.e., dynamic heterogeneity).

4. TRANS experiment: an extreme case where the clouds were made transparent. This experiment represents a radiative uncoupled plant-cloud interaction and gives us insight in the significance of the plant-cloud relation in a wide range of atmospheric conditions. Furthermore, it can be viewed as an experiment that shows the effects of a misrepresentation in the parameterizations of the diurnal cycle in cloud dynamics (e.g., radiation, surface and dynamics).

In order to cover a wide range of convective atmospheric structures, these four experiments are repeated for five wind speeds, ranging from 0 to 10 m s^{-1}, thereby moving from idealized cellular atmospheres to realistic roll-vortex situations (i.e. cloud streets) (Sikma et al., 2017).

3.3 Disentangling the plant-atmosphere system: dynamic heterogeneity and coupling regimes

Our central hypothesis is that plants strongly modulate the atmospheric flow in distinct convective atmospheres by self-regulation and adaptation. This equilibrates the responses of the land-atmosphere system at the sub-daily scales and thereby induces relevant effects on cloud cover and atmospheric convective turbulent transport. Due to our finding that the plant-atmosphere coupling is strongly affected by wind, we systematically build in complexity by starting with the windless situation (Figure 3.1) and continue by stepwise analysis of the influence of wind (Figure 3.3). We finish by disentangling a characteristic land-atmosphere system for mid-latitude region (Figure 3.4).

3.3.1 Local coupling

Under windless conditions, the plant and atmospheric states are intertwined and driven by bi-directional dynamic processes (Figure 3.1). Turbulent thermals rising from the vegetated surface act as the clouds' root by facilitating moisture transport, which is mainly determined by plant transpiration rates. At the cumulus development stage, radiative perturbations modulate the stomatal aperture, thereby affecting local transpiration (Fig. S3.3). Combined with a local decrease in surface temperature due to reduced solar radiation (Fig. S3.4), surface buoyancy rates diminish, followed by reduced updraft strengths in the cloud roots, in turn reducing moisture transport to the

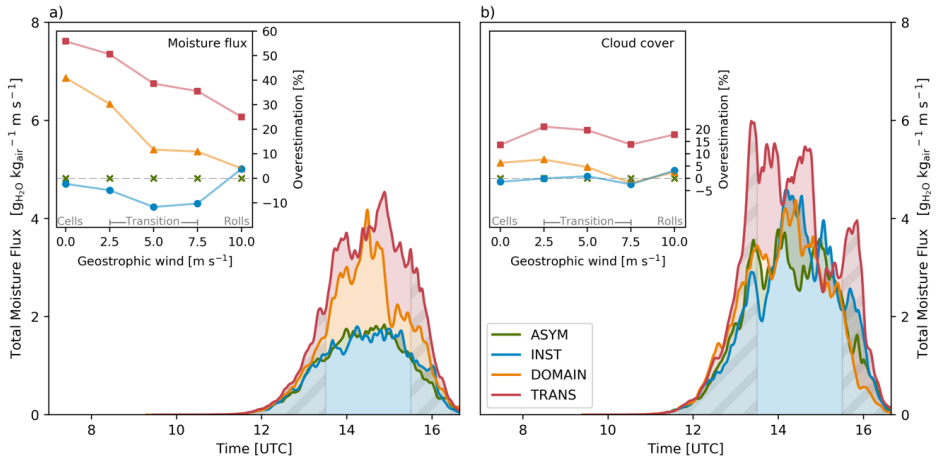

Figure 3.3 Impact of plants on vertical moisture transport toward the mid troposphere and cloud cover represented for a wide spectrum in wind conditions. The temporal evolution of the total moisture flux (i.e., over whole domain of 48 km × 48 km) from cloud base to cloud top is shown for (a) cellular and (b) roll vortex-dominated atmospheres. The insets show the overestimation of (a) the moisture flux and (b) cloud cover compared to the ASYM experiment (green crosses) in a range of atmospheric convective structures during the maximum cloud cover period (i.e., 13:30–15:30 UTC). The acronyms are described in the text and refer to changes in plant stomatal responses or homogenization of surface fluxes.

mid-troposphere (Figure 3.3a). This dynamic process is most pronounced in windless, convective cellular atmospheres, where cumuli hover directly above their shade and horizontal mixing is minimal (Figure 3.1, S3.1), thereby resulting in a local coupling. In this windless and rooted system, clouds become shallower and their horizontal extent is smaller, which is reflected in a decrease in moisture transport (inset Figure 3.3a) and cloud cover (inset Figure 3.3b) of around 56% and 14% (i.e. TRANS vs ASYM), respectively. Note that as a result of hovering cumuli and the low chance of new cloud development over the same surface area due to weakened turbulent thermals, plants are able to recover their pre-cloud state. As regards ASYM, this process is delayed due to the asymmetric stomatal response, hence the difference of ~3% compared to INST (inset Figure 3.3a).

Especially in cellular convective atmospheres, the location of the perturbed plant response proves to have a crucial influence on cumulus development. Our DOMAIN experiment, where the cumulus-perturbed surface energy from INST is homogeneously distributed, shows quantitatively that moisture transport (41%) and cloud cover (6%) continue to be overrepresented (insets Figure 3.3). This demonstrates that the regional convective atmospheric structure, which is closely related to the spatial cloud population, is predominantly influenced by local surface perturbations rather than its averaged state.

3.3.2 Transition regime

In the transition from cellular-dominated atmospheres to fully developed atmospheric rolls (i.e., under a wind speed regime of 2.5–7.5 m s^{-1}), the plant-atmosphere coupling weakens, revealing the pivotal role of the synoptic atmospheric structure in determining the strength of the plant-atmosphere coupling and subsequent preconditioning of deep convection. In this transitional atmospheric convective state, the synergy between vegetation and atmospheric state is perturbed, reducing the overestimation of moisture transport (inset Figure 3.3a). In spite of this decline, dynamic surface heterogeneity still influences cumuli development, as indicated by the misrepresentation of as much as 12% when the stomatal asymmetric response is omitted (inset Figure 3.3a; INST vs ASYM). Since most plant species respond asymmetrically to radiative perturbations (Vico et al., 2011; McAusland et al., 2015), and their responses are well within the characteristic turbulent time-scales of cumulus convection (i.e., 15-30 min), a lingered surface response emerges (Figure 3.3a; i.e., dynamic surface heterogeneity). However, in this transitional state, clouds move too slowly to maintain the lingered surface impact, as no new cloud passes within the time-span of stomatal recovery (i.e., within 10 min). As a result, the plant-atmosphere-cloud coupling is weak.

3.3.3 Regional coupling

Moving on in complexity, the effect of the asymmetric plant response once again becomes pronounced when horizontal convective rolls develop and cloud streets form in alignment with the mean horizontal flow (i.e., 10 m s^{-1}). By analyzing all of the modelled surface grid points (~1 million per case) at 14 UTC (Figure 3.4), we discover spatial and dynamic relationships between asymmetric plant responses and cloud-induced radiative perturbations that stabilize the plant-atmosphere-cloud system (Figure 3.4b-c). In this situation, the plant-atmosphere coupling is strongly influenced by the spatial distribution in cloud population and subsequent regional heterogeneity in surface energy. The combination of strong winds and shear-induced cloud tilting in the entire cloud layer, which latter impacts the radiation distribution and increases the shaded surface area, results in cloud streets that initiate a streaky dynamic surface heterogeneity aligned with the clouds' path (Figure 3.4a, S3.2). As a direct result of the roll-vortex flow, more cumuli pass over the same surface area within the period of stomatal recovery (i.e., within 10 min), which hampers the full return of the plants to their optimal state (Fig. S3.2). On the one hand, surface energy and transpiration and carbon uptake rates are reduced in the cloud-affected surface streak areas, while on the other, both those rates and the surface energy are maximized in the neighboring areas of clear

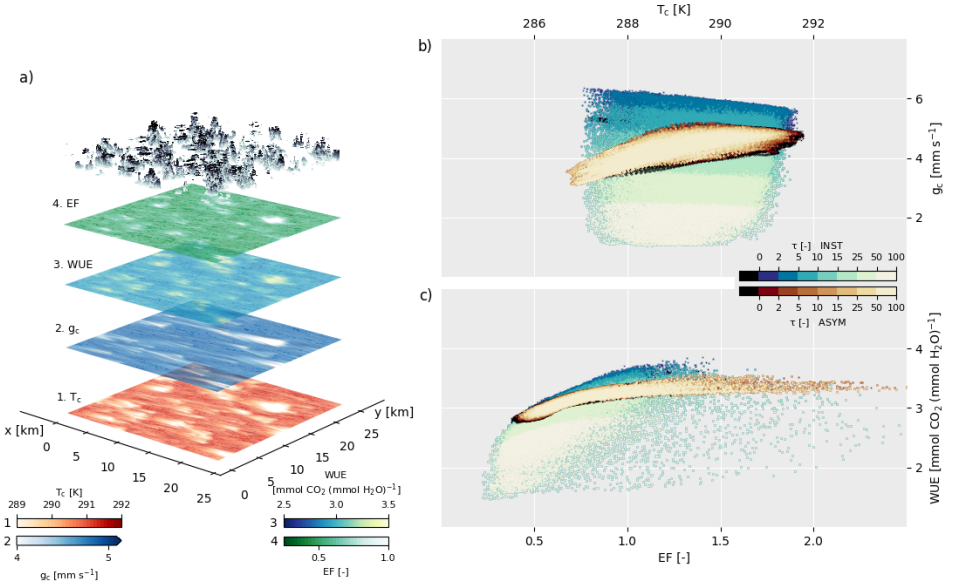

Figure 3.4 Plant responses to atmospheric and cumulus-driven perturbations in roll vortex-dominated atmospheres. An instantaneous snapshot of the surface responses to cloud shading (i.e., dynamic heterogeneity) and atmospheric perturbations under 10 m s^{-1} wind conditions is shown at 14 UTC; a time with maximum cloud cover and development. In (a) a spatial zoomed (25 km × 25 km) representation of four selected surface variables is shown, with a visualization of the cloud optical thickness on top. Water-use efficiency is defined as WUE = $-A_n$/LE, where A_n denotes assimilation of CO_2 and LE the latent heat flux, and the evaporative fraction as EF = LE/ (H + LE), with H denoting the sensible heat flux. Values above EF = 1 result from optically very thick clouds that cool the surface such that H becomes negative. In (a) and (b), all simulated surface grid points (921,600) of the total domain (48 km × 48 km) are aggregated. In (b) the relationship between canopy conductance (g_c) and canopy temperature (T_c) is visualized, while (c) shows the relationship between water-use efficiency and evaporative fraction at 14 UTC. The color gradient denotes cloud optical thickness (τ) for the INST (blue) and ASYM (red) experiments in roll vortex-dominated atmospheres. Surface points directly beneath clear sky are shown as black. Note that the increase in g_c under optically thin clouds is the result of an increase in the diffuse component (Pedruzo-Bagazgoitia et al., 2017). See Fig. S3.6 for a cellular-dominated atmosphere.

sky (Figs. S3.2, S3.5). Paradoxically, this leads to a positive contribution to regional water-use efficiency (WUE), compared to an instantaneous response (Figure 3.4c; see stabilization of WUE with increasing EF). The locked spatial surface pattern as a response to the atmospheric convective state introduces a bi-directional dynamic but significant coupling between plants and cumuli, which greatly reduces mid-tropospheric moisture transport. As shown in the inset of Figure 3.3a (i.e., 10 m s^{-1}; Rolls), the large reduction in moisture transport is of the same order of magnitude as

the underestimation of the INST situation, resulting in a relative net overestimation close to zero (i.e., INST vs ASYM). In other words, the streak-wise surface pattern locks (dampens) the atmospheric flow (convection), which causes the plant-atmosphere-cloud system to couple, resulting in a significant decrease in mid-tropospheric moisture transport similar to that of the INST case. This confirms our central hypothesis, and demonstrates the ability of plants to regulate the land-atmosphere system, which has substantial consequences for the regional hydrological and carbon cycles (Figure 3.3 & Figure 3.4). This key finding stresses that the mechanisms of ASYM and INST that lead to the almost equal reduction in mid-tropospheric moisture transport are distinct and differ greatly at the surface (Figure 3.4b-c)

3.4 Moving forward in land-atmosphere interaction studies

Our approach paves the way to a deeper understanding of local land-atmosphere interactions and gives insight in the spatiotemporal interactions on a wide range on scales. However, to systematically break down the complexity of the feedback systems and to mimic similar conditions as in numerical weather prediction models, we made assumptions in the representations of the radiation transfer and stomatal responses.

In our study, the solar inclination angle was fixed at zenith, while the amount of radiation depends on the virtual diurnal evolution in solar angle (i.e., its path through the atmosphere). Furthermore, our simulations employed a one-dimensional radiative transfer code (see Fu & Liou, 1992; Heus et al., 2010). These assumptions were necessary to make our experiments computational feasible and to understand the impact of the multilateral interactions in the plant-atmosphere system. As regards the latter, following this systematic approach gave us insight in the delayed feedback between plant stomatal responses, wind shear and speed, thus cloud movement, tilting and organization.

Although our numerical experiments reach a high-level of detail and explicitness, they miss the effects associated to three-dimensional radiative processes, as for instance lateral cloud scatter or cloud shading effects based on the diurnal change in solar inclination angle. Although this also has not been accounted for in regional and global weather models, it is known to influence in-canopy processes that ultimately affect the overlying atmosphere. For instance, Jakub & Mayer (2017) show that the three-dimensional radiative effects on the surface leads to the organization of cumulus clouds streets, while a three-dimensional in-canopy radiative transfer can improve modelled photosynthesis levels (Kobayashi et al., 2012). In relation to plant physiology, our representation of plant responses includes the essential response to light, temperature and water vapor changes. However, we foresee that future plant physiological studies can improve this description of these responses at the leaf level (e.g., Morales et al.,

2018), as well as the spatial distribution of stoma in the leaf to improve the gas exchange (de Boer et al., 2016).

Finally, and in relation to the transfer of our results to large-scale model, numerical weather prediction models generally account for the cloud shading effects through a decrease in shortwave radiation (i.e., our DOMAIN case) (Jiménez et al., 2016). However, biases are present in the global horizontal irradiance (Jiménez et al., 2016; Fig. 4b therein). The inclusion of a correction reduced the bias, but it might as well be caused by compensating errors, as sub-grid cloud (e.g., cumulus) parameterizations are prompt to errors (Lenderink et al., 2004).

An inaccurate representation of the radiative transfer might affect the partitioning in direct and diffuse radiation as well as the surface energy, which reduces the accuracy of regional and global numerical weather prediction models (Bauer et al., 2015) and impact our estimation of the carbon terrestrial sink (Le Quéré et al., 2009). Nevertheless, in order to include detailed land-atmosphere processes described in this study in coarser grid-size models, our findings need to be parameterized. Data from our large-eddy simulations is available for future studies to define, for instance, probability density functions to account for cloud shading effects and its relation to the mass flux representation, which ultimately can be used to improve its representation in larger scale models.

3.5 Conclusion

The ability of plants to regulate atmospheric perturbations under a wide range of atmospheric convective situations indicates that a dynamic relationship exists between plants and the atmospheric boundary layer. This relationship stabilizes the plant-atmosphere system and, in structured convective atmospheres (i.e., from cells to rolls), is capable of locking vegetation patterns together with atmospheric convective conditions. The asymmetric response of the plant stomata is a key process in this interaction, as it influences the preconditioning of deep convection by affecting the mid-tropospheric moisture transport under cellular and roll vortex-dominated atmospheric conditions. Due to the direct link between photosynthesis and transpiration, carbon and hydrological balances are liable to failures if the plant-coupling is misrepresented. Our results demonstrate for the first time the need to study the plant-cloud continuum holistically based on first-principles and explicit calculations of the biophysical atmospheric processes. By interconnecting spatiotemporal scales, we show that uncertainties associated with moist convection can be greatly reduced.

3.6 Acknowledgements

This study was supported by a grant from the Netherlands Organisation for Scientific Research (NWO; 823.01.012). The numerical simulations were performed with the supercomputer facilities at SURFsara and were sponsored by the National Computing Facilities (NCF) foundation and NWO under project SH-312-14. The cases and the DALES model are available on github: https://github.com/dalesteam/dales/tree/master/cases/cldveg01/model_data. Note that for this manuscript, DALES version 4.1 is used. For convenience, the executable files are saved in each folder per case.

3.7 Supplementary material

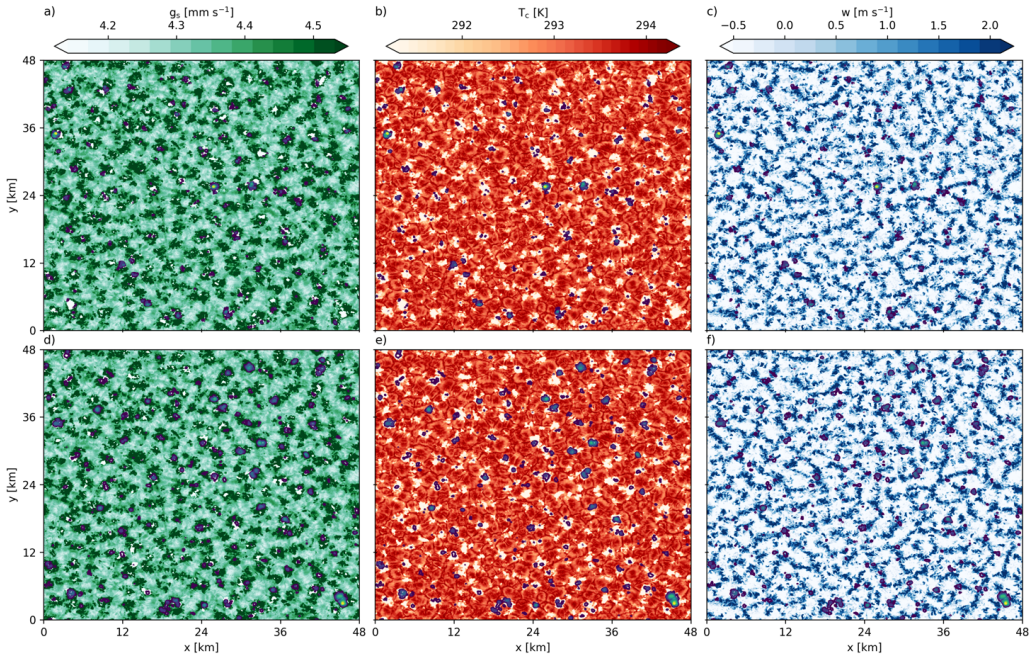

Figure S3.1 Instantaneous horizontal cross-sections at the surface for the ASYM case at 14 UTC. In a) the canopy conductance (g_c), b) canopy temperature (T_c), and c) vertical wind speed (w) at 900 m (i.e., mid-ABL) are shown for a cellular- dominated atmosphere (i.e., 0 m s^{-1}). The purple to blue contour lines represent an instantaneous snapshot of cumulus growth at 14 UTC. The lower panels (d-f) are identical in terms of horizontal cross-sections as a-c, but differ in the representation of cumulus (contour lines), which is shown as a summation over the previous half hour (i.e. 13.30-14 UTC).

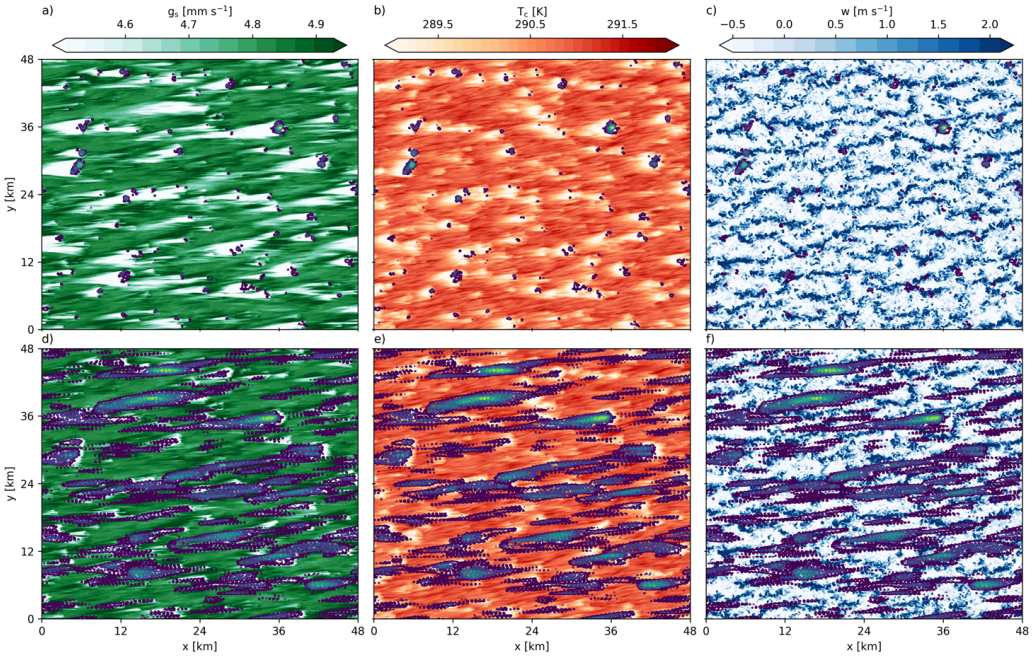

Figure S3.2 Same as in Fig. S3.1, but for a roll vortex-dominated atmosphere (i.e., 10 m s^{-1}).

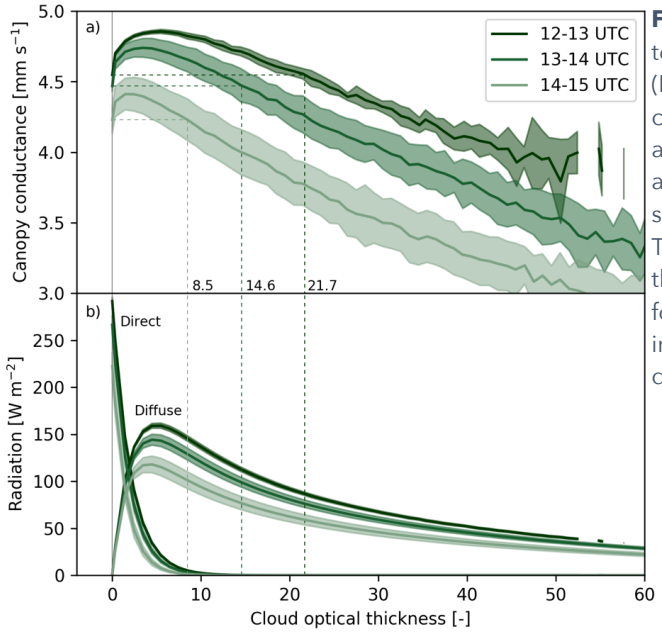

Figure S3.3 Plant stomatal response to photosynthetic active radiation (PAR) during the maximum cloud cover period for the ASYM case. The a) canopy conductance and b) direct and diffuse components of PAR are shown versus cloud optical thickness. The vertical dotted lines represent the maximum cloud optical thickness for the canopy conductance to increase, caused by an enhanced diffuse PAR component.

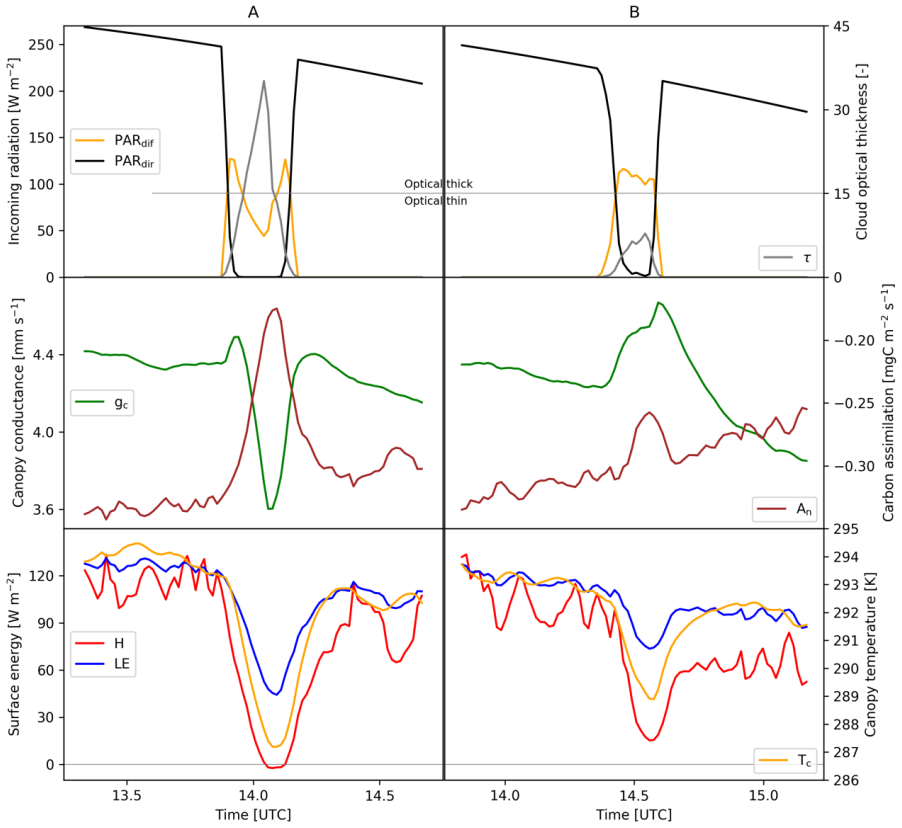

Figure S3.4 Surface and plant responses to cumulus shading for the ASYM case. The left-hand panels (A) show a surface grid point at which an optically thick cloud develops at around 14 UTC. Regarding radiation (upper panel), direct PAR is greatly diminished, while diffuse PAR increases, especially during the optically thin period. The plants (middle panel) respond by reducing their photosynthesis levels (A_n) and canopy conductance (g_c). Regarding g_c, note the brief increase during the period of high diffuse radiation. The surface energy components (lower panel) display a distinct drop in the sensible heat flux (H), and to a lesser extent, in the latent heat flux (LE). This response is mainly due to the direct relationship of canopy temperature (T_c) to H. In the right-hand panels (B), the same variables are shown for an optically thin cloud. The main differences are found in the positive g_c response and in the reduced impact on the surface energy balance and photosynthesis rates.

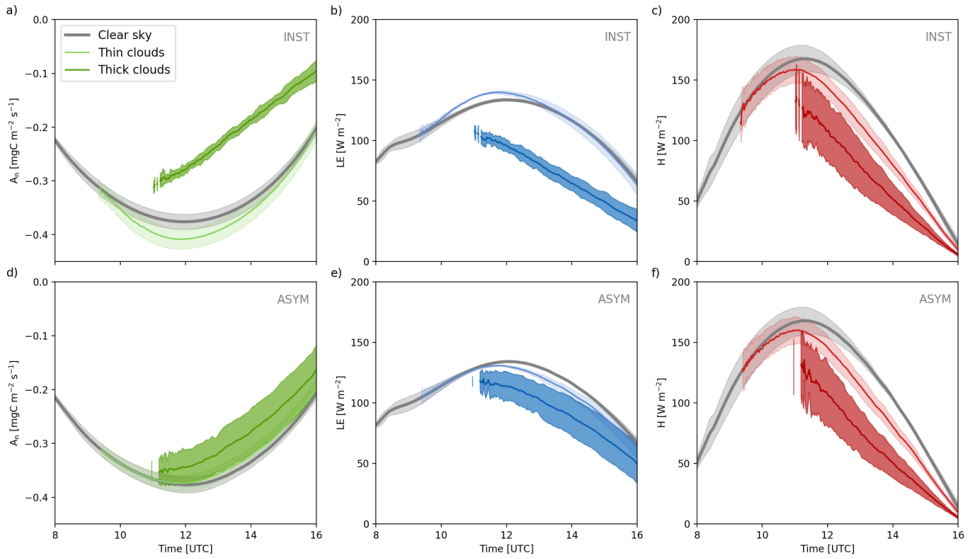

Figure S3.5 Temporal evolution of conditionally sampled carbon assimilation and latent and sensible heat fluxes. For a wide range of wind conditions (i.e., 0 to 10 m s^{-1}, with steps of 2.5 m s^{-1}), the surface data is aggregated on the basis of the effects of cloud perturbations sampled by cloud optical properties. Thin clouds are defined as clouds with an optical depth below 15, while thick clouds are defined as clouds with an optical depth greater than 15 (see for details Fig. S3.3 & S3.4). The clouds impact is determined at the surface, thereby taking into account the temporal and spatial extent due to lingered stomatal responses (Fig. S3.2). The data are then averaged (thick lines) and the standard deviation is visualized as a colored spread. The upper panels show a) carbon assimilation, b) latent heat flux and c) sensible heat flux regarding the INST case. The lower panels show the same for ASYM. Main features are the increased carbon assimilation (a) and transpiration (b) for thin clouds, and the strong negative effects of thick clouds in the INST case. No clear effects of ASYM on the carbon assimilation and transpiration are found, while a dampened response is present due to optically thick clouds. No distinct effects are found in the sensible heat flux for both cases, which is mainly radiation-driven.

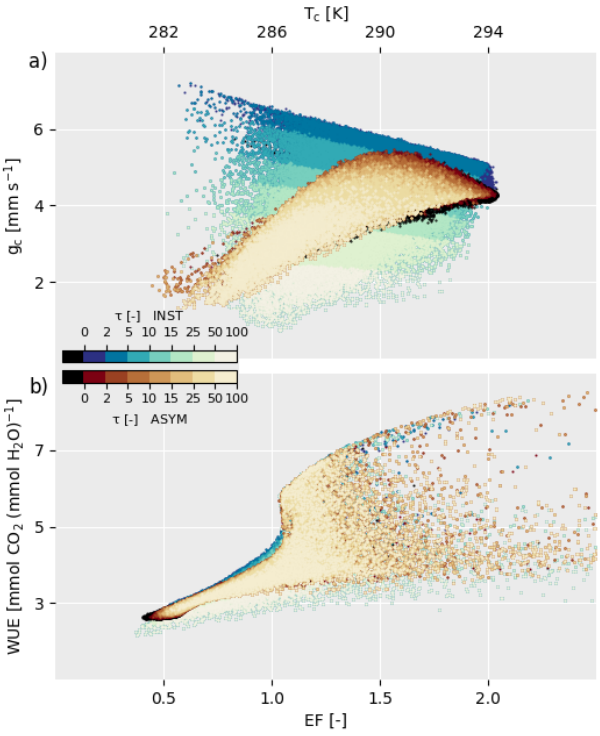

Figure S3.6 Plant and surface responses to atmospheric and cumulus-driven perturbations in cellular-dominated atmospheres. An instantaneous snapshot of the surface responses to cloud shading and atmospheric perturbations under windless conditions is shown at 14 UTC; a time with maximum cloud cover and development. In a) and b), all simulated surface grid points (921600) of the total domain (48 km x 48 km) are aggregated. In a) the relationship between canopy conductance (g_c) and canopy temperature (T_c) is visualized, while b) shows the relationship between Water-Use Efficiency and Evaporative Fraction at 14 UTC. The Water-Use Efficiency is defined as: WUE= $-A_n$ / LE, where A_n denotes the assimilation of CO_2 and LE the latent heat flux, and the Evaporative Fraction as: EF=LE / (H+LE), with H denoting the sensible heat flux. Values above EF=1 result from optically very thick clouds that cool the surface such that H becomes negative. The color gradient denotes cloud optical thickness (τ) for the INST (blue) and ASYM (red) experiments in windless (i.e., cellular) atmospheres. Surface points directly beneath clear sky are shown as black. Note that the increase in g_c under optically thin clouds is the result of an increase in the diffuse component (Pedruzo-Bagazgoitia et al., 2017).

4

Quantifying the feedback between rice architecture, physiology and microclimate under current and future CO_2 conditions

To assess the micro-meteorological consequences of rice variety choices in relation to rising CO_2 associated to climate change, we quantified the interplay between rice architecture, physiology and micro-climate in current (~385 µmol mol^{-1}) and future (~580 µmol mol^{-1}) CO_2 micro-environments. Two rice varieties contrasting in canopy structure and physiology were grown embedded in irrigated rice paddies, under elevated CO_2 (using a Free-Air CO_2 Enrichment (FACE) facility) and ambient CO_2 conditions. The high-yielding indica variety Takanari is more photosynthetically active and characterized by a more open canopy than a commonly cultivated variety Koshihikari. Our results show a strong diurnal interplay between solar angle, canopy structure, plant physiology and the overlying atmosphere. Plant architecture was identified as a strong determinant of the relation between plant physiology and micro-climate, that in turn affects the surface forcing to the overlying atmosphere. Takanari was able to maintain lower canopy temperature both in current and future CO_2 owing to the greater atmospheric mixing and stomatal conductance than Koshihikari. In the perspective of food security, a shift to such a higher-yielding variety would have consequences on the regional surface energy balance, which subsequently might alter regional weather.

This chapter has been submitted for review with H. Ikawa, B.G. Heusinkveld, M. Yoshimoto, T. Hasegawa, L.T. Groot Haar, N.P.R. Anten, H. Nakamura, J. Vilà-Guerau de Arellano, H. Sakai, T. Tokida, Y. Usui and J.B. Evers

4.1 Introduction

All terrestrial biosphere processes and their interactions exist due to the stabilizing and damping response to solar radiation. From the industrial revolution onwards, human pressure on the biosphere system has dramatically increased, causing a destabilization of biosphere processes and their interactions, resulting in the average global temperature to rise (Höhne et al., 2011). In this respect, one might consider the influence of humans as an additional internal forcing to the biosphere system. The global anthropogenic environmental footprint is expected to increase in coming decades resulting from global population growth and increasing living standards (Hoekstra & Wiedmann, 2014). Food demand will dramatically increase (e.g., Godfray et al., 2010; Tilman et al., 2011), anthropogenic and temperature-driven land-cover changes will occur (e.g., Pielke et al., 2016), which in turn will impact the local and regional radiation balance causing a change in weather patterns (e.g., Mahmood et al., 2014; de Kok et al., 2018). To anticipate on these changes, a detailed understanding of the consequences of these actions is of great importance, to be able to predict future biosphere changes and their consequences.

A key strategy towards increased food crop production involves increases in crop photosynthesis rates (e.g., Ort et al., 2015). Rice (*Oryza sativa*), is one of the three most important food crops (next to maize and wheat) and is a dominant landscape feature in many parts of the world. In addition, most of the rice in the world is grown in so-called paddy systems where soil is covered by water through much of the season. As such it has a strong surface forcing on regional weather through its high-water usage. For example, Ikawa et al. (2017) revealed that evapotranspiration from Japanese irrigated rice fields amounted to 80-90% of the seasonal precipitation, which is around one third of the annual precipitation in Japan. Especially in developing regions that are strongly affected by climate change and that experience excessive population growth rates, improving crop productivity and yields can have vast consequences on the regional weather and climate through changes in the regional energy balance. Ultimately, this might affect regional crop productivity and influence yields in turn.

In the agricultural sciences, the impact of a future climate on crop yields is determined by analyzing current crop responses (Knutti et al., 2010; Yin, 2013; Li et al., 2015). Future yield projections are developed taking into account those current responses, but do not consider the non-linear feedback of the crop to the changing atmosphere (e.g., Houghton et al., 2001; their Fig. 3; Rial et al., 2004; their Fig. 1). By so doing, weather is treated as long-term statistics. Local and regional variability is simplified to seasonal averaged or accumulated quantities of, for instance, temperature, precipitation or radiation (e.g., Pielke et al., 2007). In this respect, local weather phenomena are explained by general climate characteristics of a specific region. This

top-down approach eliminates the variability in crop responses to local weather (Pielke et al., 2007), which makes it difficult to determine their feedback on climate. To be able to assess that feedback, first a bottom-up approach is needed, in which the effects of crops on their micro-environment are identified. In rice, differences in canopy structure and physiology between varieties have been documented to have an effect on canopy functioning (e.g., Chen et al., 2014). However, to which extent these differences are caused by changes in canopy climate, and how this will change in future biosphere conditions is unclear. Therefore, in this study, we aimed to quantify the micro-meteorological consequences of crop variety choice and their responses to rising CO_2 levels. The micro-climate of two distinct rice varieties, that strongly differ in both their architectural structure and physiological traits, was investigated for current and future (year ~2050) CO_2 levels. In this study, the micro-climate is defined as the atmosphere directly affected by plant responses and structure (i.e. from 0-2 m above surface). The plants were grown embedded in irrigated rice paddies managed by Japanese farmers, to ensure that our findings reflect normal agronomic practices as they on the large scale in Japan. Future CO_2 levels were mimicked by a Free-Air CO_2 Enrichment (FACE) facility (Nakamura et al., 2012). We expected that these trait difference between these two varieties will result in different atmospheric interactions, and that the effect of elevated CO_2 on local microclimate will also differ between them.

4.2 Materials and methods

4.2.1 Site description and crop characteristics

In order to quantify the impact of plant architectural and physiological effects on the micro-climate, an experiment was conducted at the Tsukuba Free-Air CO_2 Enrichment (FACE) facility in Tsukubamirai, Ibaraki Prefecture, Japan (35° 58′N, 139° 60′ E; 10 m a.s.l.; soil type: fluvisol) between May and September 2015 (Nakamura et al., 2012). The site represented typical Japanese flood-irrigated rice (*Oryza sativa*) fields under humid subtropical conditions. The wet season was in June and September, while July and August temperatures were relatively dry with much sunshine. Four blocks were allocated in the rice fields, with each block containing one octagonal FACE plot and one ambient replicate (i.e., control plot) both with a diameter of 17 m (i.e., ~240 m^2). Pure CO_2 was fumigated from the peripheries of the octagonal rings by two horizontal tubes to ensure an average target elevation of 200 μmol mol^{-1} during daylight conditions compared to ambient conditions. The plots were separated by at least 70 m to minimize cross-contamination. During the months July and August, the average CO_2 concentration ($[CO_2]$) ± day-to-day standard deviation was 384 ± 12.5 μmol mol^{-1} in the

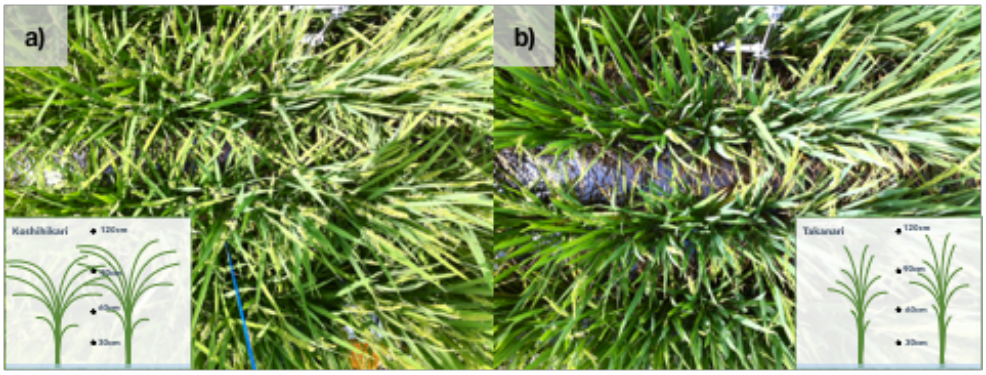

Figure 4.1 A top-down photograph of the a) Koshihikari and b) Takanari canopy during early-grain filling stage. Takanari has more erect leaves resulting in a more open canopy compared to Koshihikari, as visualized in the illustrative insets. The points represent the measurement heights for air temperature, relatively humidity, CO_2 concentration and photosynthetic active radiation.

ambient control with 578 ± 18.5 µmol mol^{-1} in FACE. The latter reflects the expected global CO_2 level in 2050 based on the RCP4.5 IPCC scenario (IPCC, 2014). For further details regarding the Tsukuba FACE system, see Nakamura et al. (2012) and Hasegawa et al. (2016).

Within the plots, two distinct rice varieties were grown; Koshihikari, a commonly grown Japanese japonica variety, and Takanari, a high yielding indica variety. Both Takanari and Koshihikari were transplanted by hand at a spacing of 30 cm (between rows) x 15 cm (along the row) with a resultant density of 22.2 hills per m^2 and grown in rows with a North-South orientation in an area of at least 3 m^2 (Fig. 4.1). Takanari has been identified as a potential future candidate to increase rice grain yield in Japan. Compared to Koshihikari, Takanari maintains higher levels of (leaf) photosynthesis (e.g., Chen et al., 2014) and exhibits higher stomatal conductance (30-40%) (Hasegawa et al., 2013; Chen et al., 2014; Ikawa et al., 2018), resulting in an increase in yields levels of up to 21% (Hasegawa et al., 2013). Furthermore, Takanari is able to achieve higher productivity in elevated [CO_2] conditions, due to its high sink capacity and photosynthetic activity, and showed greater yield enhancement under elevated CO_2 compared to Koshihikari (Hasegawa et al., 2013; Chen et al., 2014; Zhang et al., 2015; Nakano et al., 2017). Leaf area index (LAI) of both varieties ranging from approximately 4 to 5 m^2 m^{-2} in July to August, 2015, and a previous study from our FACE system reported LAI did not differ between Koshihikari and Takanari, despite a large difference in in-canopy light interception (Muryono et al., 2017).

4.2.2 Micro-climate measurements

From June to September 2015, detailed in- and above-canopy micro-climate measurements were performed in one elevated [CO_2] and one ambient plot. In the middle of each Takanari and Koshihikari plot, air temperature (T_a), relative humidity (RH) (RX-350TH, As One Co., Japan) and photosynthetically active radiation (PAR) (Apogee SQ-110; data logger: Decagon ECH2O EM50) were measured every minute at four heights (30, 60, 90 and 120 cm above soil surface). [CO_2] was also measured (LI-820, LI-COR INC., U.S.A.) at those four heights, although only one height was analyzed per minute, resulting in one [CO_2] measurement per four minutes per height. Furthermore, due to limited availability of [CO_2] profilers, the sensors were moved between Koshihikari and Takanari weekly. Water temperature (T_w) sensors (Platinum resistance thermometer Pt100) were located at the bottom of ponding water (i.e., on the soil surface) in each plot and variety, and measured continuously throughout the season every 10 minutes. The water depth was relatively constant at around 8 cm. At the North-Western (downwind) border of both ambient and elevated CO_2 plots, an eddy-covariance system (IRGASON Campbell U.S.A) was installed 15 cm above canopy top, measuring CO_2 and H_2O, sonic temperature and 3D wind at 50 Hz. Raw IRGASON data was processed to half-hourly fluxes with the software package EddyPro (LI-COR INC., U.S.A.). The IRGASON was manually raised with increasing canopy height every week such that it was consistently 15 cm above the canopy. Due to the relatively small experimental area, it was not feasible to perform separate flux measurements for both Takanari and Koshihikari in ambient and FACE conditions. As a consequence, our flux results are an aggregation of responses from the two varieties (note this only applies to the IRGASON, all other measurements were done separately per variety), but the FACE and ambient plots were measured separately. Nevertheless, to our knowledge, surface energy flux measurements in a FACE setup have not been performed, although they have been estimated using modelling approaches (Yoshimoto et al., 2005; Ikawa et al., 2018). Because the surface flux measurements were performed close to canopy top due to the limited size of each experimental plot, data sampling was performed at high frequency (50 Hz) to resolve relatively small turbulence. Canopy temperature (T_c) was measured every minute by an infrared radiative thermometer (MI-230, Apogee Instruments Inc., U.S.A.) under an angle of 45 degrees pointing South (to ensure no contamination by the water temperature) from mid-July to mid-September (i.e., harvest).

4.2.3 Data selection

In-canopy rice micro-climate conditions are strongly affected by the regional atmosphere, the vegetative state and canopy architecture. To ensure a fair micro-

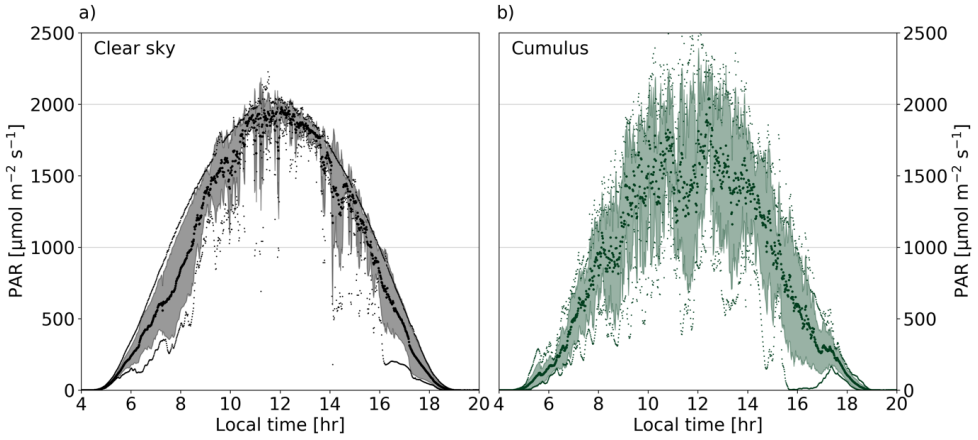

Figure 4.2 The diurnal evolution of above canopy photosynthetically active radiation (PAR) data aggregated and clustered based on radiative conditions, as described in the methodology. In a) the clear sky situations are shown, while b) shows the partly cloudy (i.e., cumulus) situations. Thick scatter points denote the average radiation, while the small scatter points indicate the minimum and maximum radiation on those days. The colored spread shows the standard deviation of the clustered data.

climate comparison between Koshihikari and Takanari, variations in those influencers need to be limited. Following from our data (Sikma, 2019), we found the period of mid-July till mid-August to be most suitable for a significant and representative evaluation: from mid-July onwards, Koshihikari and Takanari had reached their maximum height of 91 and 86 cm, respectively (i.e., no changing canopy height dependency in our data) and were close to flowering and part of the season where green LAI and associated photosynthesis are maximal. Furthermore, during this period variations in weather conditions were relatively minor and many clear and partly cloudy days occurred. Therefore, as a next step, the data were clustered based on radiative conditions (i.e., clear sky, partly cloudy) and aggregated as shown in Fig. 4.2. In total, six clear sky days (26, 27 July; 1, 2, 5, 7 August) and seven partly cloudy days (24, 25, 30 July; 10, 11, 16, 19 August) were chosen for analysis. The data has been additionally checked on wind direction and speed, to ensure no cross-contamination from FACE to ambient site occurred. In the remainder of this study, all micro-climate data are aggregated based on these two categories of radiative conditions. In the following two sections, we first focus solely on a clear sky weather regime as in these conditions the plant-atmosphere relations are pronounced. This is followed by a shorter description of the partly cloudy weather regime.

4.3 Results and Discussion

4.3.1 In-canopy micro-climate in current conditions

The different vertical structures of Takanari and Koshihikari (Fig. 4.1) resulted in distinct in-canopy radiative conditions, as apparent from the temporal distribution of photosynthetic active radiation (PAR) (Figs. 4.3a-c). Especially at 30 cm above ground level (AGL) PAR levels were low throughout the day, with the exception when the sun was at zenith. Furthermore, Takanari showed more sun spikes than Koshihikari, resulting from its more open canopy structure, despite LAI being similar (ranging from 4 to 5 m^2 m^{-2} in July & August, 2015). Light levels declined much more steeply in the canopy of Koshihikari than in the canopy of Takanari. At 60 cm AGL –around 2/3 of the canopy height– the largest differences were found between the varieties with many sun flecks from leaf blocking for Koshihikari, while the open structure of Takanari resulted in up to three times higher levels of PAR at this depth. Close to canopy top (90 cm AGL), the difference in PAR between both varieties decreased. Takanari on average intercepted less radiation and PAR at this height was closer to the maximum available PAR, while sun flecks were more common in Koshihikari. Overall, higher levels and a less steep extinction of PAR when moving from the top to the bottom of the canopy were found in Takanari (Figs. 4.3d and 3e).

The in-canopy micro-climate is influenced by both the plant architectural structure as well as its physiological response to external perturbations. With Takanari having an open canopy structure and higher photosynthesis rates and transpiration levels as

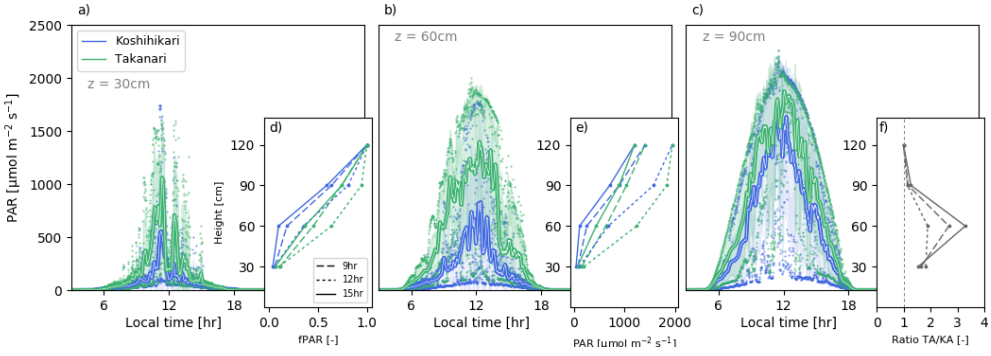

Figure 4.3 The diurnal evolution of in-canopy photosynthetically active radiation (PAR) during clear sky days of Koshihikari (blue) and Takanari (green) at a) 30cm, b) 60cm and c) 90cm above soil. Note: d), e), f) are stand-contained figures showing the PAR relation over the four measurements heights (i.e., 30, 60, 90, 120 cm). d) the PAR in-canopy profiles normalized with above canopy PAR for 9, 12 and 15LT (15min averaged). e), the absolute values of d). f), the ratio Takanari ambient (TA) vs Koshihikari ambient (KA) is visualized over three time stamps. The average height of Koshihikari was 91 cm, while Takanari was slightly shorter with 86 cm.

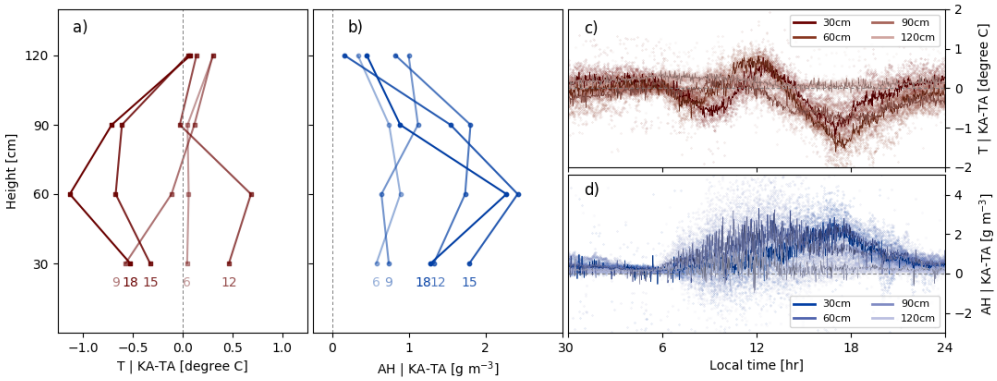

Figure 4.4 The diurnal evolution of the difference in in-canopy temperature (T; red) and absolute humidity (AH; blue) between Koshihikari ambient (KA) and Takanari ambient (TA) in clear sky conditions. In a) and b), the difference in the diurnal evolution in vertical profiles between Koshihikari ambient and Takanari ambient are shown for temperature and absolute humidity, respectively. In c) and d), the diurnal difference between KA and TA for all heights are shown. Scatter points are retrieved from actual measurements, while the lines represent a moving average (15min).

compared to Koshihikari (Chen et al., 2014), we expected vast differences in the diurnal in-canopy micro-climate. In the morning, the open canopy structure of Takanari allowed for increased radiative penetration as well as convective mixing, but for Koshihikari this mixing was hampered by the more closed canopy of this variety. Resulting from a reduced radiative in-canopy interception, daytime in-canopy temperatures of Koshihikari were lower compared to Takanari (Fig. 4.4a). However, lower (~0.5 degree C) leaf temperatures were found in Takanari, which likely resulted from the higher stomatal conductance of Takanari and its associated higher evaporative cooling rates known for this variety (Ikawa et al., 2018). Paradoxically, this did not result in a more humid canopy (Fig. 4.4b). In the case of Koshihikari, the relatively closed canopy likely hampered the vertical exchange of air, which may have resulted in a build-up of in-canopy moisture by evapotranspiration. The latter most likely did not occur as much in Takanari due to its open canopy structure, resulting to small above- and in-canopy differences in absolute humidity.

A strong interplay between canopy structure and solar angle was observed in the diurnal evolution of the temperature and absolute humidity (Figs. 4.4c & 4.4d). With the North-South row orientation and the sun at a Southerly position during zenith (i.e., ~12 local time), more direct radiation was able to reach the lower in-canopy leaves and stems, as well as the soil and water surface, causing the vertical in-canopy temperature differences to decrease (Figs. 4.4a & 4.4c). In Koshihikari, the warming effect was more

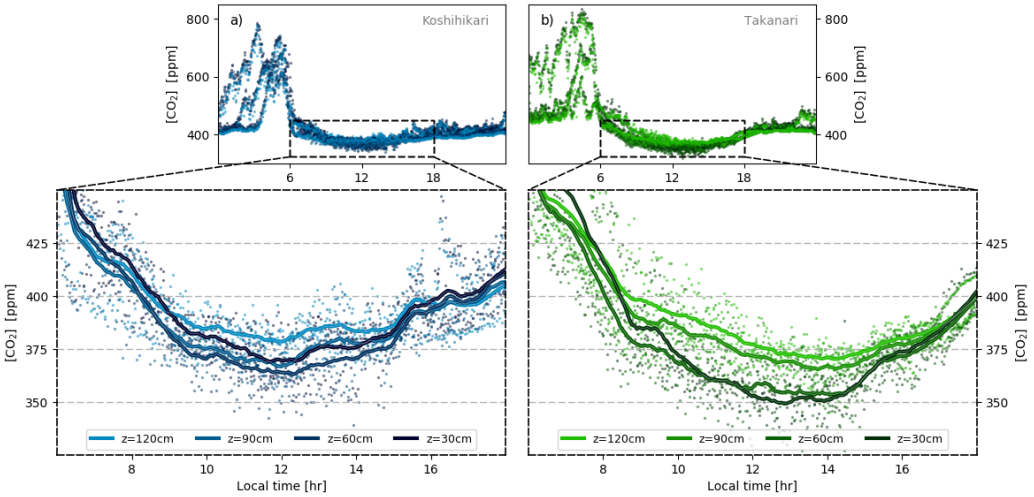

Figure 4.5 Diurnal evolution of CO_2 concentration [CO_2] for Koshihikari (left) and Takanari (right) at four measurement heights at ambient. The lower panels show a zoom over the daylight period (i.e., 6 to 18 LT). Scatter points represent all data, while the lines show a moving average of 15 min.

pronounced due to a higher canopy temperature that raises in-canopy temperatures compared to Takanari. During the afternoon, the effects of the increased water temperature became apparent when evaporation rates increased, resulting in humid Koshihikari in-canopy conditions (Fig. 4.4d). However, due to an increase in in-canopy air temperature of Takanari, which was the result of warm and dry air advection from a nearby city (explained in more detail later), absolute humidity levels were reduced. Due to the relatively closed canopy top, Koshihikari was less affected, hence the higher absolute humidity levels.

Strong differences were visible in the diurnal uptake rates of CO_2 inferred by CO_2 concentration ([CO_2]) profile measurements (Fig. 4.5). During night time, [CO_2] increased as a result of plant respiration and the absence of wind (peaks observed in Fig. 4.5), causing thermal stratification by cooling above the canopy. At sunrise, turbulent mixing started and photosynthesis activated, reducing the [CO_2]. Our results show the strong effect of canopy structure (i.e. mixing) and leaf physiology on the in-canopy [CO_2] (zoomed-in sections in Fig. 4.5). Takanari likely had higher photosynthetic activity (i.e. uptake rates) compared to Koshihikari, with Takanari having nearly similar [CO_2] at 30 and 60 cm. This confirms the higher CO_2 assimilation of Takanari than Koshihikari (Chen et al., 2014). From 90 cm upwards, atmospheric mixing leads to increased CO_2 levels, although the youngest (i.e. active) leaves were found around 90 cm during this growing stage. Although Koshihikari is less photosynthetically active (~-

20% compared to Takanari, Chen et al., 2014), reduced vertical mixing allowed for relatively low [CO_2] at 90 cm, which were comparable with values found at 30 cm. Note that the reason for the similar CO_2 levels likely differ: photosynthetic uptake rates at 30 cm were reduced, while atmospheric mixing polluted the uptake signal at 90 cm. Minimum levels of [CO_2] were found at 60 cm, where the impact of atmospheric exchange was less, resulting in higher uptake rates.

4.3.2 The effects of increasing CO_2 on the micro-climate

Increasing atmospheric levels of CO_2 cause the difference in partial pressure between plant intercellular and atmospheric levels to increase (Strain & Cure, 1985; Ainsworth & Rogers, 2007). As a consequence, the plants stomatal aperture narrows, with the subsequent effect that leaf temperatures start to rise due to decreased transpirational cooling. Especially during the flowering and grain-filling period of rice, this process might have consequences on grain quality and yield, as increased air temperatures can cause spikelet sterility (e.g., Satake & Yoshida, 1978) and exacerbate heat-induced damage in grain appearance quality (Usui et al., 2016).

Understanding the intrinsic relationships between rice micro-climate, physiology and morphology is vital in future yield and regional weather projections. In this section, we investigate the effects of an increase in [CO_2] (to ~580 μmol mol^{-1}; levels expected in the year ~2050) on the micro-climate of Koshihikari and Takanari. Note that, due to the focus of this study on current and future CO_2 levels, we did not account for other aspects of climate change, like increased air temperature and a change in radiation partitioning (e.g., diffuse, direct) or in the atmospheric dynamics.

The diurnal cycle in near-surface air temperature was closely related to the canopy temperature. For both varieties, a near-linear increase in both canopy and above-canopy air temperature was found during morning (Fig. 4.6a). Especially Koshihikari reached high canopy and air temperatures up to ~31 degree C, while Takanari stabilized around ~30 degree C (circles above one-to-one line in Fig. 4.6a). In elevated [CO_2], Koshihikari experienced stronger warming effects than Takanari. Normally during the afternoon, a sea breeze initiated advection of warm and dry air from a neighboring city, which delayed the decline in air temperature as would be expected from the daily-cycle in canopy temperature and radiation. Due to reduced winds speeds, the role of advection diminished during night time.

The high stomatal conductance, thus transpirational cooling of Takanari (e.g., Ikawa et al., 2018) becomes evident in the diurnal course of canopy temperature (Fig. 4.6b). Throughout the day, Takanari maintains a lower canopy temperature, while the canopy temperature of Koshihikari showed a strong increase (Fig. 4.6b). Furthermore, an increase in [CO_2] to ~580 μmol mol^{-1} caused the average day-time canopy temperature

to increase but this effect was larger in Koshihikari (~0.5 C) than in Takanari (~0.3) (Fig. 4.6c). On warm days, this increase even went up to periods of ~1 degree C for both varieties.

These warming effects of CO_2 elevation can have negative impacts on yields e.g. through acceleration of seed development or occurrence of spike sterility (e.g., Julia & Dingkuhn, 2013). Long-term FACE data analysis showed that yield enhancement by elevated [CO_2] (fertilization) was reduced by the increase in temperature during the grain filling (Hasegawa et al., 2016) and grain quality was severely reduced by elevated [CO_2] notably in hot years (Usui et al., 2016). Our results suggest that a shift to Takanari

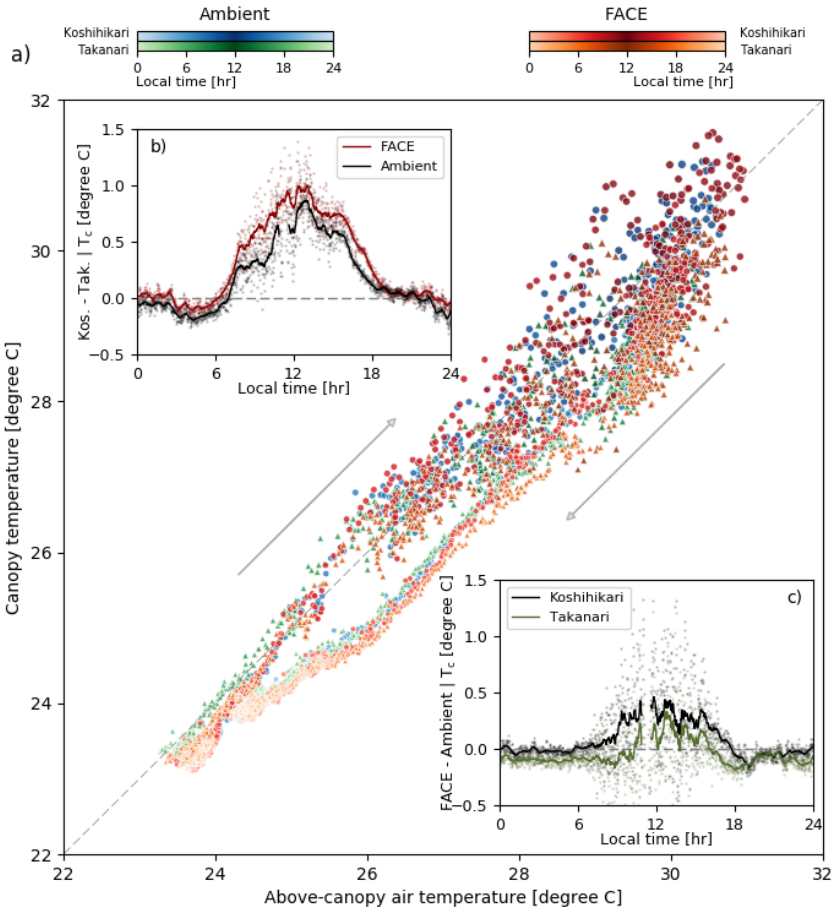

Figure 4.6 Relation between above-canopy air temperature and canopy temperature (measured under an angle of 45°). Warm colors represent FACE, while the cold colors indicate ambient. The main figure shows the diurnal evolution for both Koshihikari (circles) and Takanari (triangles). The upper inset shows the diurnal difference between Koshihikari and Takanari for FACE (red) and ambient (black) situations. The lower inset shows the effect of FACE on Koshihikari (black) and Takanari (green). For both insets, scatter points represent data, while the lines show an 15 min average. Note that there is some data missing, hence the gap in the moving average.

might be a good alternative to cope with near-future climate change as the CO_2 induced warming is smaller in this variety. This view is supported by the fact that appearance quality of Takanari was reported to be much less affected by elevated [CO_2] than that of Koshihikari (Zhang et al., 2015).

The interplay between plant architecture and physiology strongly determined the daily cycle of micro-climate. Our results show strong sensitivity to measurement height when quantifying crop micro-climate (Fig. 4.7). This is an important aspect that many studies do not consider when determining and measuring the crop micro-climate, as measurements are often performed on one pre-defined height or taken from a nearby weather station.

Due to atmospheric mixing, the impact from an elevation in [CO_2] to above-canopy air temperature was damped, resulting in similar above-canopy (i.e., 120 cm AGL) air temperature responses for both varieties (Fig. 4.7a). The impact of [CO_2] was more pronounced near the canopy top (~90cm), where stomatal closure resulted in a greater FACE-induced warming in Koshihikari than in Takanari. Moving into the canopy, the plant structure started to play a role (Fig. 4.7b, c, d). The open architecture of Takanari allowed mixing, while this mixing was hampered for Koshihikari due to its closed canopy top. Especially in the morning, in-canopy air temperatures were increased in elevated [CO_2] conditions for Koshihikari, while this was less pronounced for Takanari (Fig. 4.7c-d). This suggests that Takanari maintained high stomatal conductance and associated transpirational cooling better than Koshihikari in elevated [CO_2]. With the solar angle at zenith during noon, more direct radiation penetrated the canopy and caused air

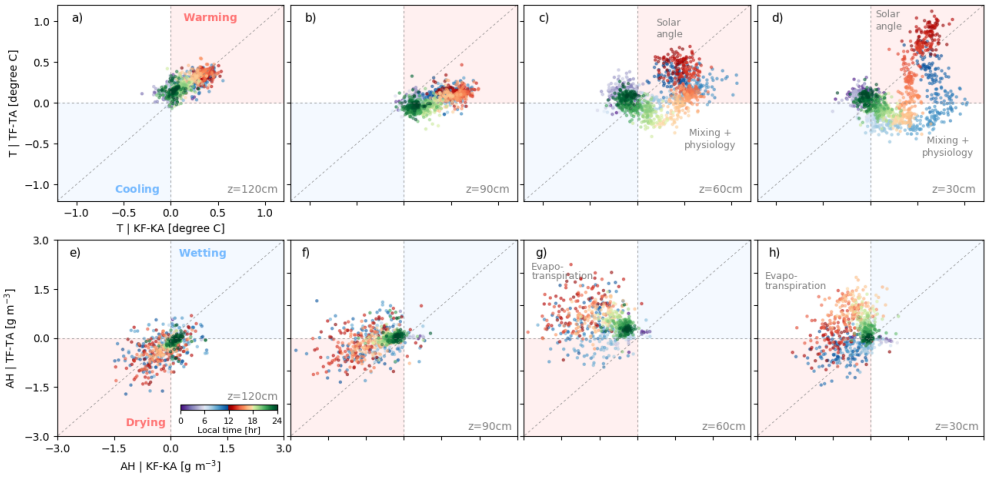

Figure 4.7 The effects of FACE on the diurnal evolution of temperature (T; upper panels) and absolute humidity (AH; lower panels) for Koshihikari (x-axis) and Takanari (y-axis) at all measurement heights in clear sky conditions. The color denotes the time of day. The average height of Koshihikari was 91 cm, while Takanari was slightly shorter with 86 cm.

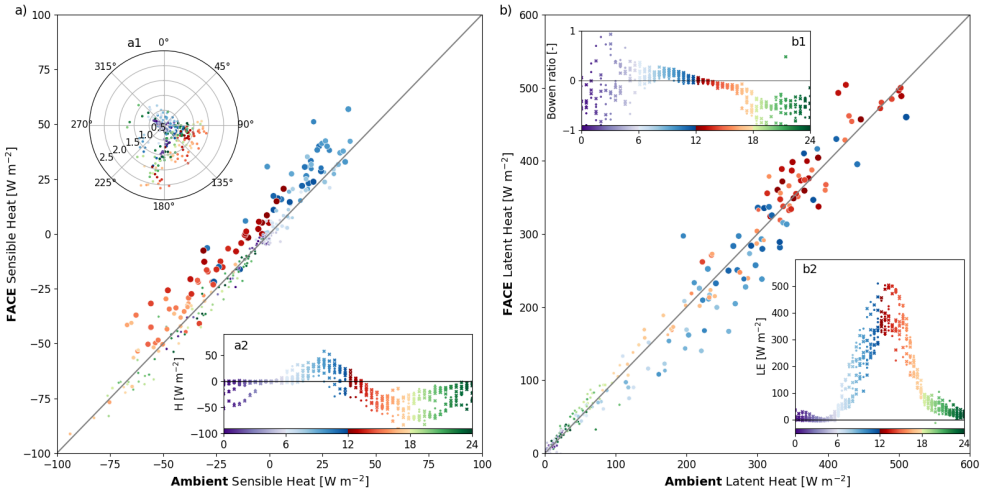

Figure 4.8 Surface flux relationship of (a) the sensible heat (H) and (b) latent heat (LE) are shown for ambient (x-axis) and FACE (y-axis). The circle size is determined by the PAR levels (Fig. 4.2a). The insets in a show wind direction and speed in m s^{-1} (a1) and the diurnal evolution in sensible heat flux (a2) for ambient (circles) and FACE (crosses) conditions. In b, the diurnal evolution in Bowen ratio (b1) and latent heat flux (b2) are shown. Ambient is represented with circles, while FACE is visualized with crosses. In all plots, the color denotes the time of day.

temperatures to rise, resulting in similar warming for both varieties. In the afternoon, a stronger increase in air temperatures was found in Koshihikari again, while in-canopy humidity levels were lower due to reduced transpiration rates (Fig. 4.7e-h). Especially close to the water surface at 30 cm, humidity levels increased faster during the afternoon in Takanari as a consequence of the increased water temperature (thus increased evaporation) and the high transpiration rates (Fig. 4.7h).

Our surface energy balance measurements show the integrated effects of plant architecture, physiology and micro-climate (Fig. 4.8). The distribution of energy over irrigated rice paddies is distinct compared to other crops. In the morning, the sensible heat flux increases as a consequence of an increased canopy temperature (Fig. 4.6), which causes the air temperature to rise. In FACE conditions, the rise in air temperature was accelerated due to stomatal responses to CO_2. Following from our in-canopy temperature and humidity measurements, we ascribe this effect mainly to Koshihikari. Especially in the morning when the wind speed was low (i.e., low mixing), strong effects of the narrowing in stomatal aperture were found in the latent heat flux (Fig. 4.8b). Those effects became less pronounced during noon. One of the reasons could be midday stomatal closure that reduced the signal in latent heat flux differences between FACE and ambient, as well as an increased water temperature and enhanced evaporation rates.

In the afternoon (~14 LT), the atmospheric synoptic condition allowed for the initiation of a daily sea-breeze circulation, causing the wind speeds and subsequently atmospheric mixing to increase. As a consequence of the fractured land-scape in Japan, meaning that rice fields and cities are alternated, warm and dry-air was advected from a nearby city to our experimental site. As a result, the sensible heat flux became strongly negative (i.e., oasis effect), while the latent heat fluxes were maximum due to the relatively dry air.

When the sun set around ~18 LT, the latent heat flux was still positive likely because evaporation was maintained. Furthermore, our results show that the sea-breeze weakened and wind speeds decreased (Fig. 4.8a1). However, since the wind direction was still from the city, the sensible heat flux remained negative, although its magnitude slowly decreased towards zero with decreasing wind speed (Fig. 4.8a).

4.3.3 Effects of shallow clouds on the plant-atmosphere interactions

In the results described above, the focus was on clear-sky weather conditions close to flowering period. In the analysis, clear differences in diurnal patterns in the relations between plants architecture, physiology and micro-climate emerged. However, this approach could cause a biased view on the plant-atmosphere interactions solely caused by the direct component of radiation. For example, a seasonal study on the effect of clear-sky and partly-clouded sky regimes on the uptake of CO_2 showed stronger uptake rates during partly-clouded skies in a mixed forest site (Freedman et al., 2001), which

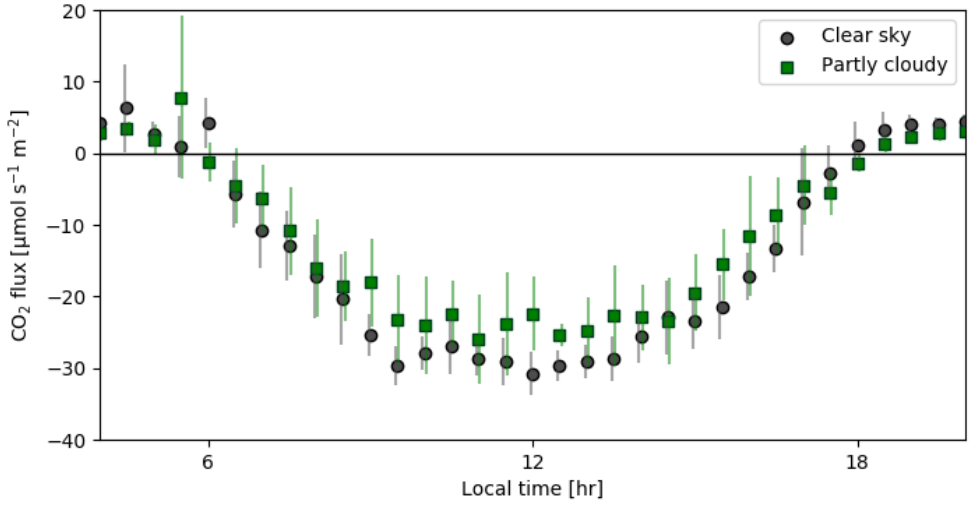

Figure 4.9 Diurnal evolution of the 30 minute CO_2 fluxes for clear sky (black) and partly cloudy (green) weather regimes in ambient conditions. Sunrise is around 6 LT, while sun set is around 18 LT. The points represent the mean flux over the aggregated data (see Fig. 4.2) and the associated error bars are visualized. Note that the error bars for both cases have been shifted slightly to avoid overlap.

was a result of an enhanced diffuse radiation component. It is well-known that the diffuse radiation component has the ability to penetrate more efficiently into the canopy, potentially causing photosynthesis levels to rise depending on conditions (Min & Wang, 2008; Pedruzo-Bagazgoitia et al., 2017). To understand the sensitivity of our results to the direct-diffuse proportion, we aggregated the data during the same time period for partly-clouded sky regimes (Fig. 4.2b). By comparing the maximum clear-sky and partly-clouded diurnal PAR (Fig. 4.2), it became clear that during partly-clouded skies the radiation levels could increase with a maximum of 10 to 20% due to cloud reflection and scattering, although the average PAR was lower compared to clear-sky situations (Fig. 4.2b). However, this did not increase the CO_2 uptake rates (Fig. 4.9). Apart from the lower in-canopy temperature and moisture levels, no large differences were found in the relative in-canopy profiles of temperature, humidity and radiation (Figs. S4.1–S4.3).

4.3.4 Putting our results in perspective

The results presented in this study show the intrinsic relation between rice architecture, physiology and micro-climate. Measurements were performed on distinct rice varieties that strongly differ in both architecture and physiology. Our results show the importance of canopy architectural differences on the surface fluxes, that might affect land-atmosphere processes. In most biogeochemical models, in-canopy variables (e.g., PAR, T_a, CO_2) are assumed to be constant throughout the canopy (e.g., Zhang et al., 2014 and refs therein), which is caused by a lack of detailed in-canopy measurements. However, with the current advancement in computational power and improved understanding of modelling concepts, it is expected that multi-layer canopy approaches including radiative transfer and calculations of the profiles of the state variables will become more a rule than an exception. Therefore, detailed in-canopy measurements are becoming essential to move forward.

Our results are based on an aggregation of days based on sky regimes (i.e., clear sky, partly cloudy), which makes our results more consistent and robust than when a single 'golden' day approach would have been followed. However, since our measurements were only performed in one region (i.e., Kanto area, Japan), extrapolation of our results to other regions needs to be done with caution. For example, the FACE facility used in this study had a strong consistent daily synoptic (i.e., regional weather) cycle. At around ~14 LT, a sea-breeze facilitated enhanced atmospheric mixing and the advection of dry and warm air from urban areas, which altered the plant-atmosphere interaction and caused an enhanced evaporative flux.

As for every FACE study, our FACE results are only capturing the plant physiological response to increasing levels of CO_2, which is only part of the equation when

considering climate change. Temperature and humidity levels will likely act as an additional external forcing to the plant-atmosphere responses, which are not taken into account in this study. Furthermore, as a consequence to an altered atmospheric composition (e.g., humidity levels), the light quality and radiation distribution will likely change. As a result, the partitioning into diffuse and direct radiation will be affected, with vast effects on the plant-atmosphere interaction. Moreover, with the expectation that urban areas expand, the influence of dry and warm air advection will likely increase in the future, impacting the rice micro-climate.

Our results show that moving from Koshihikari to Takanari as the primary variety in Japanese rice production would result in strong effects on crop micro-climate potentially leading to higher production under elevated CO_2 conditions. Although the current experimental setup did not allow for surface energy balance measurements of solely Koshihikari or Takanari, our in-canopy vertical profiles clearly showed a distinct micro-climate and subsequent surface forcing to the overlying atmosphere. Especially the increased photosynthetic capacity of Takanari results in a damped response to atmospheric warming when CO_2 levels rise, as the enhanced stomatal conductance and transpiration associated with this higher photosynthesis of Takanari resulted in a larger evaporative cooling effect compared to Koshihikari. The difference in canopy temperature between the two varieties (~0.8 degree C) is greater than that reported in our recent model study (~0.5 degree C) (Fig. 7-c in Ikawa et al., 2018), which assumed the same canopy architecture between the two varieties. This emphasizes the importance of considering differences in architectural effects between varieties in future modeling studies. Additionally, we showed that a variety that produces closed canopies such as Koshihikari may suffer from heat-induced spikelet sterility under typical climate change scenarios. Spikelet sterility occurs when a plant fails to set grain due to abiotic stresses (e.g., Satake & Yoshida, 1978). Many processes that affect grain setting are temperature driven and vulnerable to heat (i.e., 35–40 degrees C) (Hasegawa et al., 2011). Even an exposure of one hour is sufficient to induce sterility (Jagadish et al., 2007). Current crop models account for sterility by simulating the diurnal patterns in temperature, humidity, transpirational cooling and flowering time (e.g., van Oort et al., 2014 and refs therein). Some models predict variables for standardized atmospheres (e.g., sinusoidal temperature behavior), while the actual atmosphere is prone to fluctuations (Fig. 4.4c,d). Progress in the recent years, shows that modelling the panicle temperature instead of air temperature leads to more accurate results (Yoshimoto et al., 2011). Following from our results, we suggest to take into account plant architecture, solar angle and suggest to parameterize turbulent mixing (i.e., function of wind speed). By so doing, we expect a more solid evaluation on the risk of spikelet sterility in future climates.

4.4 Conclusion

The plant-atmosphere interaction is strongly influenced by both plant physiology and architecture. In this study, two contrasting rice varieties were investigated in ambient and elevated CO_2 environments: Takanari, a high-yielding indica variety with an open canopy structure and Koshihikari, a standard japonica variety with a more closed canopy top. Detailed micro-climate measurements were performed and the results were related and quantified to plant physiological and architectural characteristics. Our data are optimal for validating models related to detailed plant-atmosphere interactions in current and future climates.

Our ambient setup showed a strong diurnal interplay between solar angle (i.e., row orientation), canopy structure, plant physiology and daily recurring synoptic weather (i.e., sea breeze circulation), of which the latter initiated warm and dry air advection from urban areas. An open-canopy structure allowed for enhanced atmospheric mixing and increased in-canopy radiation levels (up to 3 times), thereby increasing in-canopy temperature and reducing the absolute humidity. In ambient conditions, Takanari had a drier and warmer in-canopy environment throughout the day, except at noon. Especially in the afternoon, Koshihikari experienced higher levels of absolute humidity (up to 2 gram per m^3 more), which was caused by increased water temperatures in combination with its closed canopy structure, allowing for a build-up in moisture.

In an elevated CO_2 environment (i.e., FACE), different results were found, where Takanari's in-canopy absolute humidity was higher and air temperature levels were lower compared to Koshihikari. This was caused by a strong physiological effect in combination with the likely enhanced evaporation rates from the water surface.

To conclude, plant architecture has a strong impact on the daily micro-climate and drives the interaction between plant physiology and boundary-layer processes through vertical exchange. Both physiology and architecture differ considerably both between and as shown here within crop species. Under elevated CO_2 conditions, an open-canopy rice variety such as Takanari will result in higher production while at the same time reducing the risk of spikelet sterility.

4.5 Acknowledgements

We thank team members of the Tsukuba FACE at the Institute for Agro-Environmental Sciences, NARO, for their help in the field and laboratory measurements, with special thanks to Hitomi Wakatsuki. This work was supported in part by the Ministry of Agriculture, Forestry and Fisheries, Japan, through a research project entitled "Development of technologies for mitigation and adaptation to climate change in agriculture, forestry and fisheries" and the Netherlands Organisation for Scientific Research (NWO; grant no. 823.01.012). Raw and processed data used in this manuscript

is stored on a public repository that can be accessed through http://doi.org/10.4121/uuid:625cf57e-aaf0-4be4-bfb0-f2f48e6c78fb.

4.6 Supplementary material

Following our data selection approach as described in the main manuscript, we show the in- canopy profiles of radiation (S4.1), temperature and absolute humidity (S4.2) and the effects of FACE (S4.3) during partly-cloudy days.

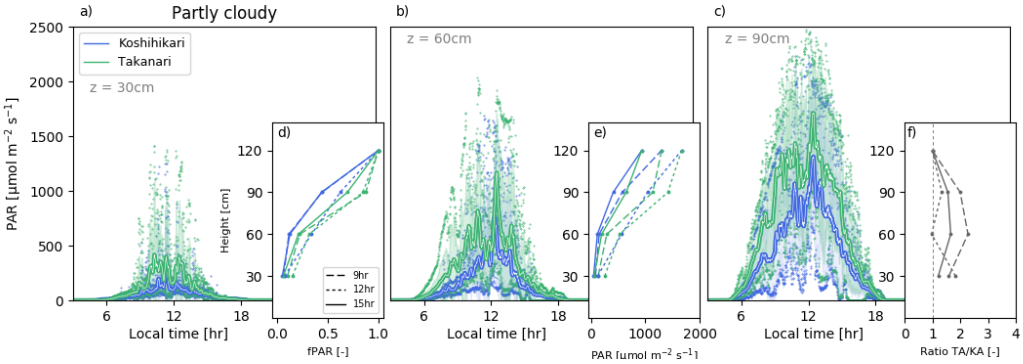

Figure S4.1 The diurnal evolution of in-canopy photosynthetically active radiation (PAR) during partly cloudy days of Koshihikari (blue) and Takanari (green) at a) 30cm, b) 60cm and c) 90cm above soil. Note: d), e), f) are stand-contained figures showing the PAR relation over the four measurements heights (i.e., 30, 60, 90, 120 cm). d) the PAR in-canopy profiles normalized with above canopy PAR for 9, 12 and 15LT (15min averaged). e), the absolute values of d). f), the ratio Takanari ambient (TA) vs Koshihikari ambient (KA) is visualized over three time stamps. The average height of Koshihikari was 91 cm, while Takanari was slightly shorter with 86 cm.

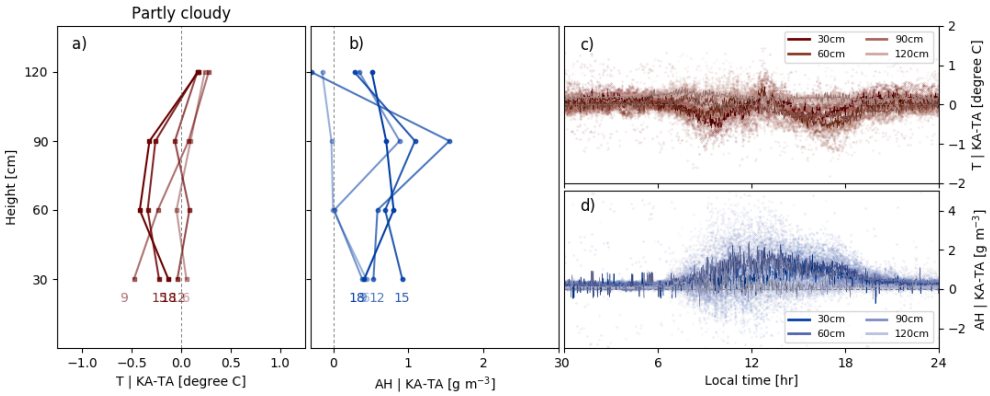

Figure S4.2 The diurnal evolution of the difference in in-canopy temperature (T; red) and absolute humidity (AH; blue) between Koshihikari ambient (KA) and Takanari ambient (TA) in partly-cloudy conditions. In a) and b), the difference in the diurnal evolution in vertical profiles between Koshihikari ambient and Takanari ambient are shown for temperature and absolute humidity, respectively. In c) and d), the diurnal difference between KA and TA for all heights are shown. Scatter points are retrieved from actual measurements, while the lines represent a moving average (15min).

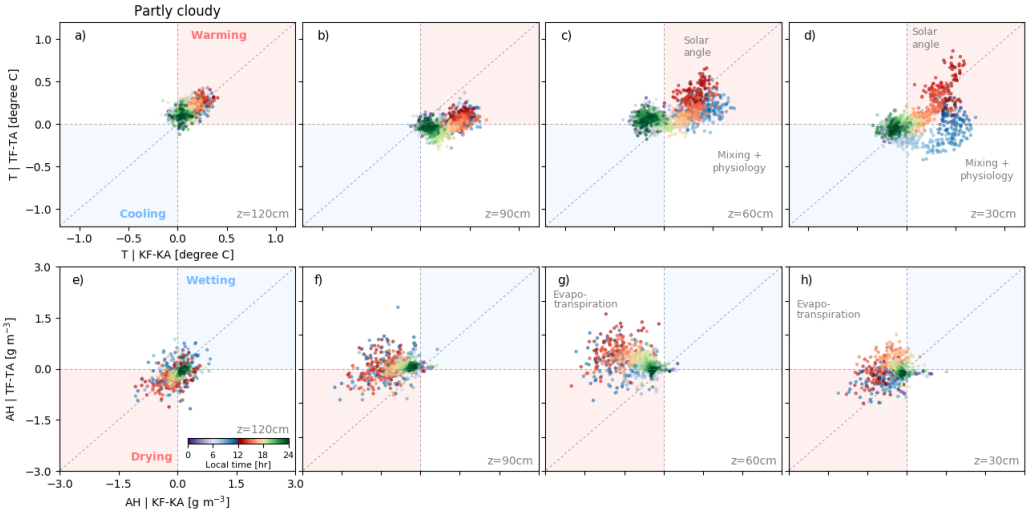

Figure S4.3 The effects of FACE on the diurnal evolution of temperature (T; upper panels) and absolute humidity (AH; lower panels) for Koshihikari (x-axis) and Takanari (y-axis) at all measurement heights in partly-cloudy conditions. The color denotes the time of day. The average height of Koshihikari was 91 cm, while Takanari was slightly shorter with 86 cm.

5

Impact of future warming and enhanced [CO_2] on the vegetation-cloud interaction

To account for the nonlinear and local vegetation-atmosphere interactions, the effects of increases in carbon dioxide and temperature on the vegetation-atmosphere-cloud interaction are studied from a bottom-up approach. Using the 3D large-eddy simulation technique coupled with a CO_2-sensitive dynamic plant physiological submodel, we aimed to spatially and temporally understand the surface and vegetation forcing on the coupled land-atmosphere interactions in future scenarios. Our simulations were based on first principles and explicitly take into account plant responses, atmospheric turbulence and cloud development on a diurnal scale. Four simulations were designed: a control simulation for current conditions, an enhanced carbon dioxide simulation (current + 200 ppm), an elevated temperature simulation (current + 2 K), and a simulation covering the combination of both elevations in temperature and CO_2. With elevations in carbon dioxide, plant transpiration reduced due to stomatal closure, resulting in reduced latent- and increased sensible heat fluxes. Although no effects on cloud cover were found in this simulation, the in-cloud moisture flux was enhanced. Elevations in temperature yielded opposite results with reduced sensible and increased latent heat fluxes, which reduced the turbulent kinetic energy and buoyancy rates, thereby negatively impacting cloud formation. Our future climate mimicking simulation shows minimal changes in the regional energy balance due to offsetting effects between increased temperature and [CO_2], while plant photosynthesis increased and transpiration decreased. Although with nearly similar surface fluxes compared to current conditions, the atmospheric boundary layer was drier, thereby hampering cloud formation and development.

This chapter has been submitted for review with Jordi Vilà-Guerau de Arellano, Xabier Pedruzo-Bagazgoitia, Bert G. Heusinkveld, Niels P. R. Anten and Jochem B. Evers

Our results highlight the necessity of small scales and interactions, which require a bottom-up approach to be able to accurately capture the nonlinear plant-atmosphere interactions. Neglecting these interactions cause the GCMs and NWPs to be liable to misrepresentations when modelling future atmospheres.

5.1 Introduction

Progress in the accuracy of Numerical Weather Prediction (NWP) and Global Climate Modelling (GCM) has been constrained by our understanding of local and regional nonlinear feedbacks on short and long time scales, our ability to translate these feedbacks into numerical equations, and the computational resources available. Although the modelling concepts and aims of NWPs and GCMs are distinct, they are generally limited by the similar lack in scientific understanding and modelling concepts. Since the seminal book of Richardson (1922), enormous progress has been made in modelling future weather and climate (e.g., Reichler & Kim, 2008; Bauer et al., 2015). Current NWP models are able to predict weather regimes up to 5 days ahead rather accurate with forecasts skills close to 90% (Bauer et al., 2015), while GCMs projections are able to constrain temperature anomaly projections between roughly +1.5 to +4.5 degrees Celsius with doubling atmospheric carbon dioxide concentration (i.e., equilibrium climate sensitivity) (Collins et al., 2013). The wide range in the projected equilibrium climate sensitivity can be ascribed to highly nonlinear processes that act on a wide range of spatiotemporal scales (Cox et al., 2013), related to, for instance, seasonal variation, ice sheet and glacier melting, increased methane release by permafrost melting (e.g., Wickland et al., 2006), et cetera. Although the increase in model complexity has not strongly reduced key uncertainties, it has revealed the sensitivity and importance of specific processes essential on the general circulation. With the identification of the representation of clouds and convective organization as one of the main reasons for the wide inter-model spread (Boucher et al., 2013; Stevens & Bony, 2013; Sherwood et al., 2014; Bony et al., 2015), it is essential to enhance our fundamental understanding of these processes and subsequently improve parameterizations to be able to improve the representation of these sub-grid processes in NWPs and GCMs.

Moist convection and cloud development are strongly affected by surface characteristics (Rieck et al., 2014; Sikma & Vilà-Guerau de Arellano, 2019). Incoming solar radiation is redistributed in soil heat and turbulent energy fluxes based on the soil moisture content, vegetation activity and characteristics, and surface roughness. With the recent improvement in computational resources and increased fundamental understanding of physical as well as modelling concepts, it is now possible to simulate the interconnected processes that drive vegetation-atmosphere dynamics. Latest

research has shown that sub-grid scale plant-cloud interactions has vast effects on processes related to the partitioning in direct and diffuse radiation (Pedruzo-Bagazgoitia et al., 2017), dynamic surface heterogeneity (Sikma et al., 2017) and in-cloud moisture transport (Sikma & Vilà-Guerau de Arellano, 2019). Furthermore, cloud shading and surface flux responses has shown to affect secondary circulations and atmospheric convection (Gronemeier et al., 2017; Xiao et al., 2018), as well as the organization of clouds (Jakub & Mayer, 2017). Although these processes and interactions occur on local and small scales, they determine the regional atmospheric state (Katul et al., 2012) and affect the development of deep convection (Keil et al., 2008), thus control the onset of extreme weather events. Therefore, it is crucial that these processes are accounted for in NWPs and GCMs.

With the gradual increase in atmospheric levels of carbon dioxide and subsequent increase in air temperature, the plant-atmosphere feedback is changing. As a consequence of the strongly non-linear behavior of the processes involved, it is very likely that current vegetation-atmosphere parameterizations do not hold in future climates. To demonstrate this, we investigated the physical processes underlying the response to increases in CO_2 and temperatures and their subsequent effect on moist convection. Our approach entailed a systematic procedure in which we cover the entire spectrum of atmospheric moisture, namely from plant transpiration, atmospheric turbulence to the development of cumulus clouds. As the latter transports moisture from the atmospheric boundary layer into the troposphere, thereby affecting the Earth's albedo, they strongly contribute to the uncertainty in climate projections (Boucher et al., 2013; Sherwood et al., 2014). Furthermore, our study highlights the sensitivity of sub-hourly and sub-kilometer small-scale interactions on the regional scale; processes that are generally neglected in GCMs and NWPs.

5.2 Research strategy

5.2.1 Methodology

Our simulations have been designed to understand the sensitivity of plant-atmosphere-cloud interactions on elevations in CO_2 and temperature and complement to our previous research for current atmospheric conditions on the cloud-plant forcing (Sikma et al., 2017) and subsequent plant-clouds feedback (Sikma & Vilà-Guerau de Arellano, 2019). Our control case has been designed based on observations and represents a typical West-European early-autumn day with cumulus development over 90% covered moist C3 grassland. Using the Dutch Atmospheric Large-Eddy Simulation (DALES4.1; model details in Heus et al., 2010; Ouwersloot et al., 2017), we simulate the first principles of atmospheric dynamics in very high detail. The surface boundary

conditions are provided by a mechanistic plant physiological sub model, A-gs (details in Jacobs & de Bruin, 1997; Ronda et al., 2001), and utilizes a two big-leaf approach that simultaneously treats direct and diffuse radiative effects caused by in-cloud scattering (details in Pedruzo-Bagazgoitia et al., 2017). Note that due to computational restrictions, we utilized a one-dimensional radiative transfer model, which does not capture the radiative aspects to elevations in CO_2. Our domain is set at 48 km x 48 km x 5.5 km (x, y, z) with resolution of 50 m x 50 m x 12 m (x, y, z).

To gain additional insight in the cloud characteristics, other than cloud cover and the liquid water path, we calculated the cloud width and cloud optical depth. These variables quantify the local impact of cloud properties on the vegetation. Namely, cloud width gives an indication on the surface area that is affected, while the cloud optical depth gives information on the radiative impact at the surface. Cloud width has been calculated using 2D autocorrelation based on Taylor (1922) and Stull (1988), details are described in Horn et al. (2015). Cloud optical depth (τ) has been calculated according to Stephens (1978), see Eq. 7 therein, and is based on the cloud droplet radius and the vertically integrated column of liquid water (i.e., liquid water path).

Model cases and the DALES model are made available on GitHub:
https://github.com/dalesteam/cases_dales/tree/4.1/futureatmosphere

5.2.2 Numerical experiments related to present and future conditions

The vegetation-atmosphere interactions are highly nonlinear and encompass a complex interrelated system. To capture the essential vegetation-atmosphere interactions, a mechanistic land surface model is coupled to our DALES model. In Figure 5.1, we show the parameterized vegetation key variables that influence the surface fluxes, and subsequently the atmosphere and cloud development. As an example, a few response curves modelled by the A-gs submodel are shown in Fig. 5.1b-d, indicating the nonlinearity in the feedbacks of Fig. 5.1a. As changes in cloudiness affect the radiation (Fig. 5.1b), the optimal temperature regime (Fig. 5.1c) as well as the water vapor deficit (D_s; Fig. 5.1d), it is essential to understand the underlying processes that control the vegetation-atmosphere interaction in future atmospheres. Inspired by the vegetation to atmosphere feedback, we designed four Large-Eddy Simulations (LES) to identify the consequences of the two main components of climate change, namely increased levels of carbon dioxide and the subsequent elevated air temperature. As visible in Fig. 5.1, these atmospheric forcings act on different vegetation components that result in distinct vegetation-atmosphere interactions. Therefore, we expect each nonlinear vegetation response to differently affect the atmospheric state.

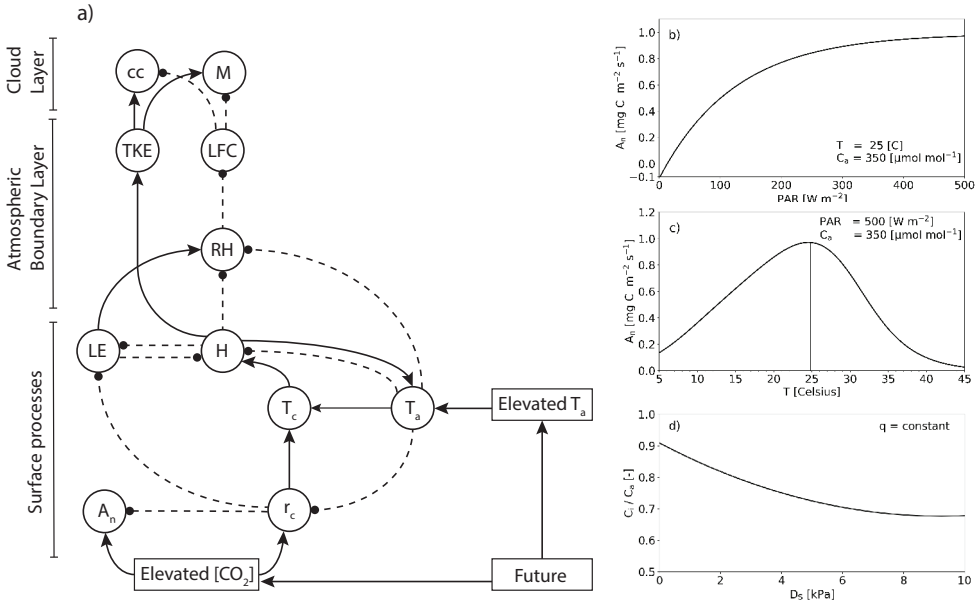

Figure 5.1 In a), the forcing diagram is visualizing simplified vegetation interactions and its effect on selected atmosphere and cloud characteristics. Positive effects are represented by solid arrows, while negative effects are shown with dashed lines and dotted arrowheads. The meaning of the variables is as follows: A_n, assimilation of CO_2; r_c, canopy resistance; T_c, canopy temperature; T_a, air temperature; H, sensible heat flux; LE, latent heat flux; RH, relative humidity; TKE, turbulent kinetic energy; LFC, level of free convection; cc, cloud cover; M, mass flux. The graphs show the non-linearity by means of response functions modelled by the A-gs submodel of b) A_n versus PAR, c) A_n versus T_c and d) ratio plant internal- and atmospheric carbon concentration (C_i/C_a) versus vapor pressure deficit (D_s).

In this study, we holistically investigate the consequences of climate change by means of four simulations:

1. **Current:** current Western-Europe temperature and [CO_2] conditions (initial boundary layer values of 284 K (~ 11 C) and 418 ppm, respectively).
2. **Carbon:** increased initial [CO_2] profile with 200 ppm (i.e., fertilization effect).
3. **Temperature:** increased initial air temperature profile with 2 Kelvin (i.e., warming effect).
4. **Future:** combination of the "Carbon" and "Temperature" simulations, of which both the air temperature and [CO_2] profiles are increased.

Note that all our simulations start with equal initial relative humidity profiles in order

to ensure similar initial thermodynamic conditions. Although uncertainty related to future changes in relative humidity is high (see e.g., Vicente-Serrano et al., 2018), this approach ensures no artificial variability based on initial conditions. Our analysis focuses on state variables that have a driving effect on the plant-atmosphere-cloud interactions. In the next section, we gradually build up by focusing on the effects of the atmospheric forcing on the vegetation response, atmospheric state and cloud development.

5.3 Results

We start our analysis at the vegetated surface, which will be followed by the atmospheric boundary-layer and subsequent effects on cloud properties. In terms of forcing and feedbacks, the Carbon and Temperature simulations initially act as a forcing to the vegetation, which will adapt and subsequently act as a forcing itself to the overlying atmosphere. As a consequence of nonlinearity, vegetation-atmosphere-cloud interactions will likely be affected compared to current atmospheres. Our aim is to understand the sensitivity of current vegetation-atmosphere-cloud interactions and feedback to the carbon and temperature forcing, and to determine the future consequences on a diurnal scale. Note that an overview of the vegetation to atmosphere-cloud forcing is summarized in Figure 5.1a.

5.3.1 Vegetation effects and responses

Plant physiological processes are affected by increased levels of carbon dioxide and elevated temperature in numerous ways. In Figure 5.2, virtual vegetation responses at canopy level that are known to influence the atmospheric state are shown at 14:00 UTC. With increasing temperature, we found the canopy resistance lowered (Fig. 5.2a), assimilation of CO_2 to be increased (Fig. 5.2b) and the water-use efficiency to be

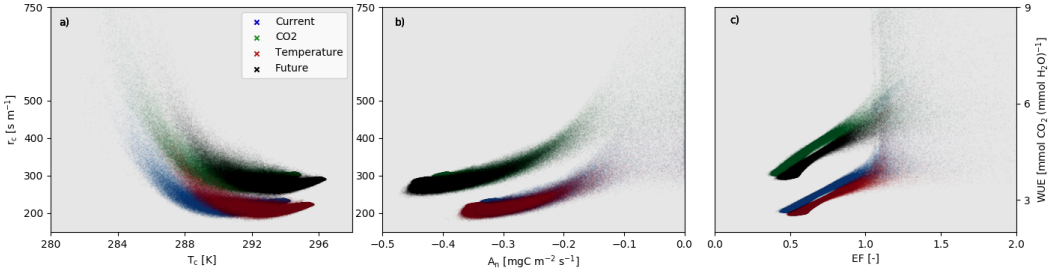

Figure 5.2 Overview of spread in plant related surface variables affected by cumulus shading and atmospheric perturbations for all 921.600 surface points at 14:00 UTC. In a) canopy resistance (r_c) versus canopy temperatures (T_c), b) canopy resistance (r_c) versus assimilation of CO_2 (A_n) and c) water use efficiency (WUE) versus evaporative fraction (EF) is shown, for current, elevated CO_2, elevated temperature and Future situations. Evaporative fraction and water-use efficiency are defined as follows: EF = LE / (H+LE), WUE = -A_n / LE, with LE and H as respectively the latent and sensible heat flux.

lowered (Fig. 5.2c). The lowering of the water-use efficiency is explained due to temperature driven nonlinearity in the assimilation of CO_2 (Fig. 5.1c) and latent heat flux. The vegetated surface has been parameterized by means of response functions (details in Jacobs & de Bruin, 1997) and as in our simulations the noon temperature (~21 C) is well below the optimal value (25 degrees C; 298 K) for maximum photosynthesis (Fig. 5.1c). With our Current simulation's canopy temperature peaking at ~21 C, there is ample room for increased photosynthesis levels when the canopy temperature would rise.

The plant physiological response to increasing [CO_2] is a narrowing of the stomatal aperture (i.e. increase canopy resistance), and the associated reduction in transpiration causes a rise in canopy temperature with ~0.5 K (Fig. 5.2a). Due to enhanced atmospheric [CO_2], the difference in partial pressure between plant intercellular and atmospheric levels increases. This led to higher photosynthesis levels (Fig. 5.2b), thus enhanced carbon assimilation. As photosynthesis increases and transpiration declines, the water-use efficiency obviously was increased (Fig. 5.2c).

When combining both the temperature and carbon effects (i.e., Future simulation), canopy temperatures increased with nearly 2.5 K compared to current situations. Mainly from the increase in [CO_2], the canopy resistance increased (25%; Fig. 5.2a). Since the optimal temperature for photosynthesis is 298 K, carbon assimilation rates are much (~30%) higher compared to current situations. Since carbon assimilation increased more strongly than transpiration, the water-use efficiency increased (Fig. 5.2c).

Cumulus shading introduces short-lived radiative perturbations that affect canopy temperature and canopy resistance. Since the effects of shading on canopy temperature and resistance are both nonlinear, it is interesting to note that the relations between these variables are affected (Fig. 5.2a), as is visible in the shifted relation between canopy resistance and canopy temperature. This is an indication that the plant-cloud interaction might be altered in future climates. An evaporative fraction of higher than 1 is reached due to hovering cumulus, which decrease the radiation vastly, thereby causing a negative sensible heat flux (Fig. 5.2c).

To get a quantitative insight in the variability of the vegetation processes that have an impact on the surface fluxes, we present all the vegetation and surface data over a period of 2 hours, as shown in Figure 5.3. Each box plot comprises nearly 110 million surface points and covers both sunlit and cloud shaded areas.

The effect of the forcing is clearly visible on the surface fluxes. With elevated levels of CO_2, latent heat (LE) fluxes were strongly reduced (13%), resulting from strong increases

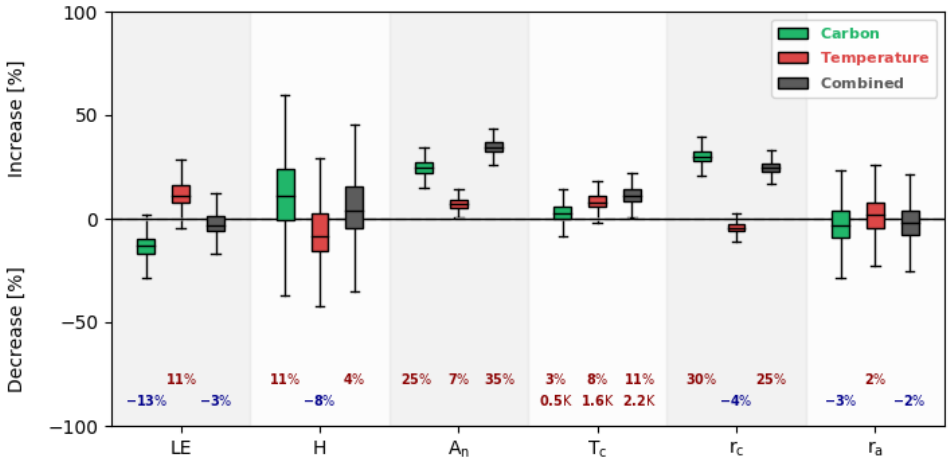

Figure 5.3 Spread in the increase or decrease in surface related variables compared to current atmospheres between 13:00 and 15:00 UTC. Each box plot encompasses ~110 million virtual surface observations. The box extends from the lower to upper quartile values, with a line at the median. The whiskers extend from the box to show the range of the data. From left to right, the latent (LE) and sensible heat (H) fluxes, assimilation of CO_2 (A_n), canopy temperature (T_c), canopy resistance (r_c) and aerodynamic resistance (r_a) are shown. The numbers on the bottom show the increase or decrease of the median compared to current atmospheres. Regarding canopy temperature, the averaged differences in Kelvin are shown as well.

in canopy resistance (30%). The sensible heat (H) fluxes were increased in a similar magnitude compared to the decrease in LE (11%), although they show a large variability due to intermittent radiative perturbations that affect the surface heating. On average, the increase in sensible heat was related to an average increased canopy temperature of 0.5 K as a response to stomatal closure. The ground heat flux was not affected much, with on average a maximum difference of 3 W m^{-2} between the simulations (not shown). Furthermore, a strong increase (25%) in carbon assimilation was found resulting from more optimal photosynthetic conditions (i.e. elevated atmospheric [CO_2]).

When increasing the air temperature with 2 K, the canopy temperature increases which subsequently resulted in lowered canopy resistance (-4%; i.e., increased canopy conductance) that increased the carbon assimilation (7%; Fig. 5.3). Note that a temperature increase larger than 2 K might result in negative carbon assimilation and transpiration effects, as is shown in Fig. 5.1c. Furthermore, due to the decreased canopy resistance, plant transpiration increased, which had an impact on the LE (11%; Fig. 5.3). Consequential, the response of H to increasing atmospheric temperatures yields to a reduction of 8%.

When combining the elevations in temperature and carbon in the Future simulation,

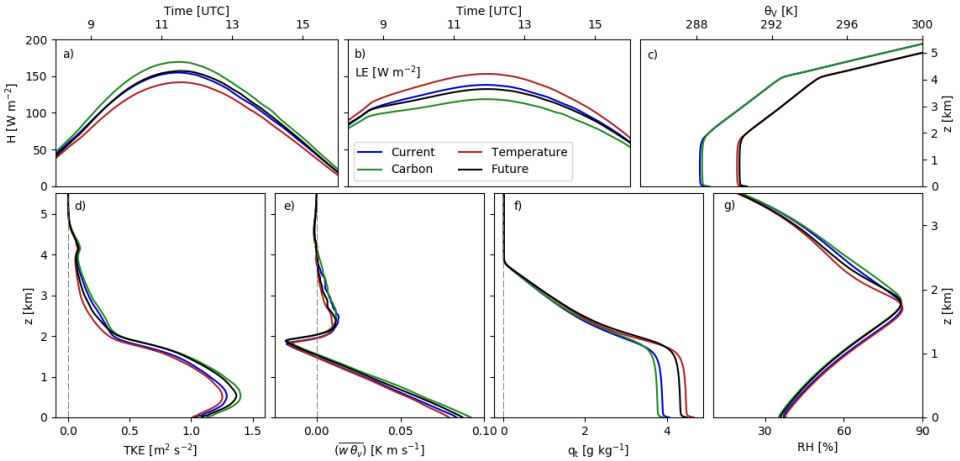

Figure 5.4 Comparison of domain averaged profiles of the simulated atmospheres at 14:00 UTC. In a) sensible heat flux (H), b) latent heat flux (LE), c) the virtual potential temperature (θ_v), d) the turbulent kinetic energy (TKE), e) the buoyancy flux ($\overline{w'\theta_v'}$), f) the total specific moisture content (q_t) and g) relative humidity (RH) is shown.

we found that the CO_2 and temperature effects on the surface energy balance are offset. Nearly similar surface energy fluxes were found compared to current situations (Fig. 5.3). However, due to the increased atmospheric temperatures and elevated [CO_2], the stomatal aperture narrows (25%) resulting in a minor reduction in transpiration (3%), higher canopy temperatures (2.2 K) and consequently higher carbon assimilation (35%). As expected, no large effects on the aerodynamic resistance were found, indicating that no large difference on the mechanistically (i.e., wind) driven vertical land-atmosphere transfer occurs.

5.3.2 Impact on the atmospheric boundary layer

With the increased air temperature and elevated CO_2 concentration, the vegetation adapts and moves into a new state (Fig. 5.2). This change could be viewed as a subsequent surface forcing on the overlying atmospheric boundary layer when compared to current atmospheres. This surface forcing, as visualized in terms of sensible (H) and latent heat (LE) fluxes in Figure 5.4a-b, affect the vertical atmospheric profiles.

Following from stomatal closure, the increase in sensible and decrease in latent heat fluxes for the Carbon run caused the atmosphere to slightly warm (0.3 K; Fig. 5.4c) with respect to the current situation. Furthermore, consequential from enhanced sensible heat, the rates of turbulent kinetic energy (TKE) were increased in the lower atmosphere (~0.1 m^2 s^2; Fig. 5.4d), as well as the buoyancy rates increased (Fig. 5.4e). This indicates

more vigorous motions in the atmospheric boundary layer that are favorable for cloud development, although the specific moisture content (Fig. 5.4f) and relative humidity levels (Fig. 5.4g) were lowered due to decreased plant transpiration, which hamper cloud development.

The increase of 2 K that has been exerted on the atmospheric profiles for the Temperature and Future simulations is well visible in Fig. 5.4c. In the Temperature simulation, lower levels of TKE and buoyancy were found, which are the effect of enhanced plant transpiration that cools the surface, thus reduce (increase) the sensible (latent) heat fluxes. The effects of plant transpiration are visible in the moisture profiles as well, where both absolute (Fig. 5.4f) and relative (Fig. 5.4g) moisture profiles show an increase.

Although the surface energy balance of the Future simulation is nearly similar compared to the Current simulation, the vegetation characteristics are distinct (Fig. 5.3). Due to stomatal closure and elevated canopy temperatures, the boundary layer temperature is slightly increased, as well as the atmospheric moisture content is decreased. An interesting finding is the relatively high TKE compared to Current, which is mainly caused by the horizontal components of momentum (not shown). With reduced plant transpiration and elevated air temperature compared to Current, the moisture profiles show a drying and the relative humidity is lowered slightly (~3%; Fig. 5.4g).

5.3.3 Consequences on moist convection

Boundary layer clouds arise on top of moist updrafts originating from the atmosphere boundary layer (ABL), where the updrafts are strongly influenced by the vegetation (LeMone & Pennell, 1976; Moeng & Sullivan, 1994). The increase in [CO_2] and atmospheric temperature has consequences on the vegetation-atmosphere interactions, which can affect cloud development through a series of nonlinear interactions. As a result of the drying effect of plant stomatal closure to elevated [CO_2] (Fig. 5.4f), the surface heat fluxes and TKE were increased (Fig. 5.4a-b, d). Although the ABL was relatively slightly drier (Fig. 5.4g), the increased vertical movements resulting from high TKE and surface fluxes compensate for this with no significant changes in cloud cover and cloud width as a result (Fig. 5.5a-b), when compared to current atmospheres. The increase in momentum followed from the increase in surface fluxes and TKE, however, increases the total moisture flux and liquid water path (LWP), which shows that clouds are able to grow deeper (i.e., reach higher altitudes). As a consequence, the clouds transport more moisture from the ABL towards the troposphere (Fig. 5.5c-d). Note that from changes in cloud width and cloud cover the spatial effects on the cloud population can be inferred. For instance, the cloud cover

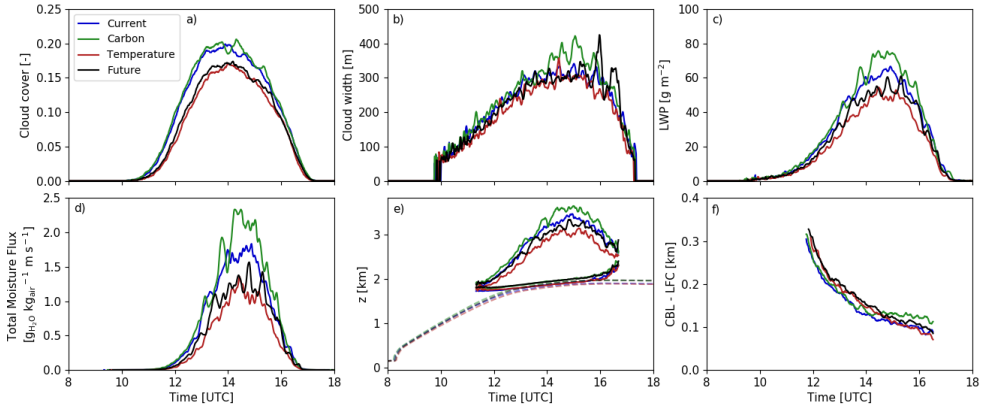

Figure 5.5 Temporal evolution of horizontally averaged cloud related variables for all simulated atmospheres. In a) the cloud cover, b) cloud width, c) liquid water path (LWP), d) total moisture flux are shown. In e) the boundary layer height (dashed) and cloud bottom and top are shown, where in f) the distance between the boundary layer height (CBL) and level of free convection (LFC) is visualized.

can be similar in cases with less and wider clouds, or with more and smaller clouds.

With elevations in atmospheric temperature a reduction in cloud cover was found (Fig. 5.5a), consequential from weak levels of TKE and buoyancy fluxes, which was a consequence of the decreased sensible heat flux and increased latent heat flux (Fig. 5.4a-b). The reduction in energy (thus momentum) was enough to reduce cloud cover to 16% (i.e., ~15% reduction compared to Current), as updrafts were not able to overcome the inversion layer and reach the level of free convection (LFC), which is the level where the latent heat release due to condensation is enough to make the clouds positively buoyant (e.g., see positive $\overline{w'\theta_v'}$ above 2km in Fig. 5.4e). It is interesting to note that the cloud width was not affected much (Fig. 5.5b), while strong reductions in the total mass flux and liquid water path were found (Fig. 5.5c-d). This indicates that more shallow clouds were developing that dissolved before reaching the LFC (i.e., forced clouds), while a similar width was maintained.

In the Future simulation, multiple interactions occur that control the ABL and cloud development (Fig. 5.1a & 5.5e). As both the elevations in CO_2 and temperature yields nonlinear responses to plant physiological processes (Fig. 5.1b-d), disentangling the plant-atmosphere interactions becomes more difficult. An example is visible in Figure 5.4a-b, d. The surface fluxes are quite similar compared to the Current run, although the TKE is larger. This indicates more turbulent energy (thus momentum) in the ABL that would be favorable for cloud development. However, as shown in Fig. 5.5a, cloud cover has reduced to 16%. We explain this finding as follows. The increased atmospheric [CO_2] reduces stomatal aperture (Fig. 5.2a), thereby enhancing the ABL TKE by more

thermal movement (Fig. 5.4d) that causes the ABL to warm and dry (Fig. 5.4c, 5.4g). However, this drying is not compensated for by increased latent heat release by transpiration, as was the case for the Temperature simulation (Fig. 5.4b). As a result, relative moisture levels were (slightly) lowered in the Future simulation compared to the Temperature simulation (Fig. 5.4g). Furthermore, with the narrowing in stomatal aperture, the ABL temperature has risen slightly (Fig. 5.4e), which additionally lowered the relative humidity levels. As a consequence, there was a ~30 minutes lag in transition layer thickness (i.e., convective boundary layer (CBL) minus the level of free convection (LFC)) compared to the Current simulation (Fig. 5.5f). In other words, an equal transition layer thickness was reached 30 minutes later in the Future simulation compared to the Current simulation. Since the sensible heat flux peaked at around 11:00 UTC, any delay in cloud development due to a too large transition layer results in less energy for cloud development. Consequential of this lag, this lowered the cloud cover and total in-cloud moisture transport and thickness (Fig. 5.5c-d).

The effects of the larger transition layer thickness can be found in Fig. 5.6, where the temporal evolution of the distribution in cloud optical depth is shown. The averaged values during maximum cloud cover (between 13:00-15:00 UTC) are shown in Table 5.1. Both visually as in Table 5.1, it is clear that the majority of the clouds in our domain are shallow (tau between 0-5 [-]). Especially in the Temperature and Future simulations, the relative contribution of shallow clouds increases. This corroborates our conclusion that the majority of clouds dissolve before reaching the LFC in the Future simulation. As a result, the amount of thicker (tau of 10+) clouds in these simulations was reduced as well.

Table 5.1 The averaged distribution of cloud optical depth between 13:00 and 15:00 UTC, as visualized in Figure 5.6. All numbers are in percentages, with the numbers between brackets showing its relative contribution to the total cloud cover.

	Cloud optical depth (tau)							
Tau [-]	0-2	2-5	5-10	10-15	15-25	25-50	50+	Total
Current	8.2 (44)	3.4 (18)	2.6 (14)	1.4 (8)	1.4 (8)	1.2 (6)	0.5 (3)	18.6 (100)
Carbon	8.2 (43)	3.4 (18)	2.7 (14)	1.5 (8)	1.5 (8)	1.3 (7)	0.6 (3)	19.2 (100)
Temperature	7.8 (50)	2.9 (18)	2.1 (13)	1.0 (6)	1.0 (6)	0.7 (4)	0.2 (1)	15.7 (100)
Future	7.7 (47)	3.0 (18)	2.2 (14)	1.1 (7)	1.1 (7)	0.9 (6)	0.3 (2)	16.3 (100)

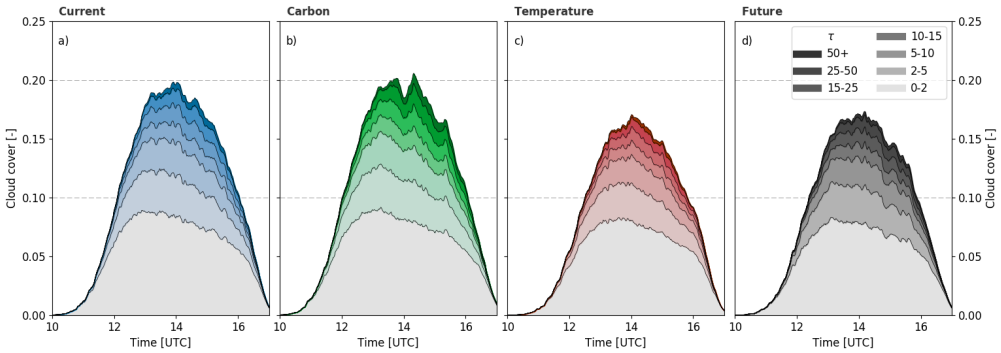

Figure 5.6 Temporal evolution of cloud cover with the distribution of cloud optical depth (τ) in shading.

5.4 Discussion

This study was designed to understand the vegetation response and its subsequent forcing to atmospheric elevations in temperature and [CO_2]. Although these atmospheric variables are essential in driving future land-atmosphere processes, there are other components of the climate system we were not able to simulate. In this section, we discuss some of these components.

The importance of modelling the full spectrum of land-atmosphere interactions becomes clear when comparing our results with the findings of Vilà-Guerau de Arellano et al. (2012), who applied a similar methodology using a spatially zero-dimensional model. In this approach, the averaged response of the atmosphere to plant dynamics was modelled, thus the spatial dynamic surface and atmospheric heterogeneity was not explicitly taken into account. Inferred from the difference between the atmosphere boundary layer height and lifting condensation level (e.g., cloud base), they concluded that boundary layer clouds are suppressed in CO_2-rich atmospheres. However, while our Future modelled results converge, the intermediate responses to CO_2 and temperature yields opposite conclusions. Interestingly, both studies are based on the same set of initial observations and utilize a similar mechanistic photosynthesis model that has been generally applied (e.g., in the European NWP model ECMWF: Boussetta et al., 2013). Although the findings on the surface energy balance broadly overlap, the interactions and turbulent exchange with the atmospheric boundary layer are distinct.

Since GCMs and NWPs neglect local and dynamic heterogeneity, as well as local land-atmosphere turbulent responses. This comparison highlights the importance of considering the sub-grid scale local land-atmosphere processes when modelling future atmospheres, as ignoring these processes might lead to serious misrepresentation of

the plant-atmosphere interactions that drive the future atmosphere.

To be able to compare the findings of our simulations, we systematically introduced elevations in air temperature and [CO_2]. However, future atmospheres will likely not be always as similar as modelled in our study, meaning that, for instance, weekly-to-monthly changes in synoptic situation (Vihma, 2014), the vegetation biomass (Brouder & Volenec, 2008) or the soil moisture state (Seneviratne et al., 2010) might occur, which latter affecting the vegetation state. However, since our focus is on the sub-hourly scale and the atmosphere has adapted to the modelled surface boundary forcing, we don't expect large deviation in the interactions as presented in this study. However, seen the nonlinearity in interactions (Fig. 5.1), it is recommended that an extensive analysis of the sensitivity of the vegetation-atmosphere-cloud interactions on all atmospheric and vegetation components is performed. Special focus on the canopy temperature is advised, as following from our submodel the assimilation of CO_2 and transpiration strongly declines above 25 degrees C. At the moment, unfortunately, the computational resources do not allow for such an extensive sensitivity study at this moment.

With increased concentrations of CO_2, the radiation balance will likely be affected with an enhancement in the longwave radiative component (Cao et al., 2010). Although the in-cloud partitioning between direct and diffuse radiation was taken into account in this study, the longwave radiative enhancement was not. An implication of an increase in longwave radiation could be an increased temperature effect. As a consequence, plant transpiration would have increased in our numerical experiments, with decreased sensible- and increased latent heat fluxes as a result. This would weaken the atmospheric vertical movements, thereby reducing TKE and buoyancy, with a likely result of hampered cloud development. Furthermore, as a consequence from the increased atmospheric temperature by longwave radiation, the atmospheric stability might increase as well, which might hamper the vertical development of clouds.

One strong uncertainty we were not able to take into account is the gradual adjustment of the vegetation to a changing climate. Examples are uncertainties related to the development in canopy structure (e.g., increase in leaf area index) (Anten et al., 2004) or leaf thickness and nitrogen allocation (Bezemer et al., 1998). Furthermore, when genotypic responses of plants to climate change are considered, the vegetation distribution might be affected through natural selection (Van Loon et al., 2015). As most plant species respond differently to atmospheric perturbations, regional or even continental changes in the surface energy balance might occur that have a strong effect on the land-atmosphere interactions.

5.5 Conclusion

The future vegetation-atmosphere-cloud interactions were simulated and systematically studied to understand whether current interactions will hold when temperature and CO_2 levels rise. We focus on the interaction occurring at the sub-hourly and sub-kilometer scale, in which the time scales of vegetation responses and cumulus development are characterized by similar time scales in the order of minutes.

Our findings show that a temperature elevation of 2 degree Celsius yields enhanced plant transpiration, thus latent heat fluxes, while reducing the sensible heat fluxes. As a consequence, the turbulent thermal intensity reduced, as quantified by lower vertical values of TKE and buoyancy. Consequently, the cloud cover and mid-tropospheric moisture transport reduced. In turn, an enhancement of 200 ppm in carbon dioxide leads to a closure of the stomatal aperture, leading to enhanced sensible- and diminished latent heat fluxes with, respectively, 11% and 13%. As a consequence, the atmospheric boundary layer became slightly warmer and drier. However, with enhanced TKE and buoyancy levels, cloud cover was maintained compared to current conditions, while the in-cloud moisture transport and thickness was increased due to enhanced momentum. Our Future simulation, which combines both elevations in temperature as [CO_2] showed an offset in the energy balance, resulting in nearly similar fluxes as in current conditions. However, with a narrower stomatal aperture, thus reduced transpiration, air temperature slightly increased and atmospheric humidity levels were reduced. As a consequence, the level of free convection (LFC) was higher, causing a thicker transition layer. Resulting from this, most forced clouds did not reach the LFC and dissolved. This caused notable reductions in cloud cover as well as moisture transport and cloud thickness.

Our results highlight the need to incorporate nonlinear plant photosynthetic responses to atmospheric perturbations and forcings in GCMs and NWPs, which is essential in the carbon and hydrological balance. Neglecting these local and small-scale processes will yield large uncertainties and misrepresentations when modelling future plant-atmosphere interactions.

5.6 Acknowledgements

The authors want to thank Tim Voskamp for his contributions. This study was supported by a grant from the Netherlands Organisation for Scientific Research (NWO; 823.01.012). The numerical simulations were performed with the supercomputer facilities at SURFsara and were sponsored by the National Computing Facilities (NCF) foundation and NWO under project SH-312-14.

6

General discussion

In this thesis, a comprehensive dataset was combined with the state-of-the-art Dutch Atmospheric Large-Eddy Simulation model. With the ability to explicitly simulate the atmosphere with the LES model, we were able to reach unprecedented detail as compared to the NWPs and GCMs and introduced novel aspects, such as dynamic plant stomatal responses, the partitioning in direct and diffuse radiation and the inclusion of a wide range in background winds, which has led to new insights on the vegetation-atmosphere-cloud interaction. However, some simplifications and assumptions were introduced. In this section, we address these assumptions and the uncertainties involved.

Furthermore, as for all field experimental designs that mimic future environments, uncertainties and unavoidable limitations are involved. Later in this section, we will discuss these uncertainties and limitations, and discuss the likely consequences.

6.1 Static heterogeneity, secondary circulations and moist convection

All our simulations entailed homogeneous and identical surface properties, as for instance vegetation type, cover, state and height, as well as soil moisture content and soil type. As a consequence, our surface is a simplification of reality, as no natural static (i.e., spatially fixed) heterogeneity is accounted for. This consequentially yields one identical initial stomatal response to atmospheric perturbations. However, we have to note that when the surface is perturbed, spatial dynamic heterogeneity will occur, which can be initiated by both atmospheric state variables or as a consequence to radiative components.

Investigations concerning static heterogeneity are often performed by prescribing the land-surface in dry or wet patches following a checkerboard pattern (e.g., Lee et al., 2018). Following from a difference in surface temperature caused by the patch's moisture content, surface energy fluxes are altered. As the sensible heat fluxes are elevated at the dry patches, convection starts to occur with subsequent moist air advection from the adjacent wet patches (Cioni & Hohenegger, 2017). Consequently, secondary circulations are formed which size is determined by the boundary layer depth and patches size (van Heerwaarden et al., 2014; Lee et al., 2018). Recent investigations indicate that heterogeneous surfaces influence the onset of convection by enhancing the upward momentum compared to homogeneous conditions (van Heerwaarden & Vilà-Guerau de Arellano, 2008; Rieck et al., 2014), thereby triggering the formation of deep convection. Lee et al. (2018) showed that a threshold patch size of 5 km triggers deep convection, while smaller patch sizes enhance atmospheric boundary layer mixing, which results in shallow clouds. The process behind this interaction is the formation of cold and moist pools above the boundary layer (van Heerwaarden & Vilà-Guerau de Arellano, 2008; Kang & Ryu, 2016), which are formed by repetitive penetrations of turbulent plumes into the free atmosphere (Kang & Ryu, 2016) that would be favorable for the development of deep convection (Zhang & Klein, 2010). However, this theory is challenged by Rieck et al. (2014), who shows that the available surface energy gradually reduces over the warm patches as a consequence of cloud formation (i.e., consequence from dynamic heterogeneity). As the LES modelling study of Rieck et al. (2014) simulates full interactions between land surface, clouds and radiation, they were able to conclude that the aforementioned decoupled studies likely overestimated the surface fluxes below cloudy areas, that might have produced too strong secondary circulations. Moreover, the observational and simulation study of Hohenegger & Stevens (2012) challenged the gradual moistening theory as well. They showed that the transition from shallow (i.e., cumulus congestus) into deep (i.e., cumulonimbus) convection normally occurred within 2 hours over land, which is much faster than the time needed to moisten the cloud layer (max. 10 hours). They imply from

their results that moisture convergence might be more important than local surface fluxes to trigger deep convection (Hohenegger & Stevens, 2012). Furthermore, as discussed by Avissar & Schmidt (1998) and Lee et al. (2018), a weak background wind of 2 to 2.5 m s^{-1} was sufficient to significantly decrease the effects of static surface heterogeneities by enhanced horizontal mixing, thereby hampering moist convection.

Apart from the research of Hohenegger & Stevens (2012) and Rieck et al. (2014), all aforementioned conclusions are based on decoupled and idealized surfaces. As Earth's surfaces are rarely similar to checkerboard patterns, the actual static heterogeneous land-atmosphere interactions are likely more chaotic and damped. The novel study of Xiao et al. (2018) combined realistic static heterogeneous land-surface with dynamic land-atmosphere interactions, and investigated the impact of static and dynamic surface heterogeneity on moist convection. In their case, they found that dynamic heterogeneity can have a larger impact on cumulus cloud development than static heterogeneity.

The discrepancy between Xiao et al. (2018) and the research described earlier in this section shows the need for more detailed land-atmosphere interactions with respect to modelling moist convection. Especially in a changing climate, where feedbacks are altered and extreme weather events become more likely, a fundamental understanding of the local feedback mechanisms is essential in order to reduce uncertainties related to the modelling of moist convection.

6.2 Radiative transfer and cloud microphysics

Over the course of writing this thesis, advancement in the development of radiative transfer parameterizations and its incorporation in high-resolution atmospheric models has occurred. Only very recently the computational resources allowed to include these 3-D radiative transfer parameterizations when modelling cumulus convection with dynamic heterogeneity. To date of writing, only Jakub & Mayer (2017) have investigated the three-dimensional radiative effects by cumulus convection over interactive surfaces. In that study the interactive component only yielded dynamic surface fluxes and neglected plant responses, with the latter being accounted for in this thesis. As in this thesis a one-dimensional radiative transfer solver has been applied, we discuss the possible limitations of our results. Furthermore, we briefly extend on the effects of cloud microphysics and its consequences on radiation later in this section.

The explorative LES study of Schumann et al. (2002) focused on the effects of cumulus shading on the turbulent flow. At the cloud shaded location an instantaneous zero heat flux was modelled. They concluded by analyzing two zenith angles that a shift in cloud shading, thus non-zero zenith angle, only had minor impact on the turbulent field. Different results were obtained by Gronemeier et al. (2017), who analyzed four zenith angles over homogeneous and striped static heterogeneous surfaces. The main

objective of their LES study was to investigate the impact and effects of cloud shading on the initiation of secondary circulations and subsequent effects on cloud-field characteristics. They found over homogeneous surfaces that cloud shadows trigger secondary circulations, whose strength depends on the solar zenith angle. Over static heterogeneous surfaces, the effect of cloud shading was found to be dependent on the solar zenith angle: the strength of secondary circulations was reduced with small solar zenith angles, while for large angles the circulation depended on the static heterogeneous pattern. With respect to cloud-field characteristics, they concluded that small zenith angles favored the development of small and short-lived clouds, while at large zenith angles the clouds grew deeper with an extended life time. Jakub & Mayer (2017) took this one step further and analyzed the potential of dynamic heterogeneity to organize cumulus convection. As their LES study compared the role of 1-D and 3-D radiative heating combined with a sensitivity on the background wind speed, solar zenith and azimuth angles, we are able to use their conclusions to put this thesis in perspective. Main findings from Jakub & Mayer (2017) show that the organization of cumulus clouds is affected by the way we are representing and treating radiative transfer models. Their 3-D radiative transfer simulation formed cloud streets in the absence of a background wind perpendicular to the sun's incident direction, whereas their 1-D approximation produced randomly positioned clouds. Comparing these findings with our work, we expect that a more realistic radiative transfer parameterization yields changes in the organization of the cumulus population. This might have consequences for the results described in Chapter 2 and 3 of this thesis, as cloud streets might form with lower background winds. As a consequence, the vegetation-cloud coupling regime in cloud street situations might be more pronounced than was initially thought. This indicates that the range in background wind for the transitional regime –as described in Chapter 3– is narrower, which implies that the cloud induced heterogeneous vegetation streaks can be formed with lower background winds. This would strengthen the vegetation-atmosphere coupling, which increases the impact on moist convection. However, this deduction is rather speculative and no strong conclusions can be given at this point.

Another assumption that has been made in this thesis is related to the clouds' droplet size. Since modelling cloud microphysical processes is rather complex and quite computationally expensive, a fixed effective droplet radius of 10 μm is considered based on observations from Baker & Latham (1979). However, in shallow cumulus clouds, variations in droplet radius of 4 to 20 μm are observed (Siebert & Shaw, 2016). As the partitioning in direct and diffuse radiation is based on cloud scattering, thus the droplet radius, our results might be affected by this assumption. This could have consequences on our photosynthesis responses to cloud shading. However, since a

sensitivity performed by Pedruzo-Bagazgoitia et al. (2017) only yielded minor effects of the droplet size on the shortwave downward radiation, we don't expect significant deviations from our current conclusions.

Furthermore, the simulated cumulus clouds in this thesis are so-called warm clouds, meaning that we neglect the development of ice crystallization (Taylor et al., 2016). Ice crystallization in intermediate stages of cloud development are normally influencing the onset of precipitation, as the ice crystals grow due to vapor deposition. When ice crystals grow, they slowly descend and initiate a chain of processes that results in precipitation (i.e., coalescence). The onset of precipitation in growing mature cumulus clouds hampers its development, as the downward directed precipitation hampers the upward going air. Furthermore, as a consequence of increased levels of soil moisture where precipitation occurs, the spatial variability in surface fluxes is increased (Chen et al., 2012). In this capacity, ice crystallization can have an influence on the formation and development of cumulus clouds. As only a minor part of fair-weather cumulus clouds precipitate, and we specifically focus on the development of the shallow variety, our conclusions on vegetation-cloud interactions are not affected. However, when simulating deep convection this process is essential and needs to be taken into account.

6.3 The Free-Air CO_2 Enrichment (FACE) experiment

Free-Air CO_2 Enrichment (FACE) experiments enable us to investigate the effects of CO_2 enhancement under natural conditions. They are primarily used to study the effects of elevated CO_2 on physiology, growth and production of plants under field conditions and there are FACE set ups for vegetation ranging from grasslands, crops (e.g., rice, wheat and soybean), temperate forests and recently there is one being developed for tropical rainforest. The FACE technique provides a strong advantage over enclosed systems (i.e., greenhouses or closed- and open-topped chambers) as it is affected by the natural fluctuations. Although in these enclosed environments it is easier to maintain stable levels of the variables under investigation (e.g., [CO_2] or temperature), they miss plant-atmosphere feedbacks and interactions that occur in nature, as for instance secondary-circulations, boundary layer dynamics, et cetera. In Chapter 4 of this thesis, results from a rice FACE experiment are presented and the interactions between two distinct rice varieties and the atmosphere are discussed. In this section, we elaborate on the discussion regarding FACE systems and focus on the possible limitations of FACE systems in general and the possible consequences this might entail on future yield projections.

By analyzing 120 primary peer-reviewed articles, including data from 12 large-scale FACE experiments, Ainsworth & Long (2004) showed that the fertilization effect of CO_2 differed between FACE experiments and enclosed chamber experiments regarding

rice and wheat. The exact reasons for the deviations remains unclear, but are very likely a consequence of the experimental setup and methodology (McLeod & Long, 1999; Long et al., 2004). For example, in chamber experiments the environmental variables are stable (i.e., managed), while in FACE experiments these are more prone to natural fluctuations. As a consequence, the experimental setup has direct effects on the microclimate, which affects the growth and interaction of these plants to an environmental forcing (e.g., elevated CO_2 or temperature). This implies that the experimental methodology has direct implications on the conclusions regarding future yield projections.

Although the FACE technique avoids many limitations as experienced by chamber methods, the results of the FACE experiments fail to match the theoretical increase in photosynthesis that could be obtained by elevated [CO_2] (Leakey et al., 2009). To understand whether this might be a consequence of the FACE technique, we need to focus on its limitations. In state-of-the-art FACE environments, CO_2 is released through tubes at the borders and carried by wind over the plots under investigation. Since wind is used as the carrier gas, it ensures minimal microclimatic perturbations compared to injection methods. The disadvantage, however, is that a spatial dilution gradient occurs across the treatment plot (McLeod & Long, 1999; Nakamura et al., 2012). Another consequence of this method, is that the operation and accuracy of the FACE system is dependent on atmospheric conditions. For instance during very calm atmospheric conditions, atmospheric air packages that contain very high [CO_2] are advected over the canopy (Fig. 6.1). If those atmospheric conditions are a consequence of the continental or regional synoptic weather, this could strongly influence the outcomes of the experiment as a prevailing wind gradient effect would occur across the plot. During windy conditions, the FACE technique will perform well on average (McLeod & Long,

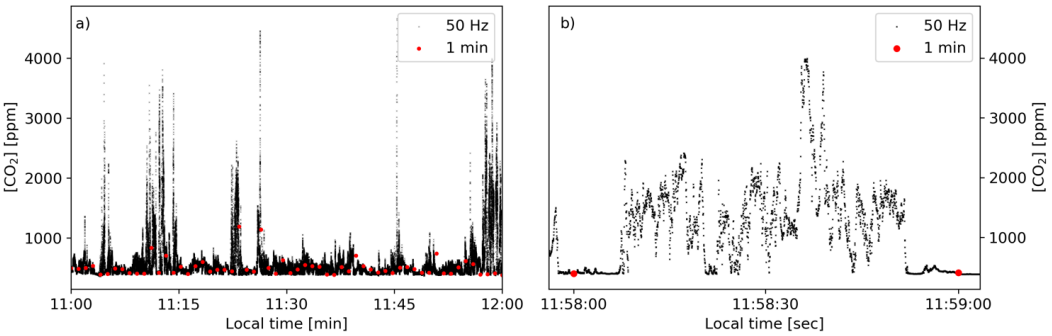

Figure 6.1 Temporal variability of CO_2 concentration ([CO_2]) in the FACE setup measured with an IRGASON at 50Hz on a clear sky day between a) 11-12 local time and b) 11:58 and 11:59. The black dots show data at 50Hz, while the red dots visualize instantaneous measurements at 1 minute.

1999; Nakamura et al., 2012). However, on very short time scales (i.e., less than 1 minute) larger fluctuations are present that arise due to turbulent mixing of the overlying air, which is visualized in Figure 6.1. It is questionable whether these fluctuations are perceived by the plants and how they would affect the net CO_2 exchange. As shown by Cardon et al. (1994, 1995), these fluctuations can have implications for the water use efficiency and could dramatically affect the time averaged stomatal conductance. This implies that the fluctuations occurring in FACE setups might have implications on future yield projections.

As FACE plots encompass a relatively small area (~240 m^2), they are isolated islands of elevated [CO_2] within an experimental field, which likely has physical and biological consequences as the surrounding atmosphere deviates significantly from that in the FACE plot (McLeod & Long, 1999). For instance, packages of ambient air pollute the FACE experimental treatment due to atmospheric turbulent mixing. In other words, the plant-atmosphere interactions of the surrounding vegetation by means of plant transpiration and surface energy balance are polluting the FACE micro-climate, with the strongest effects expected on humidity levels and the vapor pressure deficit (McLeod & Long, 1999). This might have influenced the micro-climate measurements in our FACE experiment, as these fluctuations could have affected the measurements of the open canopy of Takanari more than the closed canopy of Koshihikari.

When taking the aforementioned limitations, the findings of Cardon et al. (1994, 1995) and the conclusion from Leakey et al. (2009) into account, it strongly indicates that (unavoidable) misrepresentations in the future yield projections occur. Furthermore, the inclusion of FACE experimental data in steady-state models is another point of concern. As it is unclear how the plants perceive the fluctuations of the artificial modulated atmosphere, it is unavoidable that misrepresentations are present in the parameterizations of steady-state based plant models. As these models as well are used to assess the impact of future climate change on yield projections, and also neglect the fact that synoptic weather and regional patterns are subject to change, it is very likely that yield projections are prone to large uncertainties. However, novel modelling approaches arise that are soon able to simulate in three dimensions the interactions between the plant architecture and micro-climate. These functional-structural plant models (FSPM; see Evers et al., 2018) simulate growth and morphology of individual plants that interact with their environment. This allows for detailed simulations on the organ scale and could be used to challenge current hypothesis on plant-atmosphere interactions. Furthermore, when combined with an extensive observational dataset of micro-climate measurements, the FSPM approach could yield new knowledge on detailed plant-atmosphere interactions under current and future CO_2 conditions.

6.4 Outlook

The work presented in this thesis encompasses interdisciplinary research by combining knowledge from plant and atmospheric sciences. In the last decades, these lines of research were mostly separated. However, with the Earth's climate changing, uncertainties in both projections of the atmospheric (i.e., weather patterns) and plant processes (i.e., food security) are arising. Furthermore, the increase in understanding of vegetation-atmosphere processes as well as increased model resolution, give rise to the need for a better understanding of the vegetation-atmosphere system on small spatiotemporal scales. In this section, an outlook will be given with a focus on vegetation-atmosphere interactions.

One of the main priorities is the improvement of the carbon and hydrological balance in NWPs and GCMs. Although promising progress is already occurring, with for instance the ocean-atmosphere coupling in the European NWP model ECMWF, we expect a vast improvement of the predictive skill when more focus is laid on the inclusion of essential local land-atmosphere processes and better performing land-surface submodels. To achieve this, focus needs to be shifted from a global scale to a more regional scale, which would be in line with the advancement in model resolution over the last decades. Although current parameterizations will likely need to be adapted when more details come into play, the modelling community could be inspired from the LES studies that are currently performed with ever growing domain sizes.

Another priority is related to surface heterogeneity. Almost all LES studies are based on idealized surface conditions, albeit homogeneous surface with dynamic heterogeneity, or static checkerboard pattern heterogeneity. Although this approach allows for systematic sensitivity analysis, which highlights the areas of 'quick wins', it makes it difficult to extrapolate these results to situations with natural variability. With computational resources becoming less expensive and the availability of datasets by satellites is increasing, it would be a step forward if the LES community would introduce more realistic surface characteristics alongside the idealized cases. This entails low to high vegetation, but also a better understanding of up-scaled canopy physiological characteristics ranging from tropical forests to mid-latitude grasslands. The more natural surface characteristics and vegetation-atmosphere interactions of course need to be validated with a complete set of observations. For this, regional campaigns that encompasses a holistic approach, and focusses on minutely-to-hourly measurements of surface fluxes, soil and plant characteristics and responses, atmospheric profiles and cloud characteristic, would greatly improve the understanding of vegetation-atmosphere interactions. Furthermore, to improve the mechanistic plant physiological models and explore the sensitivity of the measured plant-atmosphere interactions, the FSPM approach could be used. Although, due to computational restrictions, no

coupled FSPM-LES approach is feasible in the coming years, the FSPM could be used to validate the mechanistic plant models used in atmospheric models and explore the sensitivity of plant-atmosphere interaction to for instance drought, increased temperature or elevated [CO_2], et cetera.

Although not incorporated in the LES model version used in this thesis, more advanced 3-D radiative transfer models are currently developed and implement. Combined with a better microphysical model, more realistic vegetation-cloud interactions will likely be obtained. This holds for the improvement of future atmosphere modelling as well, since greenhouse gases impact the longwave radiative component and aerosols scattering likely influences the shortwave component. This makes the 3-D radiative transfer model a vital component for future LES models. Incorporation of these radiative transfer models have the benefit of more interdisciplinary research, for instance to the effect of cloud microphysics, aerosols and greenhouse gases on the vegetation responses, which determines the carbon uptake and strongly affect the hydrological balance through surface flux modifications.

Regarding observational studies that aim to understand future plant-atmosphere interactions, progress would be made if observational sensitivity analysis would be performed. This would, for instance, give clarity on the FACE 'island' effect, thus shows the effect of turbulent mixing, as well as would show the nonlinearity in the plant-atmosphere interaction. Although FACE experiments are rather expensive, combining forces with other research groups would allow for more extensive and fundamental research. As a next step, the outcome from these sensitivity experiments could be compared with current modelling outcomes. This methodology might shed light on misrepresentations and would highlight the uncertainty in modelling approaches.

References

Ainsworth, E. A., & Long, S. P. (2004). What have we learned from 15 years of free-air CO_2 enrichment (FACE)? A meta-analytic review of the responses of photosynthesis, canopy properties and plant production to rising CO_2. *New Phytologist*, *165*, 351–372. https://doi.org/10.1111/j.1469-8137.2004.01224.x

Ainsworth, E. A., & Rogers, A. (2007). The response of photosynthesis and stomatal conductance to rising [CO_2]: Mechanisms and environmental interactions. *Plant, Cell and Environment*, *30*(3), 258–270. https://doi.org/10.1111/j.1365-3040.2007.01641.x

Albertson, J. D., Katul, G. G., & Wiberg, P. (2001). Relative importance of local and regional controls on coupled water, carbon, and energy fluxes. *Advances in Water Resources*, *24*(May 2016), 1103–1118. https://doi.org/10.1016/S0309-1708(01)00042-2

Anten, N. P. R., Hirose, T., Onoda, Y., Kinugasa, T., Kim, H. Y., Okada, M., & Kobayashi, K. (2004). Elevated CO_2 and nitrogen availability have interactive effects on canopy carbon gain in rice. *New Phytologist*, *161*(2), 459–471. https://doi.org/10.1046/j.1469-8137.2003.00943.x

Anthes, R. A. (1984). Enhancement of convection by Mesoscale Variations in vegetative Covering in Semiarid Regions. *Journal of Climate and Applied Meteorology*, *23*, 541–554. https://doi.org/10.1175/1520-0450(1984)023<0541:EOCPBM>2.0.CO;2

Avissar, R., & Pielke, R. A. (1989). A Parameterization of Heterogeneous Land Surfaces for Atmospheric Numerical Models and Its Impact on Regional Meteorology. *Monthly Weather Review*, *117*(10), 2113–2136. https://doi.org/10.1175/1520-0493(1989)117<2113:apohls>2.0.co;2

Avissar, R., & Pielke, R. A. (1991). The impact of plant stomatal control on mesoscale atmospheric circulations. *Agricultural and Forest Meteorology*, *54*(2–4), 353–372. https://doi.org/10.1016/0168-1923(91)90013-G

Avissar, R., & Schmidt, T. (1998). An Evaluation of the Scale at which Ground-Surface Heat Flux Patchiness Affects the Convective Boundary Layer Using Large-Eddy Simulations. *Journal of the Atmospheric Sciences*, *55*(16), 2666–2689. https://doi.org/10.1175/1520-0469(1998)055<2666:aeotsa>2.0.co;2

Baker, M. B., & Latham, J. (1979). The Evolution of Droplet Spectra and the Rate of Production of Embryonic Raindrops in Small Cumulus Clouds. *Journal of The Atmospheric Sciences*, *36*, 1612–1615. https://doi.org/https://doi.org/10.1175/1520-0469(1979)036<1612:TEODSA>2.0.CO;2

Barbaro, E. (2015). *Interaction Between Aerosols and Boundary-Layer Dynamics Over Land*. Wageningen University.

Bauer, P., Thorpe, A., & Brunet, G. (2015). The quiet revolution of numerical weather prediction. *Nature*, *525*(7567), 47–55. https://doi.org/10.1038/nature14956

Berner, J., Jung, T., & Palmer, T. N. (2012). Systematic model error: The impact of increased horizontal resolution versus improved stochastic and deterministic parameterizations. *Journal of Climate*, *25*(14), 4946–4962. https://doi.org/10.1175/JCLI-D-11-00297.1

Betts, A. K., Ball, J. H., Beljaars, A. C. M., Miller, M. J., & Viterbo, P. A. (1996). The land surface-atmosphere interaction: A review based on observational and global modeling perspectives. *Journal of Geophysical Research Atmospheres*, *101*(D3), 7209–7225. https://doi.org/10.1029/95JD02135

Bezemer, T. M., Jones, T. H., & Knight, K. J. (1998). Long term effects of elevated CO2 and temperature on populations of the peach potato aphid Myzus persicae and its parasitoid matfcariae Aphidius. *Oecologia*, *116*(1), 128–135. https://doi.org/doi.org/10.1007/s004420050

Bony, S., Stevens, B., Frierson, D. M. W., Jakob, C., Kageyama, M., Pincus, R., … Webb, M. J. (2015). Clouds, circulation and climate sensitivity. *Nature Geoscience*, *8*(4), 261–268. https://doi.org/10.1038/ngeo2398

Boucher, O., Randall, D., Artaxo, P., Bretherton, C., Feingold, G., Forster, P., … Zhang, X. Y. (2013). Chapter 7: IPCC Climate Chnage 2013: The Physical Science - Clouds and Aerosols. In T. F. Stocker, D. Qin, G.-K. Plattner, M. Tignor, S. K. Allen, J. Boschung, … P. M. Midgley (Eds.), *IPCC AR5 Climate Change 2013: The Physical Science Basis*. Cambridge university press. https://doi.org/10.1017/CBO9781107415324.016

Boussetta, S., Balsamo, G., Beljaars, A., Panareda, A. A., Calvet, J. C., Jacobs, C., … Van Der Werf, G. (2013). Natural land carbon dioxide exchanges in the ECMWF integrated forecasting system: Implementation and offline validation. *Journal of Geophysical Research Atmospheres*, *118*(12), 5923–5946. https://doi.org/10.1002/jgrd.50488

Brouder, S. M., & Volenec, J. J. (2008). Impact of climate change on crop nutrient and water use efficiencies. *Physiologia Plantarum*, *133*(4), 705–724. https://doi.org/10.1111/j.1399-3054.2008.01136.x

Cao, L., Caldeira, K., Ban-Weiss, G., Bala, G., & Nemani, R. (2010). Importance of carbon dioxide physiological forcing to future climate change. *Proceedings of the National Academy of Sciences*, *107*(21), 9513–9518. https://doi.org/10.1073/pnas.0913000107

Cardon, Z. G., Berry, J. A., & Woodrow, I. E. (1994). Dependence of the Extent and Direction of Average Stomatal Response in Zea mays L. and Phaseolus vulgaris L. on the Frequency of Fluctuations in Environmental Stimuli. *Plant Physiology*, *105*(3), 1007–1013. https://doi.org/10.1104/pp.105.3.1007

Cardon, Z. G., Berry, J. A., & Woodrow, I. E. (1995). Fluctuating [CO_2] Drives Species-Specific Changes in Water Use Efficiency. *Journal of Biogeography*, *22*(2/3), 203–208. https://doi.org/10.2307/2845911

Carleton, A. M., Travis, D., Arnold, D., Brinegar, R., Jelinski, D. E., & Easterling, D. R. (1994). Climatic-scale vegetation—cloud interactions during drought using satellite data. *International Journal of Climatology*, *14*(6), 593–623. https://doi.org/10.1002/joc.3370140602

Casso-Torralba, P., Vilà-Guerau de Arellano, J., Bosveld, F., Soler, M. R., Vermeulen, A., Werner, C., & Moors, E. (2008). Diurnal and vertical variability of the sensible heat and carbon dioxide budgets in the atmospheric surface layer. *Journal of Geophysical Research Atmospheres*, *113*(12). https://doi.org/10.1029/2007JD009583

Chen, C. P., Sakai, H., Tokida, T., Usui, Y., Nakamura, H., & Hasegawa, T. (2014). Do the rich always become richer? Characterizing the leaf physiological response of the high-yielding rice cultivar takanari to free-air CO_2 enrichment. *Plant and Cell Physiology*, *55*(2), 381–391. https://doi.org/10.1093/pcp/pcu009

Chen, F., & Avissar, R. (1994). Impact of Land-Surface Moisture Variability on Local Shallow Convective Cumulus and Precipitation in Large-Scale Models. *Journal of Applied Meteorology*, *33*, 1382–1401.

Chen, G., Xue, H., Zhang, W., & Zhou, X. (2012). The three-dimensional structure of precipitating shallow cumuli. Part one: The kinematics. *Atmospheric Research*, *122*, 70–78. https://doi.org/10.1016/j.atmosres.2012.04.007

Ciais, P., Sabine, C., Bala, G., Bopp, L., Brovkin, V., Canadell, J., … Thornton, P. (2013). Climate Change 2013: The Physical Science Basis. Contribution of Working Group I to the Fifth Assessment Report of the Intergovernmental Panel on Climate Change. In T. F. Stocker, D. Qin, G.-K. Plattner, M. Tignor, S. K. Allen, J. Boschung, … P. M. Midgley (Eds.), *Change, IPCC Climate* (pp. 465–570). Cambridge university press. https://doi.org/10.1017/CBO9781107415324.015

Cioni, G., & Hohenegger, C. (2017). Effect of Soil Moisture on Diurnal Convection and Precipitation in Large-Eddy Simulations. *Journal of Hydrometeorology*, *18*(7), 1885–1903. https://doi.org/10.1175/jhm-d-16-0241.1

Clark, C. A., & Arrit, R. W. (1995). Numerical Simulations of the Effect of Soil Moisture and Vegetation Cover on the Development of Deep Convection. *Journal of Applied Meteorology*, *34*, 2029–2045. https://doi.org/http://dx.doi.org/10.1175/1520-0450(1995)034<2029:NSOTEO>2.0.CO;2

Collins, M., Knutti, R., Arblaster, J., Dufresne, J. -l., Fichefet, T., Friedlingstein, P., … Wehner, M. (2013). Long-term Climate Change: Projections, Commitments and Irreversibility. In T. F. Stocker, D. Qin, G.-K. Plattner, M. Tignor, S. K. Allen, J. Boschung, … P. M. Midgley (Eds.), *Climate Change 2013: The Physical Science Basis. Contribution of Working Group I to the Fifth Assessment Report of the Intergovernmental Panel on Climate Change*. Cambridge University Press. https://doi.org/10.1002/mds.26688

Cox, P. M., Pearson, D., Booth, B. B., Friedlingstein, P., Huntingford, C., Jones, C. D., & Luke, C. M. (2013). Sensitivity of tropical carbon to climate change constrained by carbon dioxide variability. *Nature*, *494*(7437), 341–344. https://doi.org/10.1038/nature11882

de Boer, H. J., Price, C. A., Wagner-Cremer, F., Dekker, S. C., Franks, P. J., & Veneklaas, E. J. (2016). Optimal allocation of leaf epidermal area for gas exchange. *New Phytologist*, *210*(4), 1219–1228. https://doi.org/10.1111/nph.13929

de Bruin, H. A. R., & Jacobs, C. M. J. (1993). Impact of CO_2 enrichment on the regional evapotranspiration of agro-ecosystems, a theoretical and numerical modelling study. *Vegetatio*, *104–105*(1), 307–318. https://doi.org/10.1007/BF00048161

de Kok, R. J., Tuinenburg, O. A., Bonekamp, P. N. J., & Immerzeel, W. W. (2018). Irrigation as a Potential Driver for Anomalous Glacier Behavior in High Mountain Asia. *Geophysical Research Letters*, *45*(4), 2047–2054. https://doi.org/10.1002/2017GL076158

de Saussure, T. (1804). *Recherches chimiques sur la végétation*. https://doi.org/10.5962/bhl.title.16533

Eastman, R., & Warren, S. G. (2014). Diurnal cycles of cumulus, cumulonimbus, stratus, stratocumulus, and fog from surface observations over land and ocean. *Journal of Climate*, *27*(6), 2386–2404. https://doi.org/10.1175/JCLI-D-13-00352.1

Evers, J. B., Letort, V., Renton, M., & Kang, M. (2018). Computational botany: Advancing plant science through functional-structural plant modelling. *Annals of Botany*, *121*(5), 767–772. https://doi.org/10.1093/aob/mcy050

Ferrare, R. A., Schols, J. L., Eloranta, E. W., & Coulter, R. (1991). Lidar Observations of Banded Convection during BLX83. *Journal of Applied Meteorology*, *30*, 312–326. https://doi.org/https://doi.org/10.1175/1520-0450(1991)030<0312:LOOBCD>2.0.CO;2

Field, C. B., Jackson, R. B., & Mooney, H. A. (1995). Stomatal responses to increased CO_2: implications from the plant to the global scale. *Plant, Cell & Environment*, *18*(10), 1214–1225. https://doi.org/10.1111/j.1365-3040.1995.tb00630.x

Fischer, E. M., Seneviratne, S. I., Lüthi, D., & Schär, C. (2007). Contribution of land-atmosphere coupling to recent European summer heat waves. *Geophysical Research Letters*, *34*(6), 1–6. https://doi.org/10.1029/2006GL029068

Freedman, J. M., Fitzjarrald, D. R., Moore, K. E., & Sakai, R. K. (2001). Boundary layer clouds and vegetation-atmosphere feedbacks. *Journal of Climate*, *14*(2), 180–197. https://doi.org/10.1175/1520-0442(2001)013<0180:BLCAVA>2.0.CO;2

Fu, Q., & Liou, K. N. (1992). On the Correlated k -Distribution Method for Radiative Transfer in Nonhomogeneous Atmospheres. *Journal of the Atmospheric Sciences*. https://doi.org/10.1175/1520-0469(1992)049<2139:otcdmf>2.0.co;2

Garratt, J. R., & others. (1992). *The atmospheric boundary layer. Cambridge atmospheric and space science series*. Cambridge University Press, Cambridge.

Godfray, H. C. J., Beddington, J. R., Crute, I. R., Haddad, L., Lawrence, D., Muir, J. F., … Toulmin, C. (2010). Food Security: The Challange of Feeding 9 Billion People. *Science*, *327*(February), 812–819. https://doi.org/10.4337/9780857939388

Golaz, J. C., Jiang, H., & Cotton, W. R. (2001). A large-eddy simulation study of cumulus clouds over land and sensitivity to soil moisture. *Atmospheric Research*, *59–60*, 373–392. https://doi.org/10.1016/S0169-8095(01)00113-2

Gronemeier, T., Kanani-Sühring, F., & Raasch, S. (2017). Do Shallow Cumulus Clouds have the Potential to Trigger Secondary Circulations Via Shading? *Boundary-Layer Meteorology*, *162*(1), 143–169. https://doi.org/10.1007/s10546-016-0180-7

Grossman, R. L. (1982). An analysis of vertical velocity spectra obtained in the bomex fair-weather, trade-wind boundary layer. *Boundary-Layer Meteorology*, *23*(3), 323–357. https://doi.org/10.1007/BF00121120

Hasegawa, T., Ishimaru, T., Kondo, M., Kuwagata, T., Yoshimoto, M., & Fukuoka, M. (2011). Spikelet sterility of rice observed in the record hot summer of 2007 and the factors associated with its variation. *Journal of Agricultural Meteorology*, *67*(4), 225–232. https://doi.org/10.2480/agrmet.67.4.3

Hasegawa, T., Sakai, H., Tokida, T., Nakamura, H., Zhu, C., Usui, Y., … Makino, A. (2013). Rice cultivar responses to elevated CO2 at two free-air CO2 enrichment (FACE) sites in Japan. *Functional Plant Biology*, *40*, 148–159. https://doi.org/10.1071/FP12357

Hasegawa, T., Sakai, H., Tokida, T., Usui, Y., Yoshimoto, M., Fukuoka, M., … Okada, M. (2016). Rice Free-Air Carbon Dioxide Enrichment Studies to Improve Assessment of Climate Change Effects on Rice Agriculture. In J. L. Hatfield & D. Fleisher (Eds.), *Improving Modelling Tools to Assess Climate Change Effects on Crop Response* (pp. 45–68). Advances in Agricultural Systems Modelling. https://doi.org/10.2134/advagricsystmodel7.2014.0015

Heus, T., Van Heerwaarden, C. C., Jonker, H. J. J., Pier Siebesma, A., Axelsen, S., Van Den Dries, K., … Vilà-Guerau de Arellano, J. (2010). Formulation of the Dutch Atmospheric Large-Eddy Simulation (DALES) and overview of its applications. *Geoscientific Model Development*, *3*(2), 415–444. https://doi.org/10.5194/gmd-3-415-2010

Hoekstra, A. Y., & Wiedmann, T. O. (2014). Humanity's unsustaibable environmental footprint. *Science*, *344*(6188), 1114–1118.

Hohenegger, C., & Stevens, B. (2012). Preconditioning Deep Convection with Cumulus Congestus. *Journal of the Atmospheric Sciences*, *70*(2), 448–464. https://doi.org/10.1175/jas-d-12-089.1

Höhne, N., Blum, H., Fuglestvedt, J., Skeie, R. B., Kurosawa, A., Hu, G., … Ellermann, C. (2011). Contributions of individual countries' emissions to climate change and their uncertainty. *Climatic Change*, *106*(3), 359–391. https://doi.org/10.1007/s10584-010-9930-6

Holland, J. Z., & Rasmusson, E. M. (1973). Measurements of the Atmospheric Mass, Energy, and Momentum Budgets Over a 500-Kilometer Square of Tropical Ocean. *Mon. Wea. Rev.*, *101*(1), 44–55. https://doi.org/10.1175/1520-0493(1973)101<0044:MOTAME>2.3.CO;2

Hong, X., Leach, M. J., & Raman, S. (1995). A sensitivity study of cloud formation by vegeation forcing with different atmospheric conditions. *Journal of Applied Meteorology*, *34*, 2008–2028.

Horn, G. L., Ouwersloot, H. G., Vilà-Guerau de Arellano, J., & Sikma, M. (2015). Cloud Shading Effects on Characteristic Boundary-Layer Length Scales. *Boundary-Layer Meteorology*, *157*(2), 237–263. https://doi.org/10.1007/s10546-015-0054-4

Houghton, J. T., Ding, Y., Griggs, D. J., Noguer, M., van der Linden, P. J., Dai, X., … Johnson, C. A. (2001). Climate Change 2001: The Scientific Basis. In *Third Assessment Report of the Intergovernmental Panel on Climate Change*. (p. 881 pp). Cambridge University Press.

Hov, Ø., Terblanche, D., Jones, S., Ruti, P. M., & Tarasova, O. (2017). Five priorities for weather and climate research. *Nature*, *552*(7684), 168–170. https://doi.org/10.1038/d41586-017-08463-3

Ikawa, H., Chen, C. P., Sikma, M., Yoshimoto, M., Sakai, H., Tokida, T., … Hasegawa, T. (2018). Increasing canopy photosynthesis in rice can be achieved without a large increase in water use—A model based on free-air CO_2 enrichment. *Global Change Biology*, *24*(3), 1321–1341. https://doi.org/10.1111/gcb.13981

Ikawa, H., Ono, K., Mano, M., Kobayashi, K., Takimoto, T., Kuwagata, T., & Miyata, A. (2017). Evapotranspiration in a rice paddy field over 13 crop years. *Journal of Agricultural Meteorology*, *73*(3), 109–118. https://doi.org/10.2480/agrmet.d-16-00011

IPCC. (2014). Climate Change 2014: Synthesis Report. Contribution of Working Groups I, II and III to the Fifth Assessment Report of the Intergovernmental Panel on Climate Change. In R. K. Pachauri & L. A. Meyer (Eds.) (p. 151pp). IPCC, Geneva.

Jacobs, C. M. J., & de Bruin, H. A. R. (1997). Predicting Regional Transpiration at Elevated Atmospheric CO2 : Influence of the PBL–Vegetation Interaction. *Journal of Applied Meteorology*, *36*(12), 1663–1675. https://doi.org/10.1175/1520-0450(1997)036<1663:prtaea>2.0.co;2

Jagadish, S. V. K., Craufurd, P. Q., & Wheeler, T. R. (2007). High temperature stress and spikelet fertility in rice (Oryza sativa L.). *Journal of Experimental Botany*, *58*(7), 1627–1635. https://doi.org/10.1093/jxb/erm003

Jakub, F., & Mayer, B. (2017). The role of 1-D and 3-D radiative heating in the organization of shallow cumulus convection and the formation of cloud streets. *Atmospheric Chemistry and Physics*, *17*(21), 13317–13327. https://doi.org/10.5194/acp-17-13317-2017

Jiang, H., & Feingold, G. (2006). Effect of aerosol on warm convective clouds: Aerosol-cloud surface flux feedbacks in a new coupled large eddy model. *Journal of Geophysical Research Atmospheres*, *111*(1), 1–12. https://doi.org/10.1029/2005JD006138

Jiménez, P. A., Alessandrini, S., Haupt, S. E., Deng, A., Kosovic, B., Lee, J. A., & Delle Monache, L. (2016). The Role of Unresolved Clouds on Short-Range Global Horizontal Irradiance Predictability. *Monthly Weather Review*, *144*(9), 3099–3107. https://doi.org/10.1175/mwr-d-16-0104.1

Joseph, J. H., Wiscombe, W. J., & Weinman, J. A. (1976). The Delta-Eddington Approximation for Radiative Flux Transfer. *Journal of the Atmospheric Sciences*, *33*(12), 2452–2459. https://doi.org/10.1175/1520-0469(1976)033<2452:tdeafr>2.0.co;2

Julia, C., & Dingkuhn, M. (2013). Predicting temperature induced sterility of rice spikelets requires simulation of crop-generated microclimate. *European Journal of Agronomy*, *49*, 50–60. https://doi.org/10.1016/j.eja.2013.03.006

Kang, S. L., & Ryu, J. H. (2016). Response of moist convection to multi-scale surface flux heterogeneity. *Quarterly Journal of the Royal Meteorological Society*, *142*(698), 2180–2193. https://doi.org/10.1002/qj.2811

Katul, G. G., Oren, R., Manzoni, S., Higgins, C., & Parlange, M. B. (2012). Evapotranspiration : a Process Driving Mass Transport and Energy Exchange in the Soil-Plant-Atmosphere-Climate System. *Reviews of Geophysics*, *50*(RG3002), 1–25. https://doi.org/10.1029/2011RG000366

Keil, C., Röpnack, A., Craig, G. C., & Schumann, U. (2008). Sensitivity of quantitative precipitation forecast to height dependent changes in humidity. *Geophysical Research Letters*, *35*(L09812), 1–5. https://doi.org/10.1029/2008GL033657

Kimball, B. A. (1983). Carbon Dioxide and Agricultural Yield: An Assemblage and Analysis of 430 Prior Observations1. *Agronomy Journal*, *75*(5), 779–788. https://doi.org/10.2134/agronj1983.00021962007500050014x

Knutti, R., Furrer, R., Tebaldi, C., Cermak, J., & Meehl, G. A. (2010). Challenges in Combining Projections from Multiple Climate Models. *Journal of Climate*, *23*(10), 2739–2758. https://doi.org/10.1175/2009jcli3361.1

Kobayashi, H., Baldocchi, D. D., Ryu, Y., Chen, Q., Ma, S., Osuna, J. L., & Ustin, S. L. (2012). Modeling energy and carbon fluxes in a heterogeneous oak woodland: A three-dimensional approach. *Agricultural and Forest Meteorology*, *152*(1), 83–100. https://doi.org/10.1016/j.agrformet.2011.09.008

Kristovich, D. A. R. (1993). Mean circulations of boundary-layer rolls in lake-effect snow storms. *Boundary-Layer Meteorology*, *63*(3), 293–315. https://doi.org/10.1007/BF00710463

Lambers, H., Chapin III, F. S., & Pons, T. L. (2008). *Plant Physiological Ecology*. Springer. https://doi.org/10.1007/978-0-387-78341-3

Le Quéré, C., Raupach, M. R., Canadell, J. G., Marland, G., Bopp, L., Ciais, P., … Woodward, F. I. (2009). Trends in the sources and sinks of carbon dioxide. *Nature Geoscience*, *2*(12), 831–836. https://doi.org/10.1038/ngeo689

Leakey, A. D. B., Ainsworth, E. A., Bernacchi, C. J., Rogers, A., Long, S. P., & Ort, D. R. (2009). Elevated CO_2 effects on plant carbon, nitrogen, and water relations: six important lessons from FACE. *Journal of Experimental Botany*, *60*(10), 2859–2876. https://doi.org/10.1093/jxb/erp096

Lee, J. M., Zhang, Y., & Klein, S. A. (2018). The Effect of Land Surface Heterogeneity and Background Wind on Shallow Cumulus Clouds and the Transition to Deeper Convection. *Journal of the Atmospheric Sciences*, *76*(2), 401–419. https://doi.org/10.1175/jas-d-18-0196.1

LeMone, M. A., & Pennell, W. T. (1976). The Relationship of Trade Wind Cumulus Distribution to Subcloud Layer Fluxes and Structure. *Monthly Weather Review*, *104*(5), 524–539. https://doi.org/10.1175/1520-0493(1976)104<0524:trotwc>2.0.co;2

Lenderink, G., Siebesma, A. P., Cheinet, S., Irons, S., Jones, C. G., Marquet, P., … Soares, P. M. M. (2004). The diurnal cycle of shallow cumulus clouds over land: A single-column model intercomparison study. *Quarterly Journal of the Royal Meteorological Society*, *130*(604), 3339–3364. https://doi.org/10.1256/qj.03.122

Li, T., Hasegawa, T., Yin, X., Zhu, Y., Boote, K., Adam, M., … Bouman, B. (2015). Uncertainties in predicting rice yield by current crop models under a wide range of climatic conditions. *Global Change Biology*, *21*(3), 1328–1341. https://doi.org/10.1111/gcb.12758

Lohou, F., & Patton, E. G. (2014). Surface Energy Balance and Buoyancy Response to Shallow Cumulus Shading. *Journal of the Atmospheric Sciences*, *71*(2), 665–682. https://doi.org/10.1175/jas-d-13-0145.1

Long, S. P., Ainsworth, E. A., Rogers, A., & Ort, D. R. (2004). Rising Atmospheric Carbon Dioxide: Plants FACE the Future. *Annual Review of Plant Biology*, *55*(1), 591–628. https://doi.org/10.1146/annurev.arplant.55.031903.141610

Louis, J. F. (1979). A parametric model of vertical eddy fluxes in the atmosphere. *Boundary-Layer Meteorology*, *17*(2), 187–202. https://doi.org/10.1007/BF00117978

Mahmood, R., Pielke, R. A., Hubbard, K. G., Niyogi, D., Dirmeyer, P. A., Mcalpine, C., … Fall, S. (2014). Land cover changes and their biogeophysical effects on climate. *International Journal of Climatology*, *34*(4), 929–953. https://doi.org/10.1002/joc.3736

Manoli, G., Domec, J.-C., Novick, K., Oishi, A. C., Noormets, A., Marani, M., & Katul, G. (2016). Soil-plant-atmosphere conditions regulating convective cloud formation above southeastern US pine plantations. *Global Change Biology*, *22*(6), 2238–2254. https://doi.org/10.1111/gcb.13221

McAusland, L., Vialet-Chabrand, S. R. M., Matthews, J. S. A., & Lawson, T. (2015). *Rhythms in Plants*. Springer, Cham. https://doi.org/https://doi.org/10.1007/978-3-319-20517-5_5

McLeod, A. R., & Long, S. P. (1999). Free-Air Carbon Dioxide Enrichment (FACE) in Global Change Research: A Review. *Advances in Ecological Research*, *26*, 1–35.

Min, Q. (2005). Impacts of aerosols and clouds on forest-atmosphere carbon exchange. *Journal of Geophysical Research D: Atmospheres*, *110*(6), 1–12. https://doi.org/10.1029/2004JD004858

Min, Q., & Wang, S. (2008). Clouds modulate terrestrial carbon uptake in a midlatitude hardwood forest. *Geophysical Research Letters*, *35*(2), 1–5. https://doi.org/10.1029/2007gl032398

Miralles, D. G., Teuling, A. J., Van Heerwaarden, C. C., & De Arellano, J. V. G. (2014). Mega-heatwave temperatures due to combined soil desiccation and atmospheric heat accumulation. *Nature Geoscience*, *7*(5), 345–349. https://doi.org/10.1038/ngeo2141

Moeng, C.-H., & Sullivan, P. P. (1994). A Comparison of Shear- and Buoyancy-Driven Planetary Boundary Layer Flows. *Journal of the Atmospheric Sciences*. https://doi.org/10.1175/1520-0469(1994)051<0999:acosab>2.0.co;2

Mon. Wea. Rev. (1907). Influence of vegetation in causing rain. *Mon. Wea. Rev.*, *35*, 520–521. Retrieved from http://docs.lib.noaa.gov/rescue/mwr/035/mwr-035-11-0520.pdf

Montieth, J. L. (1995). Accommodation between transpiring vegetation and the convective boundary layer. *Journal of Hydrology*, *166*, 251–263. https://doi.org/10.1016/0022-1694(94)05086-D

Morales, A., Kaiser, E., Yin, X., Harbinson, J., Molenaar, J., Driever, S. M., & Struik, P. C. (2018). Dynamic modelling of limitations on improving leaf CO_2 assimilation under fluctuating irradiance. *Plant Cell and Environment*, *41*(3), 589–604. https://doi.org/10.1111/pce.13119

Muryono, M., Chen, C. P., Sakai, H., Tokida, T., Hasegawa, T., Usui, Y., … Hikosaka, K. (2017). Nitrogen Distribution in Leaf Canopies of High-Yielding Rice Cultivar Takanari. *Crop Science*, *57*(4), 2080–2088. https://doi.org/10.2135/cropsci2016.07.0589

Nagy, J., Lewin, K. F., Hendrey, G. R., Hassinger, E., & LaMorte, R. (1994). FACE facility CO_2 concentration control and CO2 use in 1990 and 1991. *Agricultural and Forest Meteorology*, *70*(1–4), 31–48. https://doi.org/10.1016/0168-1923(94)90046-9

Nakamura, H., Tokida, T., Yoshimoto, M., Sakai, H., Fukuoka, M., & Hasegawa, T. (2012). Performance of the enlarged Rice-FACE system using pure CO_2 installed in Tsukuba, Japan. *Journal of Agricultural Meteorology*, *68*(1), 15–23. https://doi.org/10.2480/agrmet.68.1.2

Nakano, H., Yoshinaga, S., Takai, T., Arai-Sanoh, Y., Kondo, K., Yamamoto, T., … Kondo, M. (2017). Quantitative trait loci for large sink capacity enhance rice grain yield under free-air CO_2 enrichment conditions. *Scientific Reports*, *7*(1827), 1–10. https://doi.org/10.1038/s41598-017-01690-8

Ooba, M., & Takahashi, H. (2003). Effect of asymmetric stomatal response on gas-exchange dynamics. *Ecological Modelling*, *164*(1), 65–82. https://doi.org/10.1016/S0304-3800(03)00012-7

Ort, D. R., Merchant, S. S., Alric, J., Barkan, A., Blankenship, R. E., Bock, R., … Zhu, X. G. (2015). Redesigning photosynthesis to sustainably meet global food and bioenergy demand. *Proceedings of the National Academy of Sciences*, *112*(28), 8529–8536. https://doi.org/10.1073/pnas.1424031112

Ouwersloot, H. G., De Arellano, J. V. G., H. Van Stratum, B. J., Krol, M. C., & Lelieveld, J. (2013). Quantifying the transport of subcloud layer reactants by shallow cumulus clouds over the Amazon. *Journal of Geophysical Research Atmospheres*, *118*(23), 13041–13059. https://doi.org/10.1002/2013JD020431

Ouwersloot, H. G., Moene, A. F., Attema, J. J., & Vilà-Guerau de Arellano, J. (2017). Large-Eddy Simulation Comparison of Neutral Flow Over a Canopy: Sensitivities to Physical and Numerical Conditions, and Similarity to Other Representations. *Boundary-Layer Meteorology*, *162*(1), 71–89. https://doi.org/10.1007/s10546-016-0182-5

Pedruzo-Bagazgoitia, X., Ouwersloot, H. G., Sikma, M., van Heerwaarden, C. C., Jacobs, C. M. J., & Vilà-Guerau de Arellano, J. (2017). Direct and Diffuse Radiation in the Shallow Cumulus–Vegetation System: Enhanced and Decreased Evapotranspiration Regimes. *Journal of Hydrometeorology*, *18*(6), 1731–1748. https://doi.org/10.1175/jhm-d-16-0279.1

Pielke, R. A., Adegoke, J. O., Chase, T. N., Marshall, C. H., Matsui, T., & Niyogi, D. (2007). A new paradigm for assessing the role of agriculture in the climate system and in climate change. *Agricultural and Forest Meteorology*, *142*(2–4), 234–254. https://doi.org/10.1016/j.agrformet.2006.06.012

Pielke, R. A., Mahmood, R., & McAlpine, C. (2016). Land's complex role in climate change. *Physics Today*, *69*(11), 40–46. https://doi.org/10.1063/PT.3.3364

Rabin, R. M., Stadler, S., Wetzel, P. J., Stensrud, D. J., & Gregory, M. (1990). Observed Effects of Landscape Variability on Convective Clouds. *Bulletin of the American Meteorological Society*, *71*(3), 272–280. https://doi.org/10.1175/1520-0477(1990)071<0272:oeolvo>2.0.co;2

Reichler, T., & Kim, J. (2008). How Well Do Coupled Models Simulate Today 's Climate?, *819*, 303–311. https://doi.org/10.1175/BAMS-89-3-303

Rial, J. A., Pielke Sr, R. A., Beniston, M., Noblet-ducoudré, N. D. E., & Prinn, R. (2004). Nonlinearities, Feedbacks and Critical Thresholds within the Earth's Climate System. *Climatic Change*, *65*, 11–38.

Richardson, L. F. (1922). *Weather Prediction by Numerical Processes*. Cambridge university press. https://doi.org/10.1017/CBO9780511618291

Rieck, M., Hohenegger, C., & van Heerwaarden, C. C. (2014). The Influence of Land Surface Heterogeneities on Cloud Size Development. *Monthly Weather Review*, *142*(10), 3830–3846. https://doi.org/10.1175/mwr-d-13-00354.1

Ronda, R. J., de Bruin, H. A. R., & Holtslag, A. A. M. (2001). Representation of the Canopy Conductance in Modeling the Surface Energy Budget for Low Vegetation. *Journal of Applied Meteorology*, *40*, 1431–1444. https://doi.org/10.1175/1520-0450(2001)040<1431:ROTCCI>2.0.CO;2

Satake, T., & Yoshida, S. (1978). High Temperature-Induced Sterility in Indica Rices at Flowering. *Japan. Jour. Crop Sci.*, *47*(1), 6–17.

Schumann, U., Dörnbrack, A., & Mayer, B. (2002). Cloud-shadow effects on the structure of the convective boundary layer. *Meteorologische Zeitschrift*, *11*(4), 285–294. https://doi.org/10.1127/0941-2948/2002/0011-0285

Sellers, P. J., Randall, D. A., Collatz, G. J., Berry, J. A., Field, C. B., Dazlich, D. A., … Bounoua, L. (1996). A Revised Land Surface Parameterization (SiB2) for Atmospheric GCMS. Part II: The generation of global fields of terrestrial biophysical parameters from satellite data. *Journal of Climate*. https://doi.org/10.1175/1520-0442(1996)009<0676:ARLSPF>2.0.CO;2

Seneviratne, S. I., Corti, T., Davin, E. L., Hirschi, M., Jaeger, E. B., Lehner, I., … Teuling, A. J. (2010). Investigating soil moisture-climate interactions in a changing climate: A review. *Earth-Science Reviews*, *99*(3–4), 125–161. https://doi.org/10.1016/j.earscirev.2010.02.004

Seneviratne, S. I., Lüthi, D., Litschi, M., & Schär, C. (2006). Land-atmosphere coupling and climate change in Europe. *Nature*, *443*(7108), 205–209. https://doi.org/10.1038/nature05095

Sherwood, S. C., Bony, S., & Dufresne, J. L. (2014). Spread in model climate sensitivity traced to atmospheric convective mixing. *Nature*, *505*(7481), 37–42. https://doi.org/10.1038/nature12829

Siebert, H., & Shaw, R. A. (2016). Supersaturation Fluctuations during the Early Stage of Cumulus Formation. *Journal of the Atmospheric Sciences*, *74*(4), 975–988. https://doi.org/10.1175/jas-d-16-0115.1

Sikma, M. (2019). Supplementary data of "Japan FACE 2015 experiment". 4TU.Centre for Research Data. https://doi.org/10.4121/uuid:625cf57e-aaf0-4be4-bfb0-f2f48e6c78fb

Sikma, M., Ouwersloot, H. G., Pedruzo-Bagazgoitia, X., van Heerwaarden, C. C., & Vilà-Guerau de Arellano, J. (2017). Interactions between vegetation, atmospheric turbulence and clouds under a wide range of background wind conditions. *Agricultural and Forest Meteorology*, *255*(December 2016), 31–43. https://doi.org/10.1016/j.agrformet.2017.07.001

Sikma, M., & Vilà-Guerau de Arellano, J. (2019). Substantial reductions in cloud cover and moisture transport by dynamic plant responses. *Geophysical Research Letters*, *46*, 1870–1878. https://doi.org/10.1029/2018gl081236

Soden, B. J., Shell, K. M., Kiehl, J. T., Colman, R., Shields, C. A., & Held, I. M. (2008). Quantifying Climate Feedbacks Using Radiative Kernels. *Journal of Climate*, *21*(14), 3504–3520. https://doi.org/10.1175/2007jcli2110.1

Spracklen, D. V., Arnold, S. R., & Taylor, C. M. (2012). Observations of increased tropical rainfall preceded by air passage over forests. *Nature*, *489*(7415), 282–285. https://doi.org/10.1038/nature11390

Stephens, G. L. (1978). Radiation Profiles in Extended Water Clouds. II: Parameterization Schemes. *Journal of the Atmospheric Sciences*, *35*, 2123–2132. https://doi.org/10.1175/1520-0469(1978)035<2123:rpiewc>2.0.co;2

Stevens, B., & Bony, S. (2013). What Are Climate Models Missing? *Science*, *340*(September), 1053–1054. https://doi.org/10.1126/science.1237554

Strain, B. R., & Cure, J. D. (1985). *Background on the response of vegetation to atmospheric carbon dioxide enrichment*. *Direct Effects of Increasing Carbon Dioxide On Vegetation*. https://doi.org/10.2172/6134866

Stull, R. (1988). *An Introduction to Boundary Layer Meteorology*. *Book*. Springer Netherlands. https://doi.org/10.1007/978-94-009-3027-8

Sykes, R. I., & Henn, D. S. (1989). Large-Eddy Simulation of Turbulent Sheared Convection. *Journal of the Atmospheric Sciences*, *46*(8), 1106–1118. https://doi.org/10.1175/1520-0469(1989)046<1106:lesots>2.0.co;2

Taylor, C. M., Saïd, F., & Lebel, T. (1997). Interactions between the Land Surface and Mesoscale Rainfall Variability during HAPEX-Sahel. *Monthly Weather Review*, *125*(9), 2211–2227. https://doi.org/10.1175/1520-0493(1997)125<2211:ibtlsa>2.0.co;2

Taylor, G. I. (1922). Diffusion by continuous movements. *Proceedings of the London Mathematical Society*, *20*(1), 196–212. https://doi.org/10.1112/plms/s2-20.1.196

Taylor, J. W., Choularton, T. W., Blyth, A. M., Liu, Z., Bower, K. N., Crosier, J., … Brown, P. R. A. (2016). Observations of cloud microphysics and ice formation during COPE. *Atmospheric Chemistry and Physics*, *16*(2), 799–826. https://doi.org/10.5194/acp-16-799-2016

Tilman, D., Balzer, C., Hill, J., & Befort, B. L. (2011). Global food demand and the sustainable intensification of agriculture. *Proceedings of the National Academy of Sciences*, *108*(50), 20260–20264. https://doi.org/10.1073/pnas.1116437108

Usui, Y., Sakai, H., Tokida, T., Nakamura, H., Nakagawa, H., & Hasegawa, T. (2016). Rice grain yield and quality responses to free-air CO_2 enrichment combined with soil and water warming. *Global Change Biology*, *22*(3), 1256–1270. https://doi.org/10.1111/gcb.13128

van Heerwaarden, C. C., Mellado, J. P., & De Lozar, A. (2014). Scaling Laws for the Heterogeneously Heated Free Convective Boundary Layer. *Journal of the Atmospheric Sciences*, *71*(11), 3975–4000. https://doi.org/10.1175/jas-d-13-0383.1

van Heerwaarden, C. C., & Vilà-Guerau de Arellano, J. (2008). Relative Humidity as an Indicator for Cloud Formation over Heterogeneous Land Surfaces. *Journal of the Atmospheric Sciences*, *65*(10), 3263–3277. https://doi.org/10.1175/2008jas2591.1

Van Loon, M. P., Dekker, S. C., Anten, N. P. R., Rietkerk, M., & Vilà-Guerau De Arellano, J. (2015). Understanding the impact of plant competition on the coupling between vegetation and the atmosphere. *Journal of Geophysical Research G: Biogeosciences*, *120*(11), 2212–2228. https://doi.org/10.1002/2015JG003108

Van Oort, P. A. J., Saito, K., Zwart, S. J., & Shrestha, S. (2014). A simple model for simulating heat induced sterility in rice as a function of flowering time and transpirational cooling. *Field Crops Research*, *156*, 303–312. https://doi.org/10.1016/j.fcr.2013.11.007

van Stratum, B. J. H., Vilá-Guerau de Arellano, J., van Heerwaarden, C. C., & Ouwersloot, H. G. (2014). Subcloud-Layer Feedbacks Driven by the Mass Flux of Shallow Cumulus Convection over Land. *Journal of the Atmospheric Sciences*, *71*(3), 881–895. https://doi.org/10.1175/jas-d-13-0192.1

Vicente-Serrano, S. M., Nieto, R., Gimeno, L., Azorin-Molina, C., Drumond, A., & El Kenawy, A. (2018). Recent changes of relative humidity: regional connections with land and ocean processes. *Earth System Dynamics*, *9*(2), 915–937. https://doi.org/10.5194/esd-9-915-2018

Vico, G., Manzoni, S., Palmroth, S., & Katul, G. (2011). Effects of stomatal delays on the economics of leaf gas exchange under intermittent light regimes. *New Phytologist*, *192*(3), 640–652. https://doi.org/10.1111/j.1469-8137.2011.03847.x

Vihma, T. (2014). *Effects of Arctic Sea Ice Decline on Weather and Climate: A Review*. *Surveys in Geophysics* (Vol. 35). https://doi.org/10.1007/s10712-014-9284-0

Vilà-Guerau de Arellano, J., Ouwersloot, H. G., Baldocchi, D., & Jacobs, C. M. J. (2014). Shallow cumulus rooted in photosynthesis. *Geophysical Research Letters*, *41*(5), 1796–1802. https://doi.org/10.1002/2014GL059279

Vilà-Guerau de Arellano, J., Van Heerwaarden, C. C., & Lelieveld, J. (2012). Modelled suppression of boundary-layer clouds by plants in a CO2 -rich atmosphere. *Nature Geoscience*, *5*(10), 701–704. https://doi.org/10.1038/ngeo1554

Waite, M. L., & Khouider, B. (2010). The Deepening of Tropical Convection by Congestus Preconditioning. *Journal of the Atmospheric Sciences*, *67*(8), 2601–2615. https://doi.org/10.1175/2010jas3357.1

Wang, E., Martre, P., Zhao, Z., Ewert, F., Maiorano, A., Rötter, R. P., … Asseng, S. (2017). The uncertainty of crop yield projections is reduced by improved temperature response functions. *Nature Plants*, *3*(8), 17102. https://doi.org/10.1038/nplants.2017.102

Wetzel, J., Argentini, S., & Boone, A. (1996). Role of land surface in controlling daytime cloud amount : Two case studies are modeled using, *101*, 7359–7370.

Wickland, K. P., Striegl, R. G., Neff, J. C., & Sachs, T. (2006). Effects of permafrost melting on CO_2 and CH4 exchange of a poorly drained black spruce lowland. *Journal of Geophysical Research: Biogeosciences*, *111*(2), 1–13. https://doi.org/10.1029/2005JG000099

World Meteorological Organisation. (2015). *Seamless Prediction of the Earth System :* (Vol. 41).

Wright, J. S., Fu, R., Worden, J. R., Chakraborty, S., Clinton, N. E., Risi, C., … Yin, L. (2017). Rainforest-initiated wet season onset over the southern Amazon. *Proceedings of the National Academy of Sciences*, *114*(32), 8481–8486. https://doi.org/10.1073/pnas.1621516114

Xiao, H., Berg, L. K., & Huang, M. (2018). The Impact of Surface Heterogeneities and Land-Atmosphere Interactions on Shallow Clouds Over ARM SGP Site. *Journal of Advances in Modeling Earth Systems*, *10*(6), 1220–1244. https://doi.org/10.1029/2018MS001286

Yano, J. I. I., Ziemian´ski, Mi. Z., Cullen, Mi., Termonia, Pi., Onvlee, J., Bengtsson, L., … Wyszogrodzki, A. A. (2018). Scientific challenges of convective-scale numerical weather prediction. *Bulletin of the American Meteorological Society*, *99*(4), 699–710. https://doi.org/10.1175/BAMS-D-17-0125.1

Yin, X. (2013). Improving ecophysiological simulation models to predict the impact of elevated atmospheric CO2 concentration on crop productivity. *Annals of Botany*, *112*(3), 465–475. https://doi.org/10.1093/aob/mct016

Yoshimoto, M., Fukuoka, M., Hasegawa, T., Utsumi, M., Ishigooka, Y., & Kuwagata, T. (2011). Integrated micrometeorology model for panicle and canopy temperature (IM2PACT) for rice heat stress studies under climate change. *Journal of Agricultural Meteorology*, *67*(4), 233–247. https://doi.org/10.2480/agrmet.67.4.8

Yoshimoto, M., Oue, H., & Kobayashi, K. (2005). Energy balance and water use efficiency of rice canopies under free-air CO_2 enrichment. *Agricultural and Forest Meteorology*, *133*(1–4), 226–246. https://doi.org/10.1016/j.agrformet.2005.09.010

Young, G. S., Kristovich, D. A. R., Hjelmfelt, M. R., & Foster, R. C. (2002). Rolls, streets, waves, and more: a review of quasi-two-dimensional structures in the atmospheric boundary layer. *Bulletin of the American Meteorological Society*, (July), 997–1001. https://doi.org/I 10.1 175/BAMS-83-7-Young

Zhang, G., Sakai, H., Usui, Y., Tokida, T., Nakamura, H., Zhu, C., … Hasegawa, T. (2015). Grain growth of different rice cultivars under elevated CO_2 concentrations affects yield and quality. *Field Crops Research*, *179*, 72–80. https://doi.org/10.1016/j.fcr.2015.04.006

Zhang, L., Hu, Z., Fan, J., Zhou, D., & Tang, F. (2014). A meta-analysis of the canopy light extinction coefficient in terrestrial ecosystems. *Frontiers of Earth Science*, *8*(4), 599–609. https://doi.org/10.1007/s11707-014-0446-7

Zhang, Y., & Klein, S. A. (2010). Mechanisms Affecting the Transition from Shallow to Deep Convection over Land: Inferences from Observations of the Diurnal Cycle Collected at the ARM Southern Great Plains Site. *Journal of the Atmospheric Sciences*, *67*(9), 2943–2959. https://doi.org/10.1175/2010jas3366.1

Summary

In the last decades, performance of numerical weather prediction (NWP) and global climate models (GCM) have vastly improved. As a consequence of the improvements on model physics and increased computational power, the model resolution has been increased leading to the inclusion of the regional (~10 km) scale processes. However, as our understanding of the small scale processes that act in the models 'grey-zone' is yet not sufficient enough, initially minor misrepresentations can lead to potentially large deviations in the model's progression.

The main objective of this thesis was to gain insights on the impact of diurnal and local interactions between the vegetation, atmosphere and boundary layer clouds in current and future atmospheres. Special focus was placed on the consequences on moist convection, as it is one of the main uncertainties in the global climate and weather models. Moist convection is strongly influenced by the vegetated surface characteristics, which has consequences on the sub-weekly atmospheric state. In this thesis, a balanced approach is taken, which takes into account local (meters) and short (minutes) dynamic vegetation responses to atmospheric and cloud perturbations, that subsequently influence the atmospheric boundary layer and cloud development.

To deepen our understanding of the processes that act on the smaller scales, a Large-Eddy Simulation (LES) model was employed and coupled with a mechanistic land-surface submodel. The LES model explicitly resolved the various dynamical processes at a scale of 50 m, which has an advantage over the coarser atmospheric models as minimal parametrizations are required. The investigations were based on a combined approach of advanced measurements and numerical experiments. The numerical experiments are based on observations over Western Europe, while for the future atmospheres the numerical experiments were inspired on results from a Free-Air CO_2 Enrichment (FACE) experiment in Japan and combined with findings from literature.

The **first objective** of this thesis was **to improve our understanding of the local interactions between responses of low vegetation to atmospheric perturbations and cumulus cloud development**. The impact of intermittent light perturbations on plant physiological processes, and its consequences for the atmospheric state and boundary layer cloud development, was investigated for a wide range in convective situations (i.e., cellular convection to roll vortices).

By following a systematic approach, our results highlighted the regional effects of a strong plant-atmosphere-cloud coupling (Chapter 2). In low wind and convective

situations, a lowering in surface energy fluxes resulted in stabilized cloud development, although there was a distinct response based on the cloud optical properties. With clouds identified as optically thin, there was an enhancement in both the assimilation of CO_2 and in the latent heat fluxes that was caused by an increased diffuse radiative component, with subsequent effects that favored cloud development. Clouds identified as optically thick always caused a negative surface response through shading, which had negative consequences on moist convection. In this thesis, the surface heterogeneous conditions that arose due to vegetation responses to cloud shading is called dynamic heterogeneity. To assess the validity of these results in different convective conditions, we repeated our analysis for a wide range in wind conditions in Chapter 2.

With increasing background wind, atmospheric roll vortices forced the cloud population into streets (i.e., parallel strips of clouds alternated by clear sky). As a consequence of the asymmetric stomatal plant response, vegetation streaks arose due to cloud shading that negatively affected the surface energy balance. This result shed light to a new coupling mechanism that constrained cloud development and reduced the in-cloud moisture flux (Chapter 3). Interestingly, since the sunlit areas experienced enhanced surface energy fluxes due to the increased atmospheric momentum, thus enhanced land-atmosphere exchange, the regional averaged fluxes were comparable with a free convective situation. To determine whether the plant-atmosphere-cloud coupling could be captured by homogeneous surface responses (i.e., related to a response in a NWP or GCM grid box), we performed simulations that were similar in the domain averaged surface energy, but differed in their response: interactive versus prescribed (Chapter 3). Our findings showed that large misrepresentation of up to 56% occurred in the regional moisture flux when the locality of the dynamic plant responses to atmospheric perturbations was not taken into account. This highlighted the need that these atmospheric flow dependent plant-atmosphere-cloud interactions need to be included in the parameterizations of the coarser NWPs and GCMs. When these processes are neglected, the stabilizing vegetation response to the atmospheric and cloud driven radiation perturbations is likely to be underestimated. As a consequence, the predictions of hydrological and carbon balances are liable to failure, with an overestimation in moist convection as a result.

Building up on the knowledge acquired under current conditions (Chapter 2 & 3), the **second objective** of this thesis was **to advance the understanding of how the plant-atmosphere-cloud coupling is affected by increased levels of [CO_2] and air temperature typically associated to climatic changes**. To meet this objective, a similar approach was employed as compared to the research that addressed our first objective. In Chapter 4,

a cloud to plant perspective was taken, where data from an experimental FACE campaign was used. In Chapter 5, we took a plant to cloud perspective, by simulation the key processes with an atmospheric high-resolution model.

By analyzing a comprehensive observational dataset of two distinct rice varieties in ambient and elevated CO_2 environments (+200 ppm) in Chapter 4, we identified a strong interplay between influencers on the plant-atmosphere interaction. The combination of plant architecture as well as plant physiology drove the response to atmospheric perturbations, with an open canopy leading to enhanced mixing rates, as well as a warmer in-canopy environment due to enhanced radiative penetration. In elevated CO_2 environments, the physiological response to this factor became apparent, with warmer and drier in-canopy levels in a more closed and less photosynthetic active canopy, while the opposite was found in a more open and photosynthetic active canopy. Furthermore, no clear stomatal closure effects were found in the latent heat fluxes due to enhanced evaporation rates of the irrigated surface water. This distinct response to elevations in [CO_2] shows the need to accurately account for plant physiological properties, including architecture, in modelling approaches, as they have a major influence on the surface energy balance and influence yield projections through subsequent elevations in canopy temperature, thus the risk of spikelet sterility.

Inspired by our findings of Chapter 4, we simulated and investigated the sensitivity of plant responses to elevations in both air temperature (+2 K) as [CO_2] (+200 ppm). Our findings showed contrasting responses to elevations in temperature and [CO_2] on the surface energy balance and momentum transfer. Elevations in temperature yields enhanced plant transpiration, thus latent heat flux, and reduced the sensible heat flux. As a consequence, the turbulent kinetic energy and buoyancy rates reduced, which caused reductions in cloud cover and mid-tropospheric moisture transport. With elevations in [CO_2], a distinct response occurred, leading to higher sensible heat fluxes and lower plant transpiration and latent heat fluxes. With more momentum in the atmospheric boundary layer, clouds were able to become deeper and transport more moisture into the troposphere.

When simulating a future atmosphere with both elevations in temperature and [CO_2], we found an offset in the surface energy balance with nearly identical energy fluxes as compared to current situations. However, the plant physiological state was affected, with reductions in plant transpiration and increased CO_2 assimilation. Although the turbulent kinetic energy was relatively high, the level of free convection remained at higher altitudes, which hampered cloud development, consequentially reducing the cloud cover and in-cloud moisture transport.

Acknowledgements

I am very grateful for the flexibility, commitment and freedom my promotion team has provided me. Although my side activities might have caused some distractions along the way, their support and critical comments brought this PhD thesis to a higher level. For that I am very thankful.

Jochem, it was great to experience your enthusiasm and your drive to share your knowledge on modelling plant canopies. For me, it led to a better understanding of processes and feedbacks in plants of which I was unaware when starting my PhD. In your comments, you often asked me to clarify certain statements that I thought were obvious. However, they were not, which has greatly helped to put this thesis in perspective. When abroad in Japan or China we were often, for some reason, ending up in a karaoke bar with a group of researchers. It was great to have this level of contact.

Niels, I am very grateful for your help on the scientific as well as management level. With your solution-oriented mindset, we could always tackle the issue and find a solution. I am very thankful you approved my part-time construction, which allowed me to gain work experience outside academia. Your sharp comments definitely had a great impact on the quality of the thesis.

Jordi, we have been working together for over 8 years and I have never experienced a moment when you were not available for a discussion, talk or brainstorm session. We have experienced some great and fun moments over the years and am really thankful for your Spanish influence and mindset along the way. One thing I particularly liked was our dinners over the years, it is good to realize how these have been gradually improving! Definitely one of my highlights during the PhD was the conference you organized in Barcelona. Although the whisky was a bit pricy, it was great to see Messi play and experience the amazing parts of Barcelona. I hope me finishing the PhD doesn't mean I won't receive the invitation to Ibiza, I am still waiting!

Bert, our discussions and brainstorm sessions have been great. Your enthusiasm and creativity were leading to many novel and great ideas. It was a pleasure to have you with me in Japan; I still remember a certain lunch we had in Akihabara, Tokyo! You also managed to show me how extreme suffering can be pleasant. For instance the time we decided to go for a short bike ride on our racing bike with only having one biscuit packed. In 4 hours, all the hills between Wageningen and Arnhem ticked of our list and

109 km later, we finally ate our biscuit and I still remember its taste… Not to speak of our "morning" MTB ride, it took me a while before I could normally walk again! Many thanks for the great times off-work relaxing, and always having your door open for me to ask a question, provide me help on a problem or have a discussion.

During my time in Japan, I have been working closely together with the Tsukuba FACE team; thanks all for the nice lunches and good laughs. There are a few persons I would like to give my special thanks to; who helped me out, made my life more pleasant or helped me overcome some of the cultural "obstacles".

Toshi, many thanks for your supervision, help, overview and guidance during my stay. I have learned a lot and you were always eager to teach me new things. Our collaboration really grew during the time and I was very happy I got the opportunity to visit you again in Morioka; the *Onsen* on the volcano was exceptional!!

Hiroki, it was a real pleasure to work, learn from and hang out with you. Many thanks for helping me getting settled in the first weeks, it meant a lot to me. I also greatly appreciated the driving to and from the field, helping me with the micro-meteorological observations and all the off-work relaxation. You were always in for something nice and I still remember our great surfing trips! Hope to meet you somewhere soon in Europe so I can finally return a dinner.

Mayumi, it was great to work with and learn from you. Your knowledge of micro-meteorological measurements was invaluable during the start of the project and helped to the success of my project. Thanks for the fine dinners and pleasant company!

Hitomi, many thanks for helping me out in the field every Friday: the only day of the week when it literally always rained! Your spontaneous and down-to-Earth attitude was great and always cheered my mood!

I would also like to thank the other members of the FACE and NIAES team, with special thanks to Nakamura-san, Harigae-san, Charles Chen, Kuwagata-san, Ono-san and all other team members who helped me with the biomass and micro-climate measurements.

My time as a PhD wouldn't be as nice without the fun moments with my colleagues both at CSA and MAQ, thank you all! Especially Xabi and Luuk; Xabi, thanks for the great lunches, dinners, discussions and fun moments. Our USA trip was memorable! Luuk, it

was great to share the office with you! It was nice to have a good laugh and be able to share our thoughts on some matters. Thanks for organizing all the drinks and other nice activities at CSA as well! Ali, Ambra, Daniel, Jorad, Bei, Shuangwei, it was really nice to share the office with you!! I would also like to mention some PhDs with whom I really enjoyed the lunches, dinners, discussions or drinks with: Marcello, Dennis, Alba, Imme, Marie, Alejandro, Goufang, Herman, Giovanni, Rachel, Ningyi, Arian, Ioannis, Kailei, Wenjing, Uta, Niteen, Frank, Thomas and Thomas, thank you all!

Huug, although you were not directly involved in my project, you have had an enormous influence on it by mentoring me the years prior. You really taught me to think critically and never take something for granted. I am certain that this mindset has helped me greatly during my PhD and want to thank you for all the energy and time you have spent on me. It was great fun working together!

Chiel, I really enjoyed our discussions. Your experience on atmospheric modelling was invaluable. Sjanie, Alex-Jan, Nicole and Petra, thank you for your great (administrative) help along the way.

Luuk, Jeroen, Tim, Zhoucen, Yiming, Janno and Tianyao thanks for helping me on my project by working on your thesis. You have taught me a great deal and have provided me valuable insights by analyzing the FACE data or LES modelling.

Sem, Max and Michiel, I am really lucky to have you in my life for already a very long time! Sem, thank you for your willingness to design the thesis cover and being a great friend for more than half my life. The same holds for Max and Michiel; I am grateful and proud you are sitting alongside me while defending this thesis. Anneroos, it is great to have you as a good friend! Although you didn't believe 10 years ago that I said we probably would be still friends at this moment, I think it's safe to say that we can at least add another 10 years on top that! Bart, we both started the journey as a student together, and I'm very happy we're still in touch. I've had so much fun with you during our time in Wageningen!! I also would like to thank the rest of my "SHSO" friends, although we don't see each other that regularly anymore, I feel very fortunate to have you in my life.

Mom, Dad, Leander, Shanna and the rest of the family: I would like to thank you for your support and interest during my studies and PhD. It made a difference!

Last but definitely not least, Pleun. Some people say that two PhD's living in one house is asking for trouble but I think we have successfully shown the opposite. My PhD has had some ups and downs and I am very grateful you were there for me all the time. Let's finish this ride soon and aim for a better and more fun road for the coming years ahead!

List of journal publications

1. **Sikma, M.** and Ouwersloot, H.G. (2015). Parameterizations for convective transport in various cloud-topped boundary layers. Atmos. Chem. Phys., 15, 10399-10410

2. Horn, G.L., Ouwersloot, H.G, Vilà-Guerau de Arellano, J. and **Sikma, M.** (2015). Cloud Shading Effects on Characteristic Boundary-Layer Length Scales. Bound. Lay. Meteorol., 157(2), 237-263

3. Pedruzo-Bagazgoitia, X., Ouwersloot, H.G., **Sikma, M.**, van Heerwaarden, C.C., Jacobs, C. and Vilà-Guerau de Arellano, J. (2017) Direct and diffuse radiation in the shallow cumulus-vegetation system: Enhanced and decreased evapotranspiration regimes, J. Hydromet., 18, 1731-1748

4. **Sikma, M.**, Ouwersloot, H.G., Pedruzo-Bagazgoitia, X., van Heerwaarden, C.C., Vilà-Guerau de Arellano (2017) Interactions between vegetation, atmospheric turbulence and clouds under a wide range of background wind conditions. Agri. For. Meteorol. 205: 31-43.

5. Ikawa, H., Chen, C.P., **Sikma, M.**, Yoshimoto, M., Sakai, H., Tokida, T., Usui, Y., Nakamura, H., Ono, K., Maruyama, A., Watanabe, T., Kuwagata, T. and Hasegawa, T. (2018). Increasing canopy photosynthesis in rice can be achieved without a large increase in water use—A model based on free-air CO2 enrichment. Global Change Biology, 24, 1321-1341. DOI: 10.1111/gcb.13981

6. **Sikma, M.** and Vilà-Guerau de Arellano (2019). Substantial reductions in cloud cover and moisture transport by dynamic plant responses. Geophys. Res. Lett. DOI: 10.1029/2018GL081236

7. **Sikma, M.**, Ikawa, H., Heusinkveld, B.G., Yoshimoto, M., Hasegawa, T., Groot Haar, L.T., Anten, N.P.R., Nakamura, H., Vilà-Guerau de Arellano, J., Sakai, H., Tokida, T., Usui, Y. and Evers, J.B. (2019) Quantifying the feedback between rice architecture, physiology and microclimate under current and future CO_2 conditions. J. Geophys. Res.: Biogeosciences. Under review

8. **Sikma, M.**, Pedruzo-Bagazgoitia, X., Heusinkveld, B.G., Evers, J.B., N.P.R. Anten, Vilà-Guerau de Arellano, J. (2019) Plant-atmosphere-cloud interactions in future climates. J. Geophys. Res.: Atmospheres. Under review

PE&RC Training and Education Statement

With the training and education activities listed below the PhD candidate has complied with the requirements set by the C.T. de Wit Graduate School for Production Ecology and Resource Conservation (PE&RC) which comprises of a minimum total of 32 ECTS (= 22 weeks of activities)

Review of literature (4.5 ECTS)

- Quantifying feedbacks between plant architecture, physiology and microclimate to analyze crop climate responses

Post-graduate courses (3 ECTS)

- GroIMP workshop (2016)
- Dynamic models in R (2017)

Laboratory training and working visits (4.5 ECTS)

- Free-Air CO_2 enrichment experiment; National Institute for Agro-Environmental Sciences, Japan

Invited review of (unpublished) journal manuscript (2 ECTS)

- Annals of Botany: phytomer growth and development in perennial C4 grass (2016)
- Journal of Advances in Modelling Earth Systems: comparison of high-resolution model with global model-like approach with respect to plant-atmosphere interactions and radiative responses (2018)

Competence strengthening / skills courses (2.1 ECTS)

- Scientific publishing; PE&RC (2016)
- PhD Carousel; WGS (2016)
- Career perspectives; WGS (2018)

Discussion groups / local seminars / other scientific meetings (5.9 ECTS)

- Atmospheric turbulence and cloud development discussion group (2015-2016)
- Plant form and function group (PFF) (2015-2018)
- Photosynthesis discussion group (2016)

International symposia, workshops and conferences (12.1 ECTS)

- 7th GroIMP user and development meeting; Angers, France (2015)
- BBOS-BLT; Delft (2016)
- BBOS-BLT; Barcelona, Spain (2016)
- AMS-BLM-AFM; Salt Lake City, Utah, USA (2016)
- FSPMA; Qingdao, China (2016)
- AGU Washington DC; USA (2018)

Lecturing / supervision of practicals / tutorials (3 ECTS)

- Boundary-layer processes (2015-2016)

Supervision of MSc students (24 ECTS)

- Sensitivity of cloud growth to Amazonian midday plant depression
- The rice-atmosphere interaction in present and future climate
- The vegetation-cloud interaction in a future climate
- The interaction between rice morphology and microclimate in present and future conditions
- Investigating the morphological response and yield change of two rice varieties to increasing temperature and radiation
- Determining canopy stomatal response on a large scale
- Interaction between plant responses to dynamic light
- The rice morphology and in-canopy microclimate interaction under ambient and elevated CO_2 concentration

The research described in this thesis was financially supported by the Netherlands Organisation for Scientific Research (NWO – ALW Open competition grant 823.01.012 to J.B. Evers)

Layout by author
Cover design by Studio Katt

Printed by GVO drukkers & vormgevers, Ede, The Netherlands

Propositions

1. Our knowledge and understanding of current plant-atmosphere feedbacks is insufficient to be used to extrapolate for future scenarios.
   (this thesis)

2. Understanding sub-grid scale land-atmosphere processes at the fundamental level is essential to make progress in numerical weather prediction and global climate modelling.
   (this thesis)

3. Our current definition of climate directly undervalues the risk for weather extremes in a changing climate.

4. More emphasis on fundamental research is necessary to maintain long-term societal progress.

5. Democracy is an unsuitable political system for solving global issues.

6. The quality of coffee strongly correlates with the efficiency in writing a thesis.

Propositions belonging to the thesis, entitled

Quantifying feedbacks in the plant-atmosphere-cloud continuum

Martin Sikma

Wageningen, 16 October 2019